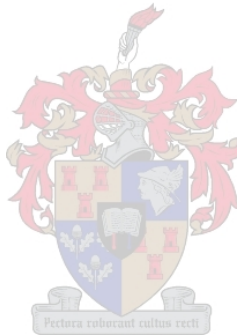


# Development of a vital signs monitoring wireless ear probe

by

André Bestbier



*Thesis presented in partial fulfilment of the requirements for  
the degree of Master of Engineering (Mechanical) in the  
Faculty of Engineering at Stellenbosch University*

Supervisor: Prof. PF. Fourie

September 2017

# Declaration

By submitting this thesis electronically, I declare that the entirety of the work contained therein is my own, original work, that I am the sole author thereof (save to the extent explicitly otherwise stated), that reproduction and publication thereof by Stellenbosch University will not infringe any third party rights and that I have not previously in its entirety or in part submitted it for obtaining any qualification.

Date: ..... 2017/09/09

Copyright © 2017 Stellenbosch University  
All rights reserved.

# Abstract

## Development of a vital signs monitoring wireless ear probe

A. Bestbier

*Department of Mechanical and Mechatronic Engineering,  
University of Stellenbosch,  
Private Bag X1, Matieland 7602, South Africa.*

Thesis: MEng (Mech)

September 2017

Add abstract.

# Uittreksel

## Ontwikkeling van n kritieke sein moniteering draadlose oor probe

(“*Development of a vital signs monitoring wireless ear probe*”)

A. Bestbier

*Departement Meganiese en Megatroniese Ingenieurswese,  
Universiteit van Stellenbosch,  
Privaatsak X1, Matieland 7602, Suid Afrika.*

Tesis: MIng (Meg)

September 2017

Voeg uittreksel by.

# Acknowledgements

I would like to express my sincere gratitude to the following people and organisations ...

# Dedications

*Hierdie tesis word opgedra aan ...*

# Contents

<b>Declaration</b>	i
<b>Abstract</b>	ii
<b>Uittreksel</b>	iii
<b>Acknowledgements</b>	iv
<b>Dedications</b>	v
<b>Contents</b>	vi
<b>List of Figures</b>	x
<b>List of Tables</b>	xiii
<b>Nomenclature</b>	xiv
<b>1 Introduction</b>	1
1.1 Aim and Objectives . . . . .	2
1.2 Motivation . . . . .	2
<b>2 Literature Review</b>	4
2.1 Ear Anatomy . . . . .	4
2.1.1 Auricle . . . . .	4
2.1.2 Ear Canal . . . . .	5
2.1.3 Tympanic Membrane . . . . .	6
2.2 Vital Sign Physiology . . . . .	7
2.2.1 Core Temperature . . . . .	7
2.2.2 Heart Rate . . . . .	8
2.2.3 Respiratory Rate . . . . .	9
2.2.4 Blood Oxygen Saturation . . . . .	9
2.3 Vital Signs Measurement Theory . . . . .	10
2.3.1 Core Temperature Measurement . . . . .	10
2.3.2 Commercial Temperature Monitoring Devices . . . . .	14

2.4	Heart Rate . . . . .	14
2.4.1	Electrocardiography . . . . .	15
2.4.2	Photoplethysmography . . . . .	16
2.4.3	Ballistocardiography . . . . .	19
2.4.4	Other Heart Rate Methods . . . . .	20
2.5	Respiratory Rate . . . . .	21
2.5.1	Respiratory Rate Ear Sensors . . . . .	21
2.5.2	Respiratory related Heart Rate Characteristics . . . . .	22
2.6	Blood Oxygen Saturation . . . . .	23
2.6.1	Pulse Oximetry Theory . . . . .	23
2.6.2	Work done by others in ear pulse oximetry . . . . .	26
<b>3</b>	<b>Concept Selection</b>	<b>27</b>
3.1	Temperature . . . . .	27
3.1.1	Temperature measurement method . . . . .	27
3.1.2	Temperature measurement sensor . . . . .	29
3.2	Heart Rate . . . . .	31
3.2.1	Heart rate measurement method . . . . .	31
3.2.2	Heart rate measurement sensor . . . . .	34
3.3	Respiratory Rate . . . . .	36
3.3.1	Respiratory rate measuring method . . . . .	36
3.4	Blood oxygen saturation . . . . .	38
3.5	Final concept . . . . .	38
<b>4</b>	<b>Detailed Design</b>	<b>40</b>
4.1	Hardware . . . . .	40
4.1.1	Temperature sensor . . . . .	40
4.1.2	Pulse Oximeter . . . . .	42
4.1.3	Control and Communication Hardware . . . . .	44
4.2	Software . . . . .	46
4.2.1	Sensor Communication Software . . . . .	47
4.2.2	Temperature related software . . . . .	48
4.2.3	Calculating $T_{OBJ}$ . . . . .	49
4.2.4	PPG signal processing . . . . .	50
4.2.5	Beat Detection . . . . .	53
4.2.6	$SpO_2$ Calculation . . . . .	58
4.2.7	Current Balancing . . . . .	58
4.2.8	Moving average $SpO_2$ . . . . .	60
4.2.9	PC Interface . . . . .	60
<b>5</b>	<b>Trial Period</b>	<b>62</b>
5.1	Participant Selection . . . . .	62
5.2	Benchmark Validation . . . . .	63
5.3	Method . . . . .	64

<b>6 Calibration</b>	<b>67</b>
6.1 Temperature Calibration . . . . .	67
6.1.1 Group Calibration Approach . . . . .	67
6.1.2 Intra-participant calibration approach . . . . .	68
6.2 SpO <sub>2</sub> Calibration . . . . .	68
<b>7 Results and Discussion</b>	<b>70</b>
7.1 Temperature Results . . . . .	71
7.1.1 Group Calibration Results . . . . .	71
7.1.2 Intra-participant Calibration Results . . . . .	72
7.1.3 Temperature Results Discussion . . . . .	73
7.2 Heart Rate Results . . . . .	75
7.2.1 Beat Detection Algorithm Evaluation Results . . . . .	75
7.2.2 Beat Period and Average Heart Rate Results . . . . .	77
7.2.3 Heart Rate Results Discussion . . . . .	79
7.3 Respiratory Rate Results . . . . .	79
7.3.1 Respiratory Rate Discussion . . . . .	81
7.4 SpO <sub>2</sub> Results . . . . .	82
7.4.1 SpO <sub>2</sub> Results Discussion . . . . .	83
7.5 Results Summary . . . . .	84
<b>8 Conclusion</b>	<b>85</b>
8.1 Device development . . . . .	85
8.2 Experimental Trial . . . . .	86
8.3 Data Analysis and Results . . . . .	86
8.3.1 Core Temperature . . . . .	86
8.3.2 Heart Rate . . . . .	86
8.3.3 Respiratory Rate . . . . .	87
8.3.4 SpO <sub>2</sub> . . . . .	87
8.4 Suggestions for Future Work . . . . .	87
8.5 Conclusion . . . . .	88
<b>Appendices</b>	<b>89</b>
<b>A Calculations</b>	<b>90</b>
A.1 Ear-Monitor power supply . . . . .	90
<b>B Data Tables</b>	<b>91</b>
B.1 Temperature Results . . . . .	91
B.2 PhysioNet Beat Detection Results . . . . .	92
B.2.1 Respiratory Rate Results . . . . .	94
B.2.2 Ball mass and inertia parameters . . . . .	94
<b>C Discrete Element Method Theory</b>	<b>96</b>
C.1 Ball elements . . . . .	96

C.1.1 Ball mass and inertia parameters . . . . .	96
<b>List of References</b>	<b>97</b>

# List of Figures

2.1	Anatomical structures of the auricle . . . . .	5
2.2	Structure of the ear (Drake et al: Gray's Anatomy for Students) . . . . .	6
2.3	The results from 20 studies reviewed by Sund-Levander <i>et al.</i> (2002) . . . . .	8
2.4	Dominant radiation wavelength at 37°C using Planck's law . . . . .	13
2.5	Infrared thermometer diagram (Karaki and Polyziev, 2014) . . . . .	13
2.6	CAD model of the Degree from the Cusinuss website (Cosinuss, 2017b) . . . . .	14
2.7	Ear-worn device developed by Winokur <i>et al.</i> (2012) . . . . .	15
2.8	The two modes of Photoplethysmography (Tamura <i>et al.</i> , 2014) . . . . .	16
2.9	Basic operating principles of PPG (Tamura <i>et al.</i> , 2014) . . . . .	17
2.10	Wearable ear PPG device by Poh <i>et al.</i> (2010) . . . . .	18
2.11	Comparing ear PPG to finger PPG and chest ECG (Da He <i>et al.</i> , 2010) . . . . .	19
2.12	Cosinuss One® ear worn heard rate device (Cosinuss, 2017a) . . . . .	19
2.13	Device to measure in ear pulse waves due to the heart beat (Park <i>et al.</i> , 2015) . . . . .	20
2.14	Breathing detected through microphones inside the ear canal (Goverdovsky <i>et al.</i> , 2016) . . . . .	21
2.15	Baseline oscillations in behind the ear BCG due to breathing (Da He <i>et al.</i> , 2010) . . . . .	22
2.16	Absorption spectra of oxy- and deoxyhemoglobin . . . . .	23
2.17	Bragi Dash . . . . .	26
3.1	ST60Micro diagram from the datasheet . . . . .	30
3.2	NJL5501R diagram from the datasheet . . . . .	34
3.3	MAX30100 block diagram from the datasheet . . . . .	35
3.4	Ear-Monitor concept with components labelled . . . . .	39
4.1	Flow of information in a typical telemedicine set-up . . . . .	40
4.2	TMP006 PCB . . . . .	41
4.3	MAX30100 package diagram with required connections for operation. . . . .	43
4.4	(a) is the layout as designed on EAGLE PCB with the outline of the MAX30100 shown in black and (b) is the finished flexible PCB with copper tracks . . . . .	44

4.5	Block diagram of the Ear-Monitor's hardware components . . . . .	45
4.6	Ear probe with TMP006 visible . . . . .	46
4.7	Hardware of the Ear-Monitor . . . . .	46
4.8	Block diagram of the flow of information through the various software functions. Final calculated vital signs are shown in blue . . . . .	47
4.9	How the software reads 16-bit values from the TMP006 registers . .	47
4.10	Plot of the $T_{OBJ}$ equation with recommended calibration parameters over the operating temperature range of the Ear-Monitor . . .	50
4.11	The raw PPG signal, $x_n$ , is sent through AC and DC extraction and filtering functions . . . . .	51
4.12	(a) the raw infrared signal contaminated by DC offset and drift and (b), the extracted AC component of the signal . . . . .	52
4.13	(a) the AC component of the infrared signal before filtering and (b), after filtering . . . . .	53
4.14	Filtered AC component of PPG with important features labelled . .	54
4.15	(a) the AC component of the infrared signal before filtering and (b), after filtering . . . . .	55
4.16	SSF with detected beats and threshold plotted. . . . .	56
4.17	Peak detection example . . . . .	57
4.18	Plots of heartbeat periods and chest expansion. . . . .	58
4.19	Plot showing the effect of the current balancing function implemented on the MAX30100 lowering the difference in detected light between red and infrared LED by adjusting the current to the infrared LED. . . . .	59
4.20	Ear-Monitor user interface . . . . .	61
5.1	Benchmark devices: (a) Nexus-10, (b) SureSigns VM1 and (c) EM 100-A . . . . .	63
5.2	Diagram showing how devices are connected to the participant during the recording session . . . . .	65
5.3	Recording session set-up with participant . . . . .	66
6.1	Temperature errors before and after calibration . . . . .	68
7.1	Temperature through the Group calibration method: ET 100-A vs. Ear-Monitor . . . . .	72
7.2	Temperature through the Intra-participant calibration method: ET 100-A vs. Ear-Monitor . . . . .	73
7.3	Temperature errors of the Group calibration and Intra-participant calibration methods . . . . .	74
7.4	Plots of (a) the Ear-Monitor SSF with detected beats and (b) the Nexus-10 PPG signal with annotated beats . . . . .	76
7.5	Number of beats: Nexus-10 vs. Ear-Monitor . . . . .	77
7.6	Beat period: Nexus-10 vs. Ear-Monitor . . . . .	78

7.7	10-beat average heart rate: Nexus-10 vs. Ear-Monitor . . . . .	78
7.8	Number of breaths detected: Nexus-10 vs. Ear-Monitor (Excluding outliers) . . . . .	81
7.9	SpO <sub>2</sub> : SureSigns VM1 vs. Ear-Monitor . . . . .	83
C.1	Ball Element Parameters . . . . .	96

# List of Tables

2.1	Results of the respiratory rate extraction through neural networks (Johansson, 2003) . . . . .	23
2.2	SpO <sub>2</sub> Accuracy . . . . .	25
3.1	Contact thermometers evaluation . . . . .	28
3.2	Non-contact thermometers evaluation . . . . .	29
3.3	Ear ECG . . . . .	31
3.4	Ear PPG . . . . .	32
3.5	Ear BCG . . . . .	33
3.6	Ear Phonocardiogram . . . . .	33
3.7	Ear Accelerometer . . . . .	36
3.8	Ear Microphone . . . . .	37
3.9	Respiratory related heart rate characteristics . . . . .	37
4.1	T <sub>DIE</sub> example calculation . . . . .	48
4.2	T <sub>DIE</sub> example calculation . . . . .	49
5.1	Demographic summary of participants . . . . .	63
7.1	Mean errors of the respiratory rate measurements . . . . .	80
7.2	Summary of Statistical Results . . . . .	84
B.1	Summary of the temperature results . . . . .	91
B.2	Results of the beat detection algorithm on the PhysioNet data . . .	92
B.3	Results of the beat detection algorithm on the PhysioNet data . . .	93
B.4	Summery of breaths recorded during each recording session . . . . .	94

# Nomenclature

## Constants

$$g = 9.81 \text{ m/s}^2$$

## Variables

$Re_D$	Reynolds number (diameter)	[ ]
$x$	Coordinate	[m]
$\ddot{x}$	Acceleration	[m/s <sup>2</sup> ]
$\theta$	Rotation angle	[rad]
$\tau$	Moment	[N·m]

## Vectors and Tensors

$\vec{v}$  Physical vector, see equation ...

## Subscripts

a	Adiabatic
$a$	Coordinate

# Chapter 1

## Introduction

This thesis reports on a project undertaken in die biomedical field of wearable electronics. Great advances in the miniaturization of electronics and wireless communication have challenged and transformed the norm of how we use electronics to listen to the language of our bodies.

This project revolves around the continuous measurement of vital signs. These signs are objective parameters that give an indication of physical well-being and the state of essential physiological functions. For example, infections are indicated by a rise in core temperature (DerSarkissian, 2016), pneumonia can be detected by a shortness of breath (Mayo Clinic, 2017), an abnormal decrease in blood oxygen saturation during sleep can be a warning sign for sudden infant death syndrome (Thach, 2008) and a rise in heart rate can indicate physical stress (Karriem-Norwood, 2017). These signs can be detected electronically before traditionally observable symptoms appear. In many cases, the deciding factor in the success of a treatment is whether the illness is detected early enough.

Because of this, the importance and usefulness of a continuous, wearable health monitor should not be underestimated. Access to accurate, long term data can lead to improved diagnosis of health issues and a better understanding of how our bodies react to drugs, exercise, emotions and the environment around us. Traditionally, vital sign monitoring is done with a stationary, dedicated device for each signal to be measured. Due to the many large, stationary equipment needed for traditional patient monitoring, it is obvious that this is not suitable for continuous and mobile vital sign monitoring.

This project concerns the design, development and evaluation of a proof of concept device that will overcome the limitations of these traditional methods. The device is to be worn in the ear like an earphone or hearing aid. It will make multi-parameter vital sign measurements and transmit collected data through a wireless connection to a supporting system for storage and analysis. In this project, the supporting system is on a laptop, but it can also be on the smart-phone of the wearer or on a cloud server. This supporting system

can be used by a physician, caretaker or the wearer self, to monitor and track his/her health.

From here onwards, this device is referred to as the *Ear-Monitor*. This report will discuss the project aim and objectives, relevant literature and the design, manufacturing and testing of the Ear-Monitor.

## 1.1 Aim and Objectives

To develop and test a proof of concept wearable device that can monitor vital signs through the external ear and transmit collected data wirelessly to a storage system. Vital signs include core temperature, heart rate, respiratory rate and blood oxygen saturation.

In order to achieve the aim of this project the following three objectives have to be met:

- Develop a device to measure core temperature, heart rate, respiratory rate and blood oxygen saturation through the external ear of the wearer.
- Conduct a trial experiment to test the device on a sample of human participants.
- Use the data collected from the trial to evaluate the accuracy of the measurements made by the device.

## 1.2 Motivation

This project originated from a need found in medical practice and expressed by the proposer/advocate of this topic. It is the need for better vital sign monitoring methods for neonates and infants in hospital nurseries and at home. High-risk patients are placed in ICUs and are thoroughly monitored, whereas lower risk patients are left in the nursery or sent home (Barfield *et al.*, 2012). These patients are poorly monitored while at a fragile age, increasing the risk of health issues. Insufficient health monitoring for neonates and infants is due to the lack of a practical monitoring method. The solution to this issue is the development of an unobtrusive, wearable health monitor.

While contemplating and researching this idea, it was found that a much larger group can benefit from such a device. This lead to the project pivoting toward a more general purpose vital sign monitoring device. This device will prove if it is practical to measure the mentioned vital signs through the external ear canal. If this proof of concept is successful, the methods developed during this project can be used to develop specialized ear-worn devices for various applications. In practice, such a device can transmit health statistics and warnings in real time to a physician or caretaker. Applications include:

- Monitoring neonate- and infant health in nurseries and at home.
- Monitoring health of patients with chronic illnesses.
- Studying the effect of prescription drugs or other treatments.
- Monitoring the health of people working under strenuous conditions like heavy machinery operators and soldiers.
- Tracking the health and fitness of athletes.

The ear was chosen as location for various reasons. Firstly, the anatomy of the ear and the proximity of an ear-worn device to the tympanic membrane, means that all the mentioned vital signs mentioned can theoretically be measured from this location. This eliminates the need for multiple devices or the need for wires connecting sensors on different parts of the body. The absence of sensors on traditional locations such as the chest or limbs and the absence of connective wires mean that the ear-worn device is minimally obstructive for the wearer, especially through freeing up the hands and allowing free movement. Secondly, the shape of the external ear is ideal for supporting a device without the need for straps or adhesives. Furthermore, the head remains relatively still in relation to the rest of the body. This reduces the risk of motion artefacts corrupting the signals of interest. An ear-worn device can be embedded in the already familiar shape of an earphone or hearing aid. The final motivation for using the ear as location for the health monitor is its novelty. As will be apparent from Chapter 2 of this document, there is opportunity for research to be done in the unsaturated field of ear-worn health monitors.

# Chapter 2

## Literature Review

This chapter aims to describe the biological context within which the project is undertaken. An overview of the anatomy of the ear, which is relevant to this study, is given. Thereafter, background is given of the physiology of each of the four vital signs. Finally, the technology relevant to the measurement of each vital sign required of the Ear-Monitor is discussed in terms of theory and the work done by others.

### 2.1 Ear Anatomy

The area that is available for the Ear-Monitor to make the vital sign measurements is the external ear. It includes the auricle, ear canal with surrounding tissue and the lateral side of the tympanum. Each part of the ear anatomy is discussed, especially with regards to its ability to emit information related to vital signs or to support the device in another way.

#### 2.1.1 Auricle

The auricle is the visible part of the ear. It forms a C-shaped funnel that protrudes from the scull. Its structure is predominantly formed by yellow elastic cartilage covered in skin. Its complex folded shape differs from person to person, but certain structures are present in all normal auricles and have been named. As can be seen on Figure 2.1, the concha is the indented part next to the ear canal. This area is an ideal location for a wearable device. The device can be held in place by the tragus and a probe can easily extend into the ear canal.

The external ear is supplied with blood from the auricular arteries. These arteries branch from the carotid artery which supplies the rest of the brain with blood. Being made mostly of cartilage and located at an extremity of the body, the auricle is not a suitable location for taking temperature measurements for its temperature is easily influenced by the ambient conditions.

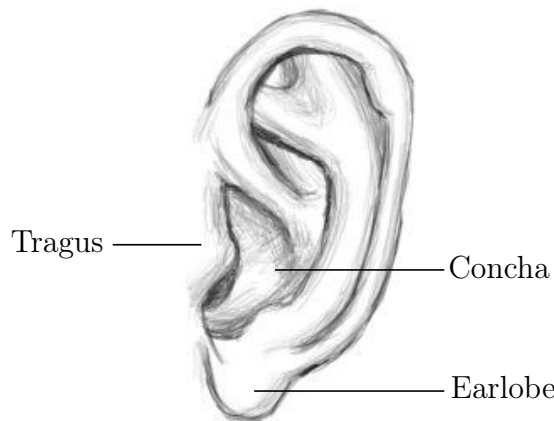


Figure 2.1: Anatomical structures of the auricle

The layer of skin covering the auricle contains blood vessels and therefore the earlobe is a popular location for traditional pulse oximetry measurements. This is a possible location for an ear-worn device to make a heart rate and peripheral blood oxygen saturation ( $\text{SpO}_2$ ) measurement (Poh *et al.*, 2010). The earlobe's blood vessels are, however, susceptible to vasoconstriction due to cold or hypovolaemia (World Health Organization, 2011). This will reduce the blood perfusion of the subcutaneous tissue making it harder to record accurate heart rate and  $\text{SpO}_2$  measurements.

### 2.1.2 Ear Canal

The external ear canal is the tube running from the floor of the auricle to the middle ear, ending blindly at the tympanic membrane or tympanum. Figure 2.2 depicts the structure of the ear as seen from a coronal plane section. The auricle is visible and the shape and relative size of the canal can be observed. The ear canal in adults is approximately 25 mm long and have a diameter of 5 to 7 mm (Alvord and Farmer, 1997). The outer third of the external ear canal is surrounded by cartilage and fibrous tissue (Encyclopædia Britannica, 2015). The inner two thirds is surrounded by the temporal bone. Thin skin forms the lining of the canal and contains glands secreting ear wax. Hairs are found in the outer part of the canal. The ear canal of infants starts out relatively straight, but obtains a definite S-shape as the head develops (Alvord and Farmer, 1997). This S-shape is important to keep in mind when placing a sensor to measure tympanic temperature. Ear canal size also varies from person to person. Therefore, an ear probe should be designed to fit in a variety of ear canal shapes and sizes.

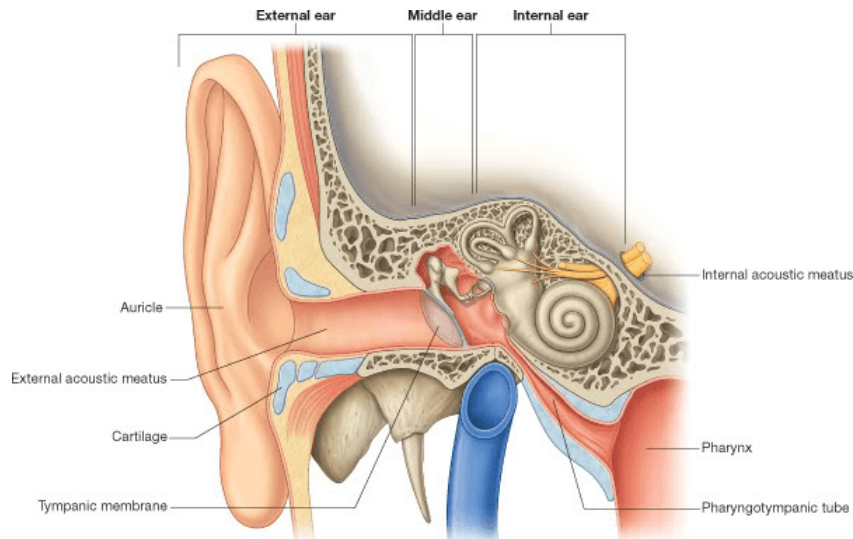


Figure 2.2: Structure of the ear (Drake et al: Gray's Anatomy for Students)

The secluded nature of the ear canal means that it has a relatively constant temperature. Air trapped in the canal by a plug of high thermal resistance will reach thermal equilibrium close to the temperature of the canal wall and tympanum. This is a better location for a core temperature measurement, but will still be influenced by the ambient temperature. The wall of the ear canal is well supplied with blood. Blood vessels just beneath the thin layer of skin make the ear canal a possible location for measuring heart rate and blood oxygen saturation. The still nature of the head will minimize movement artefacts.

### 2.1.3 Tympanic Membrane

The tympanum forms the medial boundary of the external ear canal. It is a smooth elliptical membrane with a thickness of about 0.074 mm (Alvord and Farmer, 1997). The membrane is slanted relative to the external ear canal.

As with the rest of the external ear, the tympanum is supplied with blood from a branch of the carotid artery, therefore sharing its supply with the brain, including the hypothalamus, the thermoregulation centre of the body. It is the most medial part of the external ear, and is therefore the least susceptible to be influenced by the ambient temperature. This is the reason why the tympanum is one of the best locations to measure core body temperature. The location is used by physicians to measure core temperature, for it is quick and minimally invasive (Gasim *et al.*, 2013). Variations in body temperature can be sensed faster on the tympanic membrane than on other locations on the body. Contact with the tympanum can cause discomfort and harm to the patient, so non-contact infrared thermometers are usually used.

## 2.2 Vital Sign Physiology

This section reviews the theory and research done on the physiological aspects of each vital sign that the Ear-Monitor is required to measure. The importance of each of the four vital signs are discussed, including the typical range of measurements expected from healthy adults and the causes and implications of deviations from these measurements.

### 2.2.1 Core Temperature

Thermoregulation is the body's way of keeping its internal temperature within certain limits to create a favourable environment for chemical reactions to take place (Holland, 2016). The temperature control centre of the body is in the hypothalamus and it regulates temperature by maintaining a fine balance between heat production and heat loss. Normal human core temperature varies between 36.5 °C and 37.5 °C (Jones, 2010). Inability to maintain this balance may indicate problems in the well-being of a person. Elevated temperature (hyperthermia) due to a fever can indicate the presence of an infectious disease. Abnormally low temperature (hypothermia) can be caused by exposure to cold, metabolic disorders or infection. Both hyper- and hypothermia can be life threatening. A core temperature measurement is often a key indication to start a treatment or not. Therefore, temperature measurement is part of a full clinical examination.

The location where temperature is measured is a key factor, for temperature is not constant throughout the body. This is because heat production and heat loss are not constant throughout the body, which means extremities are usually cooler than the core. Traditional locations for measuring temperature are the tympanic membrane, axilla, mouth, rectum, oesophagus, forehead and urinary bladder. The mean temperature of these areas varies as well. A systematic literature review done by Sund-Levander *et al.* (2002) combined the results of 20 studies to identify oral, rectal, tympanic and axillary temperature ranges in healthy humans. Figure 2.3 illustrates the results.

Studies have also been done comparing measurements at distinct locations to pulmonary artery temperature in ill patients. One of these found the following standard errors for temperatures at different locations: to ear-based  $0.07 \pm 0.41$  °C; urinary bladder  $0.03 \pm 0.23$  °C; oral  $0.05 \pm 0.26$  °C; and axillary  $-0.68 \pm 0.57$  °C. The accuracy of each method varied with the level of pulmonary artery temperature. Repeated measurements with all four methods had mean standard deviation values within  $\pm 0.2$  °C (Erickson and Kirklin, 1993).

A second study done by Lefrant *et al.* (2003) showed the following standard errors: oesophageal  $0.11 \pm 0.30$  °C, rectal  $-0.07 \pm 0.40$  °C, axillary  $0.27 \pm 0.45$  °C, inguinal  $0.17 \pm 0.4$  °C and urinary bladder  $-0.21 \pm 0.20$  °C.

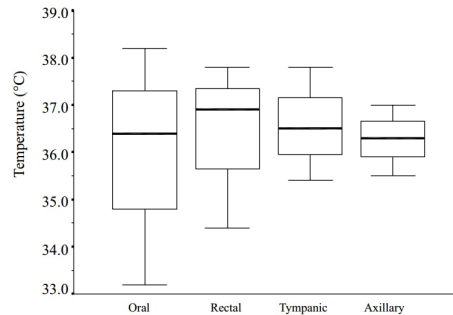


Figure 2.3: The results from 20 studies reviewed by Sund-Levander *et al.* (2002)

The location of the device in development is restricted to the ear, therefore the tympanic membrane is the preferred location for temperature measurements. The referenced studies show that the tympanic membrane is a valid location to measure accurate core temperature.

### 2.2.2 Heart Rate

The presence of a heart beat is paramount to sustain the vital cardiac output, supplying blood to the whole body. Heart rate can be controlled or maintained through two different regulatory systems: The intrinsic conduction system and the nervous system. The intrinsic conduction system works through the rhythmic contraction and relaxation of the heart muscle tissue. The heart rhythm is regulated by the sinoatrial node. The nervous system can influence the heart rate through sympathetic and parasympathetic nerves running from the cardiovascular centre in the medulla oblongata to the heart. The heart beat rate is varied to control the blood flow and blood pressure in the body.

The heart is the source of a group of bio-signals. The firing of nodes and propagation of electrical charges through neurons and the conductive cardiac muscles emit electrical signals that can be detected. The contraction of the ventricles forces blood into the arteries, causing a temporary increase in blood pressure. This pressure increase propagates through the arteries as a wave, causing a temporary local increase in blood volume. Pressure- and volume changes can be detected. Blood turbulence and the opening and closing of heart valves cause the characteristic heart sound and chest movements, both indications of heart rate.

Heart rate is influenced by numerous physiological factors including  $O_2$ ,  $CO_2$ ,  $H^+$  levels, blood pressure, stress and exercise. Pathological factors can include fever, sepsis, heart disease and anaemia. Tachycardia is abnormally high resting heart rate, generally above 100 bpm, whereas bradycardia is a lower than normal resting heart rate, usually below 60 beats per minute (bpm)

(Laskowski, 2015). Although these two conditions are not necessarily danger signs, it may be an indication of health problems and therefore heart rate measurement is part of any medical examination.

### 2.2.3 Respiratory Rate

Respiration is the first step in the chain of events to get oxygen to the body's cells for metabolism to provide the body with energy. Respiration ventilates the lungs with air through inhalation and exhalation. The respiratory rate of a healthy adult at rest is usually between 12 and 20 breaths per minute (Charbek, 2015). This can vary drastically if the body is experiencing physical or emotional stress. An increase in respiratory rate can be caused by a fever, pulmonary dysfunction or any one of numerous medical conditions.

Respiratory rate monitoring is especially useful for diagnosing sleep apnoea. Symptoms include regular pauses in respiration or periods of shallow breathing (hypopnea) during sleep. This causes an oxygen deficiency in the body and lowers the quality of sleep. Short term symptoms include excessive daytime sleepiness, morning headaches, impaired alertness, and vision problems. If left untreated, sleep apnoea can lead to high blood pressure, diabetes, depression, worsening of ADHD, stroke, heart failure, irregular heartbeats, and heart attacks (Blahd, 2016). Sufferers may be unaware of their condition and a sure-fire method of diagnosing it is by monitoring respiratory rate during sleep, traditionally done during an overnight sleep study.

### 2.2.4 Blood Oxygen Saturation

Haemoglobin is the oxygen transporter protein found in red blood cells of blood. Blood gets oxygenated in the lungs and then carries O<sub>2</sub> to the rest of the body for aerobic respiration necessary to produce energy. The correct levels of oxygen in the blood are vital to the health of the individual.

Arterial oxygen saturation, SaO<sub>2</sub>, refers to the concentration fraction of oxygenated haemoglobin to total concentration of haemoglobin in arterial blood. This fraction can be calculated by Equation 2.1.

$$SaO_2 = \frac{C(HbO_2)}{C(HbO_2) + C(Hb)} \quad (2.1)$$

Where C(HbO<sub>2</sub>) is the concentration of deoxygenated haemoglobin (deoxyhaemoglobin) and C(Hb) is the concentration of oxygenated haemoglobin (oxyhaemoglobin).

Blood oxygen saturation of 95-100% is normal in healthy humans. Hypoxaemia is the condition when the saturation is below 90%. This can be an indication of circulatory or ventilatory problems, anaemia or sleep apnoea.

Levels below 80% can impede organ function and can lead to organ failure and cardiac- or respiratory arrest. The brain is extremely susceptible to damage when deprived of oxygen. Cerebral hypoxia is the insufficient supply of oxygen to the brain. This can cause brain damage and in severe cases, brain death.

## 2.3 Vital Signs Measurement Theory

This section will accumulate a thorough understanding of the theory and current state of technology relevant to the measurement of each vital sign required of the Ear-Monitor. Attention is given to the different methods available to determine each vital sign. This section will also make reference to various articles and studies done by other researchers in this field of study. The aim is to gather all the relevant information to make an informed selection of the methods and sensors the Ear-Monitor will use to measure each vital sign.

### 2.3.1 Core Temperature Measurement

Various methods are available for measuring core temperature. Non-electric, fluid-filled thermometers was the first to be used (Pearce, 2002). The mercury-filled thermometer was used by early physicians to study the thermoregulation of the human body and crudely identify fevers. Since then, the mercury has been replaced by coloured alcohol or another heat sensitive liquid, due to toxicity of mercury.

Another type of fluid-filled thermometer is the liquid-crystal thermometer. It contains liquid crystals that change colour at different temperatures. The use of these two types of fluid-filled thermometers has decreased significantly due to the accuracy, speed and convenience of digital thermometers.

Digital thermometers are now the industry standard of measuring core temperature. Central to any digital thermometer lies a transducer that convert temperature to an electrical signal. Resistance temperature detectors, thermocouples thermistor and thermopiles are discussed. They can be divided into contact and non-contact thermometers.

#### 2.3.1.1 Contact Thermometers

These are a family of thermometers that measure their own temperature with the assumption they and the object whose temperature is of interest, are in thermal equilibrium. Therefore, they are usually placed in contact with the object. When using a contact thermometer in the ear, the sensor part of the thermometer can be placed in contact with the ear canal wall, the air inside the canal or with the tympanic membrane itself. Several types of contact thermometers exist, including resistance temperature detectors, thermocouples and thermistors.

### Resistance Temperature Detector

Resistance temperature detectors (RTDs) use the temperature-resistance relationship for metals to measure temperature. Thin wire coils or films of platinum, copper or nickel are usually preferred for they have a stable and repeatable temperature-resistance relationship over a wide temperature range.

### Thermocouple

Thermocouples make use of the thermo-electric effect to make a temperature measurement. They consist of two dissimilar conductors connected at the one end, known as the hot junction (measuring junction). The other ends of the two wires are known as the cold junction (reference junction) and are connected to a voltage meter via common conductors. A voltage is generated dependent on the temperature difference between the measuring- and reference junctions. Thermocouples do not respond to absolute temperature; therefore, their accuracy depends on how well the reference temperature can be defined. Reference temperatures are usually determined by a precise thermistor. Thermocouples are very versatile and widely used in clinical applications, but the downside is that their output signal is low and non-linear, therefore requiring a sensitive and stable voltage measuring device (Jones, 2010).

Thermocouples can be connected in series and are then called thermopiles. This configuration sums the output voltages, resulting in temperature averaging. This method improves accuracy by reducing noise.

### Thermistor

A thermistor is a type of semiconductor whose resistance varies with changes in temperature. They differ from RTDs in that they are usually made of ceramics, they have higher precision over a smaller temperature range and they can have a negative relation to temperature. Thermistors are preferred above RTDs and thermocouples for use as biomedical sensors due to their faster response time and higher sensitivity over a smaller range. The smaller range does not matter, for the temperature range of interest in bio-sensors is small and well defined.

### Contact Thermometer Application

In the case of RTDs and thermistors, the measuring element is placed in position and a current is sent through the sensor. By measuring the voltage across the resistive element, it is possible to calculate the voltage and subsequently determine the temperature. In the case of a thermocouple, the hot junction can be placed in contact with the canal wall or tympanum. Typically, the hot junction is enclosed in a soft material to protect the canal and tympanum. The canal is sealed off and time is allowed for the area to equilibrate to tympanic temperature.

Placing a thermometer in contact with the tympanic membrane gives an accurate measurement, but can cause discomfort to the wearer. There is also a risk of harming the tympanic membrane. Sensors in contact with the ear canal wall or the air inside the canal run the risk of making errors by measuring the temperature of objects that are not in thermal equilibrium with the tympanic membrane. Therefore, non-contact thermometers are considered.

### 2.3.1.2 Non-contact Thermometers

Thermopiles can be used to detect thermal radiation without being in contact with the object. All matter with temperatures above 0 K radiates electromagnetic radiation according to the Stefan-Boltzmann law. The thermal radiation,  $Q$ , per unit area is given by Equation 2.2.

$$Q = \varepsilon\sigma T^4 \quad (2.2)$$

Where  $\varepsilon$  is the emissivity,  $\sigma$  the Stefan-Boltzmann constant and  $T$  the temperature of the object. The wavelength distribution varies according to the temperature of the object and is described by Planck's law, given by Equation 2.3.

$$B_\lambda(\lambda, T) = \frac{2hc^2}{\lambda^5} \frac{1}{e^{\frac{hc}{\lambda k_B T}} - 1} \quad (2.3)$$

Where  $B_\lambda$  is the spectral radiance,  $\lambda$  the radiation wavelength,  $h$  Planck's constant,  $k_B$  Boltzmann's constant  $c$  the speed of light and  $T$  the temperature of the object. By maximizing  $B_\lambda$ , it is possible to find the dominant wavelength that is emitted at a certain temperature. Figure 2.4 depicts a plot made of spectral radiance versus wavelength at  $T = 37^\circ\text{C}$ , the core temperature of humans. It is evident that the dominant wavelength is at  $9.35\text{ }\mu\text{m}$ . This is in the infrared range, and therefore this type of thermal radiation thermometer is called an infrared thermometer.

In the case of measuring the temperature of the tympanic membrane, the temperature of the hot junction is determined by the radiation received from the tympanum minus the radiation radiated by the sensor itself.

When dealing with thermal radiation, an important aspect is emissivity. Emissivity is the ability of an object to radiate thermal energy. It is quantified as a ratio of thermal energy emitted by a surface relative to the thermal energy emitted by an ideal blackbody at the same temperature. A blackbody has an idealized surface that reflects no radiation, which means all energy radiated from the surface is due to the temperature of the surface. Thus, a blackbody has an emissivity of 1 and has the maximum theoretical thermal radiation at a given temperature. The accuracy of an infrared sensor depends on the ability of the object to emit sufficient thermal radiation for the sensor to detect.

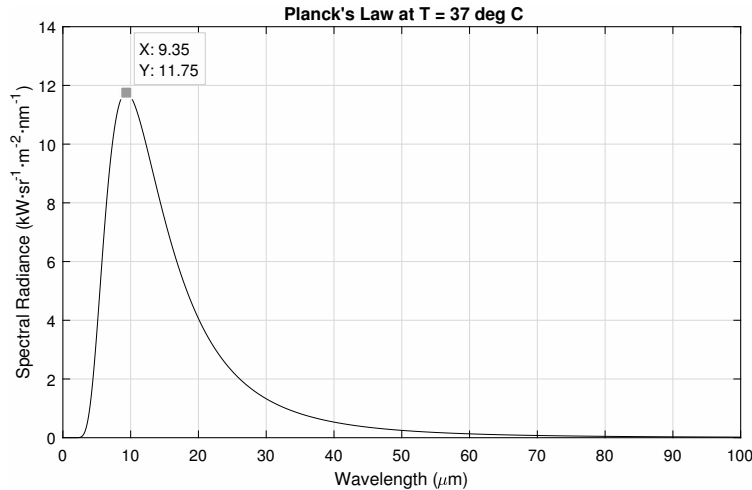


Figure 2.4: Dominant radiation wavelength at 37 °C using Planck's law

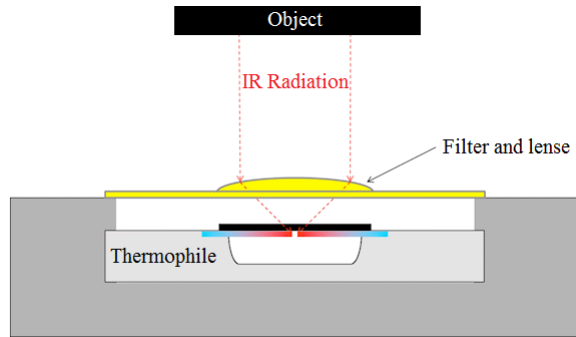


Figure 2.5: Infrared thermometer diagram (Karaki and Polyziev, 2014)

Cross-referencing various emissivity tables, it was found that the emissivity of human skin is 0.98, which means that it is an excellent emitter of thermal energy (Stumme *et al.*, 2003; ThermoWorks; Optotherm, 2017). The ear drum is covered with skin, making it an ideal target object for a non-contact thermometer.

An infrared thermometer generally consists of a thermophile attached to a blackbody and shielded by an infrared filter that also acts as a lens to focus infrared waves (Karaki and Polyziev, 2014). This setup, depicted in Figure 2.5, allows for the non-contact temperature sensing of the tympanic membrane. Unlike pulse and respiratory rates, core body temperature varies slowly. It takes minutes to vary significantly. Therefore, the sampling period of core temperature can be as long as 10 seconds.

### 2.3.2 Commercial Temperature Monitoring Devices

Ear thermometers are widely used at home and in hospitals. Ear contact thermometers like Novatemp® and Starboard® claim a  $\pm 0.2^\circ\text{C}$  accuracy (Novatemp, 2011; Starboard, 2016). Non-contact infrared ear thermometers usually have a similar rated accuracy. None of these are, however, wearable devices.

The Degree®, Figure 2.6, is a continuous in-ear thermometer for children, developed by Cosinuss, a company specialising in wearable sensors. The bulk of the device is worn behind the ear, and a wire runs over the auricle to the ear canal, in which a probe is placed. The device takes its temperature measurements with a sensor placed in contact with the canal wall. The manufacturer claims an accuracy of  $\pm 0.1^\circ\text{C}$  (Cosinuss, 2017b). It monitors temperature continuously and sends real time data to a mobile phone.

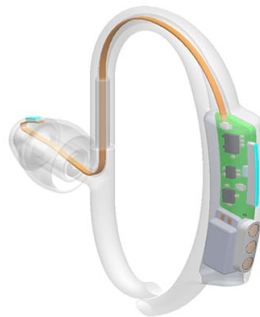


Figure 2.6: CAD model of the Degree from the Cusinuss website (Cosinuss, 2017b)

Apart from the Degree, there is not much literature on wearable ear thermometers. Two patents were found describing similar devices: US 6556852 B1 and US 20090221888 A1. The first proposes the use of an infrared sensor pointed at the tympanic membrane, and the latter does not specify the method of measuring. The trial planned as part of this project will add to this insufficient body of knowledge.

## 2.4 Heart Rate

There are many options available to monitor heart rate. Electronic monitoring methods include electrocardiography, photoplethysmography, ballistocardiography, phonocardiography and doppler flow-meters.

### 2.4.1 Electrocardiography

Electrocardiography (ECG) is a recording of the electrical activity of the heart over a period of time. Electrical activity arises from the depolarization and repolarization of the heart muscle during the cardiac cycle. The most prominent electrical charge is the QRS complex, which corresponds to the ventricular depolarization and is visible on the electrocardiogram as a sharp peak in the millivolt range. ECG is the recommended way of monitoring heart rate in most intensive care units. A cardiologist will use a 12 lead ECG with 10 electrodes placed in a specific configuration on the chest. Various wearable devices use ECG to measure heart rate. Fitness monitors normally use a chest strap with electrodes to detect the electrical activity of the heart.

Studies have been done developing wearable ECG devices for clinical use. The latest in wearable ECG electrodes is the use of dry polymer-based materials (Wang *et al.*, 2010) or non-contact electrodes that can be placed on top of clothing (Lin *et al.*, 2013). This is an improvement on the standard conductive gels or adhesives and can be used repeatedly. But these electrodes still need to be placed on the chest.

An ear located ECG monitor has been developed by Winokur *et al.* (2012). This device uses a single lead setup with one electrode placed on the mastoid bone behind the ear and a reference electrode placed on the neck. This configuration relies on the conductive properties of human tissue to carry electrical charges from the heart to the ear. They were able to use the electrocardiogram in conjunction with PPG and BCG to determine various heart intervals and track changes in mean arterial blood pressure. Figure 2.7 depicts Winokur *et al.* (2012)'s device and a plot of its electrocardiogram. No heart rate information was extracted.

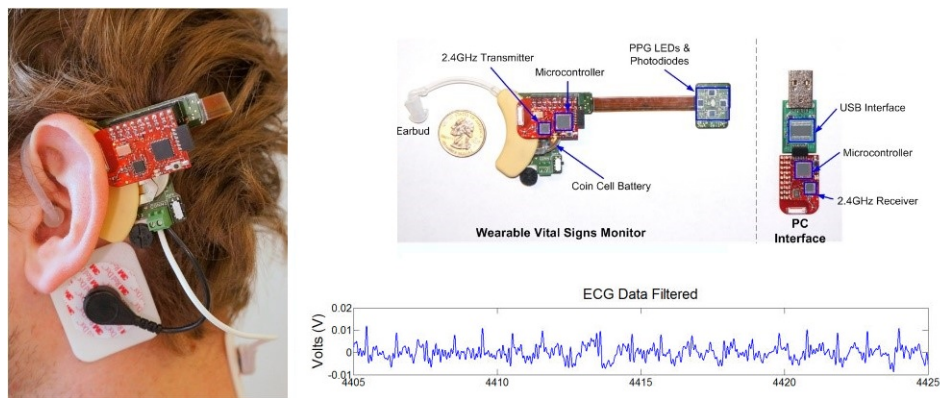


Figure 2.7: Ear-worn device developed by Winokur *et al.* (2012)

### 2.4.2 Photoplethysmography

Photoplethysmography (PPG) produces an optically obtained plethysmogram, which plots the volume of an organ over time. PPG can be used to measure the change in the volume of blood vessels close to the skin surface. When the left ventricle contracts a pressure pulse propagates through the arteries from the heart to the extremities of the body. This wave corresponds to the systolic blood pressure. Blood vessel walls contain elastic fibres that allow it to stretch. This means that the diameter of vessels will increase when the blood pressure increases, causing arteries to stretch and contract with each cardiac cycle. PPG can be used to determine heart rate by measuring this volumetric variation.

A photoplethysmograph can non-invasively determine peripheral arterial blood volume by shining light through the skin surface, into the dermis and subcutaneous tissue and collecting the light transmitted or reflected. Light shined into the tissue can either be reflected, absorbed or allowed to transmit through. This leads to the two modes of PPG operation depicted by Figure 2.8.

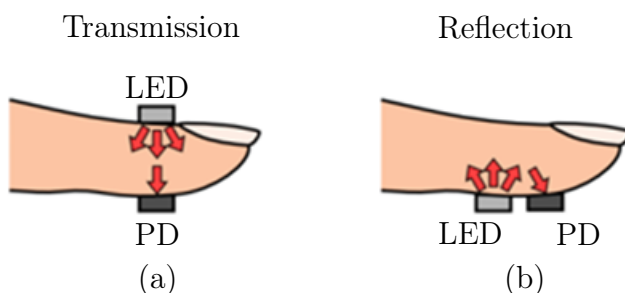


Figure 2.8: The two modes of Photoplethysmography (Tamura *et al.*, 2014)

In (a) the emitter and detector face each other and are separated by tissue that can transmit the light, leading to a transmission mode PPG. Transmission mode PPG is limited to locations on the body where transmitted light can be detected, like the finger, ear lobe, concha and tragus. These locations have limited blood profusion, especially at low temperatures. In (b) the emitter and detector are placed on the same plane and both faces towards the tissue. Light from the emitter is reflected by the tissue and captured by the detector, leading the reflection mode PPG. The emitter and detector need to be optically isolated so that light cannot pass from the one to the other without going through the tissue. Reflectance mode PPG can be used at more locations, but is more susceptible to motion artefacts (Tamura *et al.*, 2014).

According to Lambert's law, the amount of light absorbed is proportional to the length of the path that the light has to travel in the absorbing substance (Encyclopædia Britannica, 2009). Therefore, a change in blood vessel diameter

will increase the distance the light has to travel causing a change in light absorption. This can be detected by measuring reflected or transmitted light. Variation in the light reflected or transmitted is synchronised with the heart rate.

Shorter light wavelengths are mostly absorbed by the tissue, while longer wavelengths can penetrate deeper. Red and near infrared light are preferred for transmission PPG. Green light is becoming more popular for shallow reflectance PPG, due to larger light variations during the cardiac cycle and less noise than near infrared PPG (Tamura *et al.*, 2014).

The signal read by the photo detector of the pulse oximeter consists of an AC component superimposed on a DC signal. The DC component is due to the constant transmission or reflection of light by the body's tissue: skin, fat, venous blood and the non-pulsating arterial blood. The AC component is the variation in transmitted or reflected light due to the change in diameter of the arteries and therefore synchronised to the heart rate. The AC component is usually between 0.5 - 2% of the DC component (Tavakoli Dastjerdi, 2006). Figure 2.9 illustrates the way in which the heart rate is visible in a photoplethysmograph. It can be seen that the blood volume increases with each heartbeat, and that this causes more light to be absorbed, thus less detected by the photodiode.

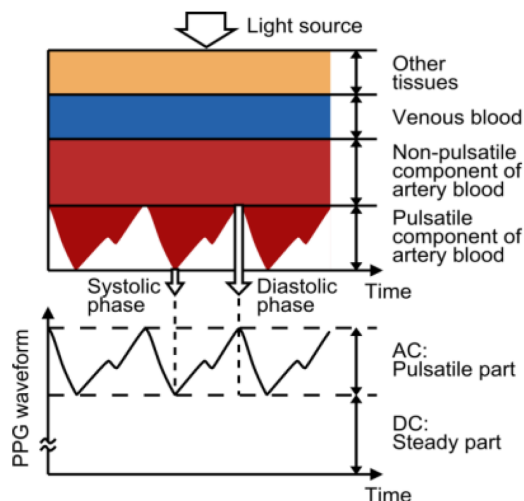


Figure 2.9: Basic operating principles of PPG (Tamura *et al.*, 2014)

#### 2.4.2.1 Work done by others in Ear PPG

A review of work done by others in the field of ear PPG reveals six devices relevant to this study.

Shin *et al.* (2009) present a wearable music headset with an integrated transmission PPG ear clip that attaches to the ear lobe. The device includes an accelerometer to aid in the removal of motion artefacts. Evaluation was done through a study comparing the heart rate from the device to that made with a conventional ECG recorder. This study revealed a heart rate error of 0.6%.

Poh *et al.* (2010) designed a wearable PPG with a magnetic earring sensor. The bulk of device sits in front of the ear and is held in place by a band around the auricle, as can be seen from Figure 2.10. A reflective PPG sensor is held against the ear lobe by placing a magnet on the opposite side. The device also includes an accelerometer to make baseline measurements for motion artefact cancellation. A study was conducted to compare the PPG signals measured by the wearable device to chest ECG signals collected by a FDA-approved commercial system. Whilst standing motionless, the study found a very high correlation between the ear PPG and the chest ECG with a mean bias of  $0.62 \pm 4.51\%$  with ECG reference measurements.

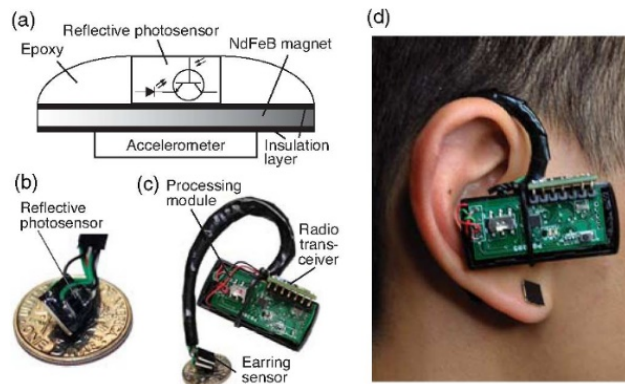


Figure 2.10: Wearable ear PPG device by Poh *et al.* (2010)

Da He *et al.* (2010) researched an ear worn heart rate monitor containing a PPG sensor in reflectance mode. Red light is shined into the tissue behind the ear and collected by a photodiode chip with an integrated transimpedance amplifier. Signals were not digitalised on the device, but recorded and processed on MATLAB. The collected signal was compared with a transition finger PPG and a chest ECG. Figure 2.11 illustrates this comparison.

Winokur *et al.* (2012) developed a similar device that shines 660nm and 940nm light waves through tissue at the mastoid bone and collecting the reflected light with 4 photodetectors. A PPG front end conditioned the signals and their device sent the raw heart beat information to a PC through a radio connection. This is the same device that records ECG and is used to analyse heart intervals and mean blood pressure rather than heart rate.

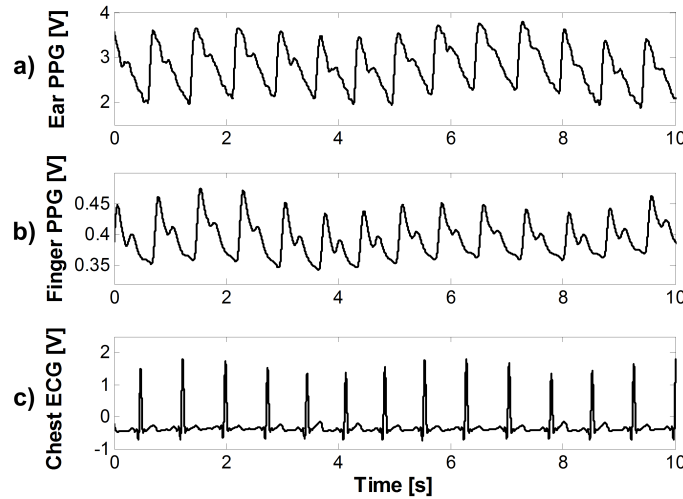


Figure 2.11: Comparing ear PPG to finger PPG and chest ECG (Da He *et al.*, 2010)

Buske *et al.* (2009) proposed yet another location. They modified a pair of headphones to measure a transmission PPG from the concha. During the testing phase, the device showed a mean heart rate accuracy of around 85% when compared to an ECG.

The Cosinuss One<sup>®</sup> is a commercial device that monitors heart rate through the ear canal. The earpiece presses against the ear canal wall and records a PPG in reflection mode. It targets athletes that want to monitor their bodies during exercise.



Figure 2.12: Cosinuss One<sup>®</sup> ear worn heard rate device (Cosinuss, 2017a)

### 2.4.3 Ballistocardiography

Ballistocardiography (BCG) is the measurement of the mechanical effects of the beating heart on the body over time. Typically, accelerometers or pressure

sensors are used to measure movement or forces on the surface of the body. BCG has been researched for use in ear heart rate extraction.

In a wearable device proposed by Da He *et al.* (2010), mechanical vibrations associated with heart rate are converted to electronic signals through capacitive sensing electrodes placed behind the ear. This method works by measuring the change in capacitance between the two electrodes as the distance between them changes due to heart rate vibrations.

A study by Winokur *et al.* (2012) proposed measuring the head-to-foot axis recoil due to the blood-volume shift during cardiac ejection. This is done by placing a MEMS accelerometer behind the auricle. Due to the movement dependent method of operation this technology is extremely susceptible to motion artefacts and it can only be used when the body is stationary.

A variation of this technology is discussed in an article by Park *et al.* (2015). They propose using a scissor shaped hinge mechanism in the ear canal that measures the change in the canal size due to the in-ear blood pulse waves. The mechanical movement is converted to an electrical signal through a piezoelectric film sensor. Figure 2.13 shows a drawing of this device from Park's 2015 article.

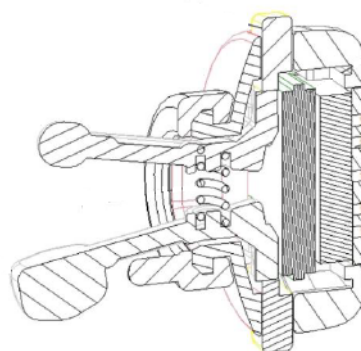


Figure 2.13: Device to measure in ear pulse waves due to the heart beat  
(Park *et al.*, 2015)

#### 2.4.4 Other Heart Rate Methods

Electronic stethoscopes use a microphone to record heart sounds. The heart makes a distinct series of sounds during the cardiac cycle due to blood turbulence and the shutting of heart valves. A plot of the heart sounds is known as a phonocardiogram. The period of this sound series can be used to determine heart rate and it does not require skin-contact.

A Doppler flow-meter can be used to detect the alternating blood current component in near-surface arteries. This component is synchronised to the

heart rate frequency. The device can use ultrasound or electromagnetic waves to achieve the Doppler shift.

A study done at Stanfort Medicine by Shcherbina *et al.* (2017) reviewed seven commercially available wearable (wristband) heart rate monitors. They found mean errors ranging from 2.5 to 8.8%.

## 2.5 Respiratory Rate

Unlike the other vital signs, a person cannot measure his or her own respiratory rate. As soon as a person is consciously thinking about respiration, breathing usually slows. Measuring needs to happen while the person's thoughts are otherwise occupied. Therefore, a continuous measuring method is preferred. Typically, a nasal mask or chest strap is used to measure respiration.

### 2.5.1 Respiratory Rate Ear Sensors

Ear located devices that extract respiration information are rare, but some literature sources are available.

Goverdovsky *et al.* (2016) tested an ear probe with two embedded microphones. The microphones could detect the sound created by turbulence in the airways for breathing rates higher than 12 breaths per minute. Figure 2.14 shows a plot of the normalised sound amplitude at two different breathing rates. Variation during breathing can be seen in both recordings.

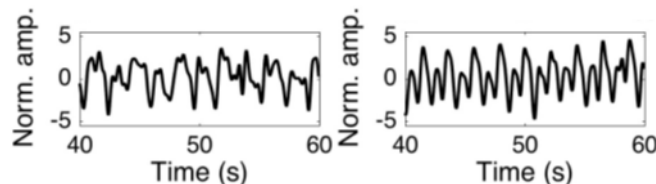


Figure 2.14: Breathing detected through microphones inside the ear canal  
(Goverdovsky *et al.*, 2016)

Da He *et al.* (2010) did extensive research on the ear as a location for vital sign monitoring. They extracted respiratory rate from baseline oscillations in a BCG signal recorded by capacitive electrodes placed behind the ear. Mechanical movement is converted to electrical signals by these electrodes. Therefore, the movement of the head due to respiration is seen on the BCG as baseline oscillations, Figure 2.15.

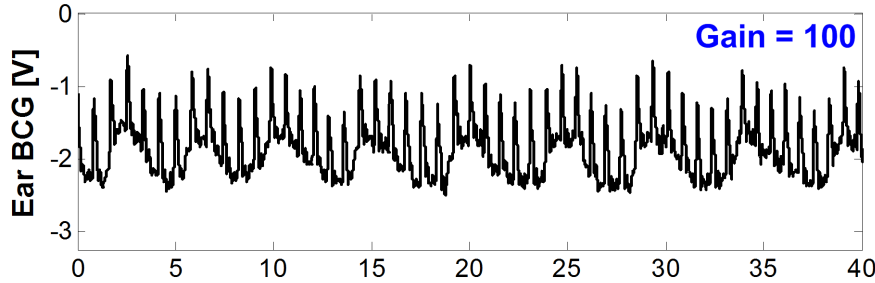


Figure 2.15: Baseline oscillations in behind the ear BCG due to breathing  
(Da He *et al.*, 2010)

### 2.5.2 Respiratory related Heart Rate Characteristics

A different approach is to extract respiratory rate by analysing the heart rate. A PPG signal contains three distinct respiratory related characteristics: amplitude modulation (AM), respiratory-induced intensity variation (RIIV) and frequency modulation (Johansson, 2003).

Amplitude modulation is due to blood pressure changes during the respiratory cycle called Pulsus Paradoxus. RIIV is changes in the volume of the dermis and subcutaneous capillary bed. It is visible as baseline variation in the PPG signal. Frequency modulation of the heart rate synchronised to respiration rate, called respiratory sinus arrhythmia (RSA).

RSA can also be detected in ECG, but differs from the fluctuations seen in chest ECG, due to electrodes movement relative to the heart and changes in chest impedance during the respiratory cycle (Moody *et al.*, 1986). These fluctuations cannot be detected in the ear. RSA is observed as baseline oscillation in heart rate in synchrony with the respiratory rate. Heart rate increases during inspiration and decreases during expiration (Yasuma and Hayano, 2004). According to a study done by Stratton *et al.* (2003), the variation in heart rate due to RSA is higher in younger test subjects, with a 74% increase in children versus a 52% increase in adults.

Research has been done to develop algorithms to utilise these characteristics to extract respiratory rate from PPG signals. Clifton *et al.* (2007) used wavelet analysis and achieved a respiratory rate accurate to within 1 breath per minute and Leonard *et al.* (2006) documented a respiratory rate error of 7.9%. Johansson (2003) developed two neural network algorithms that use the different respiratory related characteristics of PPG signals to detect breaths. Table 2.1 shows the results of the best algorithm.

Table 2.1: Results of the respiratory rate extraction through neural networks  
(Johansson, 2003)

Respiratory Related Characteristics	False Positive (%)	False Negative (%)
RSA	3.7	6.9
AM	5.2	4.7
RIIV	5.2	5.9

## 2.6 Blood Oxygen Saturation

Oxygen saturation can be measured by means of an arterial blood gas test resulting in an arterial oxygen saturation reading. This requires drawing a blood sample for testing and therefore is not relevant to this study. An alternative method is pulse oximetry. This method estimates peripheral capillary oxygen saturation,  $\text{SpO}_2$ , through the spectrophotometric analysis of PPG signals captured at two different wavelengths. This is a clinically accepted estimation of the arterial oxygen saturation (Aoyagi, 2003).

### 2.6.1 Pulse Oximetry Theory

Blood oxygen saturation estimation through pulse oximetry relies on the different adsorption spectra of oxyhaemoglobin and deoxyhaemoglobin. Figure 2.16 shows the absorption spectra of oxy- and deoxyhaemoglobin.

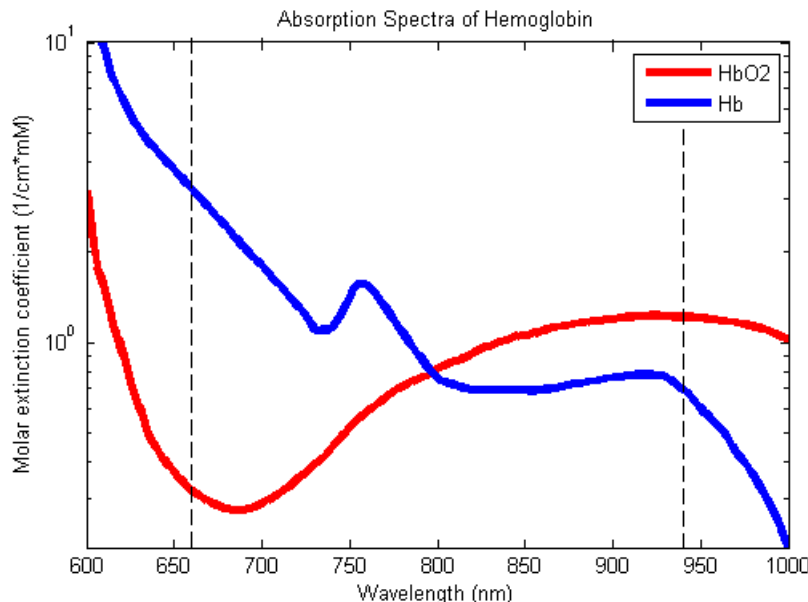


Figure 2.16: Absorption spectra of oxy- and deoxyhemoglobin

It can be noted that deoxyhaemoglobin has a significantly higher absorption of red light while oxyhaemoglobin has a slightly higher absorption of infrared light.

According to Beers law, the amount of light absorbed by a dissolved substance is proportional to its concentration (Encyclopædia Britannica, 2009). Therefore, oxygenated blood (with a higher concentration of oxyhaemoglobin) will absorb more infrared light and reflect more red light. Whereas deoxygenated blood (with a higher concentration of deoxyhaemoglobin) will absorb more red light and reflect more infrared light. This explains why oxygenated blood appears bright red, while deoxygenated blood is a darker shade of red.

Red and infrared light are shined into the peripheral tissue and the light reflected or transmitted is measured for both wavelengths. Literature and commercial devices usually use wavelengths of 660 nm (red) and 940 nm (near infrared) (Tytler and Seeley, 1986; Chan and Underwood, 2005; Bagha and Shaw, 2011; Bheema lingaiah *et al.*, 2013; Duun *et al.*, 2007). The ratio of reflected or transmitted light is unique to a certain level of blood oxygen saturation and is used to estimate blood oxygen saturation.

The Beer-Lambert law describes the absorption of a specific wavelength of light by a substance in a homogeneous solution (Bagha and Shaw, 2011). It can be used to calculate light intensity as shown by Equation 2.5 or it can be manipulated to give what is called the unscattered absorption factor as shown in Equation 2.4 (Kennedy, 2015).

$$I = I_o e^{-\varepsilon \lambda c L} \quad (2.4)$$

$$A = \varepsilon c L = \ln \left( \frac{I_o}{I} \right) \quad (2.5)$$

$A$  is the dimensionless adsorption factor,  $\varepsilon$  is the wavelength dependant molar absorptivity,  $c$  is the concentration of the substance and  $L$  is the path length the light needs to travel through the substance.  $I_o$  is the intensity of the light entering the solution and  $I$  is the intensity of light passing though the solution.

Equation 2.4 can be used to calculate the concentration of oxyhaemoglobin in the blood of the peripheral tissue, provided that the absorptivity and path length of all materials inside the tissue is known. This is not practical, for the thickness and absorptivity of skin and subcutaneous tissue varies between individuals. Furthermore, this equation is also not valid when taking into account the reflection of light, which is fundamental when the application requires reflection mode pulse oximetry.

To solve this problem, a modulated relationship, seen in Equation 2.6, is used that compensate for the different DC absorption between patients (König

*et al.*, 1998; Duun *et al.*, 2007; Bheema lingaiah *et al.*, 2013; Bagha and Shaw, 2011; Nitzan *et al.*, 2014; Oak and Aroul, 2015).

$$R = \frac{\left(\frac{AC}{DC}\right)_{\text{red}}}{\left(\frac{AC}{DC}\right)_{\text{IR}}} \quad (2.6)$$

Where  $R$  is the  $\text{SpO}_2$  modulation ratio. This ensures that the  $\text{O}_2$  saturation of only the arterial blood is calculated. The ration can be checked against an empirical determined curve. The standard formula for this curve is found in literature as  $\% \text{ SpO}_2 = 110 - 25R$ , (Oak and Aroul, 2015) but it can vary from device to device.

As mentioned,  $\text{O}_2$  can be calculated using reflected or transmitted light. Light that is not absorbed or scattered by tissue can be either reflected, or transmitted. Thus, both reflected and transmitted light is proportional to the mount of light absorbed. Transmittance mode pulse oximeters are more common, but their use is restricted to parts of the body that allow light to pass through, like a fingertip or earlobe.

Pulse oximetry is clinically accepted and currently the most accurate way to monitor  $\text{O}_2$  saturation non-invasively (Aoyagi, 2003; DeMeulenaere, 2007; Chan *et al.*, 2013; Lee *et al.*, 2016). This being said, note should be taken of the limitations of this method. Pulse oximeters measures  $\text{O}_2$  saturation indirectly by analysing differences in light absorption, rather than directly measuring oxygen concentration in the blood as is done during a blood gas test. This allows ease of use and non-invasive measurement abilities, but sacrifices some accuracy. Various studies have been conducted to quantify the accuracy of the pulse oximeter. Table 2.2 sums up some of these studies.

Table 2.2:  $\text{SpO}_2$  Accuracy

Accuracy	Source
$\pm 2\%$	Fahy <i>et al.</i> (2011)
$\pm 2.1\%$	Louw <i>et al.</i> (2001)
$\pm 3\%$	Sinex (1999)
$\pm 4\%$	DeMeulenaere (2007)

The results differ in their exact quantities, but there is no doubt about a uncertainty factor of at least  $\pm 2\%$  that should be kept in mind when taking measurements with an pulse oximeter, especially during the trial period of this project.

## 2.6.2 Work done by others in ear pulse oximetry

Standard locations for pulse oximetry include the fingertip, earlobe, ankle and forehead. A study comparing fingertip and earlobe pulse oximetry to an arterial blood gas test found that finger pulse oximetry differed by a mean of -0,71% and earlobe pulse oximetry differed by a mean of +4.2% (Olive *et al.*, 2016). Literature and commercial wearable pulse oximeters typically utilise a finger clip to measure SpO<sub>2</sub> (Watthanawisuth *et al.*, 2010; Pujary *et al.*, 2003; Huang *et al.*, 2014; Khalifa *et al.*, 2014). This location is not ideal for continuous monitoring and is especially susceptible to motion artefacts. Although the fingertip location is not of interest to this study, the literature is still reviewed for similar principals can be applied to ear pulse oximetry.

Ear lobe pulse oximetry is usually done through a sensor that clips to the ear lobe, and is attached to a stationary device. Wearable ear pulse oximetry is still novel and not well covered in literature. There are some patents filed for wearable ear SpO<sub>2</sub> devices (US 20050177034 A1, US 4086915 A, US 3412729 A and US 6556852 B1) and the Bragi Dash (Bragi, 2017), as can be seen in Figure 2.17, is one of the first commercial devices to claim this ability. However, little academic material is available.



Figure 2.17: Bragi Dash

A study done by (Aziz *et al.*, 2006) tested a wireless earlobe-mounted pulse oximeter on a group of subjects. Subjects were tested while sitting, walking and running. During the sitting and walking phases they recorded an SpO<sub>2</sub> reading of above 95%, which is “as expected” according to them. But during the running phase they could not obtain any accurate reading.

# Chapter 3

## Concept Selection

This chapter builds on the knowledge gained in the literature review and explains the logic used to select the methods and sensors to realize each vital sign monitoring requirement of the Ear-Monitor. Selections are made by analysing advantages and disadvantages of each option and combining it with sound engineering judgement.

### 3.1 Temperature

The Ear-Monitor measures core temperature from the inside of the ear canal. The main criteria are sensor size and measurement accuracy. The method- and sensor selection are discussed separately.

#### 3.1.1 Temperature measurement method

Two temperature measuring methods are considered, namely contact- and non-contact thermometers.

##### 3.1.1.1 Contact thermometers

A contact RTD, thermocouple or thermistor is placed in contact with the canal wall, canal air or tympanic membrane. Table 3.1 summarises the evaluation.

Table 3.1: Contact thermometers evaluation

 <b>IMAGE</b>	<p><b>Advantages</b></p> <ul style="list-style-type: none"> <li>• Available in small sizes, ideal for the size restrictions of the ear canal.</li> <li>• Good accuracy.</li> <li>• Converting transducer voltage to temperature is simpler than with non-contact thermometers.</li> </ul>
<p>Sensor size: <math>0.5 \times 2.3</math> mm Measurement accuracy: <math>0.15^\circ\text{C}</math></p>	<p><b>Disadvantages</b></p> <ul style="list-style-type: none"> <li>• Canal wall and canal air temperature measurements can easily be influenced by ambient temperature conditions.</li> <li>• Tympanic membrane contact can cause discomfort and harm to the wearer.</li> <li>• More time is needed to take measurements, for the sensor needs to be in thermal equilibrium with the object.</li> </ul>

### 3.1.1.2 Non-contact Thermometers

A non-contact, infrared sensor is placed inside the ear canal and pointed at the tympanic membrane. Table 3.2 summarises the evaluation.

Table 3.2: Non-contact thermometers evaluation

IMAGE	<b>Advantages</b>
Sensor size: 1.6 - 4 mm $\varnothing$ Measurement accuracy: 0.2-0.5 °C	<p><b>Advantages</b></p> <ul style="list-style-type: none"> <li>The sensor can measure the temperature of the tympanic membrane directly, which is the best representation of core temperature in the ear.</li> <li>Temperature conversion compensates for different ambient temperature conditions.</li> <li>No contact with the tympanic membrane significantly lowers the injury risk to the user.</li> </ul> <p><b>Disadvantages</b></p> <ul style="list-style-type: none"> <li>Non-contact temperature sensors are typically bigger than contact thermometers, adding to the size limitation challenge.</li> <li>If the tympanic membrane does not fill a considerable fraction of the sensor's field of view, erroneous measurements can occur.</li> </ul>

### 3.1.1.3 Temperature measurement method choice

A non-contact, infrared sensor is selected for the Ear-Monitor. User safety, without significant performance compromise gives it superiority over contact thermometers for this application. The lower accuracy is justified by the fact that the tympanic membrane is a better representation of the core body temperature.

## 3.1.2 Temperature measurement sensor

To realize non-contact temperature measurement, two infrared sensors are considered: The ST60 Micro from Dexter Research Center Inc and the TMP006 from Texas Instruments.

### 3.1.2.1 ST60 Micro

The ST60 Micro is a one channel, 80-junction, completely analogue temperature sensing device. It is enclosed in a Micro-TO package which is 4.09 mm in diameter as shown in Figure 3.1. The manufacturer emphasizes the ST60

Micro's versatility and proposes use in tympanic ear thermometers. A die temperature thermistor is available for ambient temperature compensation. Four wires are used to supply the sensor with power and to read transduced voltages.

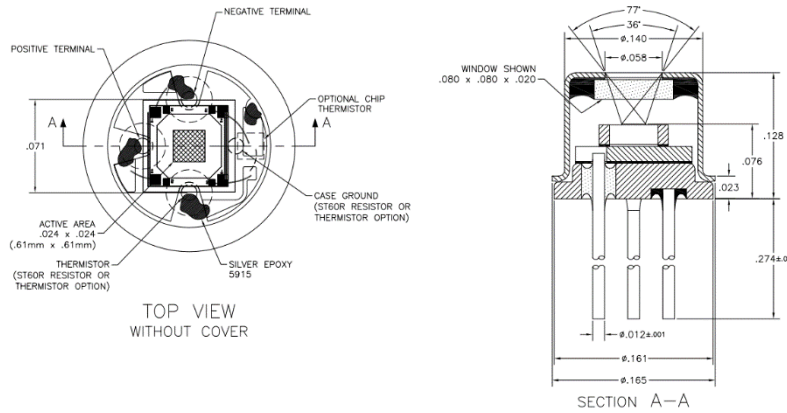


Figure 3.1: ST60Micro diagram from the datasheet

### 3.1.2.2 TMP006

The TMP006 is a fully integrated infrared sensor measuring only  $1.6 \times 1.6 \times 0.8$  mm, ideally suited for a narrow ear canal. Thermophile voltage and sensor temperature are made digitally available through hardware registers. These two values can be used to calculate the object temperature. Registers are accessed by a MCU though I<sup>2</sup>C communication. Values are digitalized by a 16-bit on-chip ADC, eliminating the need for supporting analogue filters and amplifiers. The user guide of the TMP006 suggests that it be used to calculate the surface temperature of target objects with emissivity values greater than 0.7, and preferably greater than 0.9. The literature study revealed that the emissivity of the eardrum is 0.98, placing it well within the required range.

### 3.1.2.3 Temperature measurement sensor choice

The simple shape of the ST60 Micro makes it easy to mount, but the diameter of the package may not fit in smaller ear canals and leave little room for the other sensors. Therefore, the ST60 Micro is eliminated.

The smaller package size and on-chip ADC justify the selection of the TMP006 for use in the Ear-Monitor. The TMP006 needs no separate analogue filter and amplifier. Furthermore, the manufacturer supplies detailed calibration documentation, allowing for more accurate and time effective calibration.

## 3.2 Heart Rate

The Ear-Monitor extracts heart rate from in or around the ear canal. The main criteria are sensor size, unobtrusiveness and the susceptibility of the signal to noise. The method- and sensor selection are discussed separately.

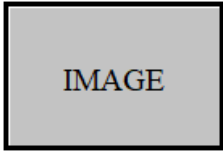
### 3.2.1 Heart rate measurement method

The following five methods from literature are considered to measure heart rate.

#### 3.2.1.1 Ear ECG

As shown by Winokur *et al.* (2012), an electrocardiogram can be detected behind the ear. One electrode is placed behind the ear on the mastoid bone and the other on the back of the neck. A differential amplifier and ADC is used to acquire the signal. Table 3.3 summarises the evaluation.

Table 3.3: Ear ECG

 <b>IMAGE</b>	<p><b>Advantages</b></p> <ul style="list-style-type: none"> <li>• ECG is the standard method used by cardiologists to measure heart rate.</li> <li>• Other cardiac information can be extracted from ECG i.e. heart rhythm, heart damage and the state of the conductive heart tissue.</li> <li>• No pulse transit time delay.</li> </ul>
Sensor size: 10 mm $\varnothing$ electrodes Unobtrusiveness: Bad - electrode needed behind ear and on neck Signal robustness: Noisy (Winokur <i>et al.</i> , 2012).	<p><b>Disadvantages</b></p> <ul style="list-style-type: none"> <li>• The sensor cannot be fitted entirely inside the ear canal.</li> <li>• Two electrodes are needed.</li> <li>• Separate signal acquisition electronics are needed.</li> </ul>

#### 3.2.1.2 Ear PPG

A LED and photodiode are used to detect variation in subcutaneous tissue blood volume due to the beating heart. Literature identifies three possible locations: inside the ear canal, the earlobe and the concha. With unobtrusiveness in mind, the ear canal method is selected. This means reflective PPG is used. Table 3.4 summarises the evaluation.

Table 3.4: Ear PPG

 <b>IMAGE</b>	<p><b>Advantages</b></p> <ul style="list-style-type: none"> <li>• A substantial pressure pulse can be detected in and around the ear.</li> <li>• Pulse oximetry, a type of PPG, is a tried and tested way of measuring heart rate and SpO<sub>2</sub>.</li> <li>• Respiratory related characteristics like amplitude modulation, respiratory-induced intensity variation and frequency modulation can be found only in PPG signals and can be used to determine respiratory rate.</li> </ul>
Sensor size: Smallest - 1.9×2.6×0.8 mm Unobtrusiveness: Good - fits inside ear canal Signal noise: Low - clear pressure wave visible (Da He <i>et al.</i> , 2010)	<p><b>Disadvantages</b></p> <ul style="list-style-type: none"> <li>• PPG is susceptible to motion artefacts and variation in blood profusion.</li> <li>• Few PPG sensor packages are available to fit inside the ear canal.</li> <li>• Using separate LEDs and photo detectors increases the complexity and size for the proof of concept Ear-Monitor.</li> </ul>

### 3.2.1.3 Ear BCG

A pressure sensitive sensor or accelerometer is placed inside the ear canal to detect the mechanical effects of the pulsating heart. Table 3.5 summarises the evaluation.

Table 3.5: Ear BCG

 <b>IMAGE</b>	<p><b>Advantages</b></p> <ul style="list-style-type: none"> <li>• Pressure sensors can be made small enough for the limited space in the ear canal.</li> <li>• Accelerometer can also be used to measure respiratory rate.</li> </ul>
Sensor size: Smallest - $3 \times 3 \times 1$ mm (ST Electronics, 2016a) Unobtrusiveness: A part of the sensor protrudes from the ear, can be made smaller Signal noise: High (Da He <i>et al.</i> , 2010; Winokur <i>et al.</i> , 2012)	<p><b>Disadvantages</b></p> <ul style="list-style-type: none"> <li>• The signal detected by Da He <i>et al.</i> (2010) and Winokur <i>et al.</i> (2012) appears noisy and detecting beats are troublesome.</li> <li>• This method is influenced by motion artefacts to such an extent that it is unusable for most forms of practical use.</li> </ul>

### 3.2.1.4 Phonocardiogram

A microphone is placed inside the ear canal and identifies heart beats by analysing the sound produced by the cardiac cycle. Table 3.6 summarises the evaluation.

Table 3.6: Ear Phonocardiogram

 <b>IMAGE</b>	<p><b>Advantages</b></p> <ul style="list-style-type: none"> <li>• Can be used to detect breathing as well, as shown by Goverdovsky <i>et al.</i> (2016).</li> </ul>
Sensor size: $3.35 \times 2.5 \times 0.98$ mm (ST Electronics, 2016b) Unobtrusiveness: Can fit inside the ear canal Signal noise: High	<p><b>Disadvantages</b></p> <ul style="list-style-type: none"> <li>• Sounds from other sources like movement and speaking can corrupt the signal.</li> </ul>

### 3.2.1.5 Heart rate method choice

Ear PPG is selected as the Ear-Monitor's method of measuring heart rate. PPG produces a clear signal that will allow for accurate beat detection. This

method can also be incorporated into the SpO<sub>2</sub> measurement sensor, eliminating the need for two different sensors. The entire sensor fit inside the ear canal, making it unobtrusive. This method is also less susceptible to noise than ear BCG or a phonocardiogram.

### 3.2.2 Heart rate measurement sensor

Reflexive ear canal PPG is selected to measure heart rate. Three PPG sensors options are considered namely: separate LEDs and photodetector, the NJL5501R from JRC and the MAX30100 by Maxim Integrated.

#### 3.2.2.1 Separate LEDs and photodetector

SMD LEDs are used with one or more photo detectors. The components are mounted on a thin PCB and placed in the ear probe. The LEDs and photo detectors can be placed in various precise configurations and a wider choice of individual transducers can be used. Additional analogue electronics are needed to drive the LEDs, conditioning the detector signal output and compensate for ambient lighting. A commercial integrated analogue front-end chip like Texas Instruments' AFE4400 is used to perform this task.

#### 3.2.2.2 NJL5501R

The NJL5501R is a surface mounted photo-emitter and -detector contained in one 1.9×2.6×0.8 mm package shown in Figure 3.2. Red and infrared LEDs make it suitable for reflective pulse oximetry and heart beat detection. Its small size allows it to fit in the ear canal while leaving adequate space for other sensors. It requires all the same supporting electronics such as using the separate LEDs and a photo-detector method.

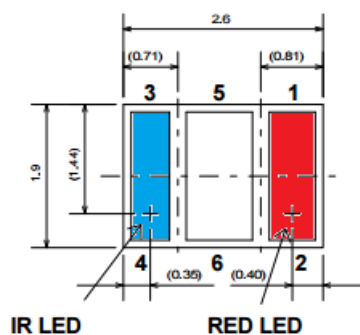


Figure 3.2: NJL5501R diagram from the datasheet

### 3.2.2.3 MAX30100

The MAX30100 is a single chip pulse oximeter and heart rate detector. It has red and infrared LEDs, a photodetector, a 16-bit ADC and digital filters all in one  $5.6 \times 2.8 \times 1.2$  mm, 14-Pin package. The LEDs and photodetector are in the same plane, which means it operates in reflective mode. Like the TMP006 it uses the I2C protocol to communicate with a MCU. Configuration registers allow the designer to specify sample rate, LED currents and LED pulse width. Figure 3.3 shows a block diagram of the internal systems of the MAX30100.

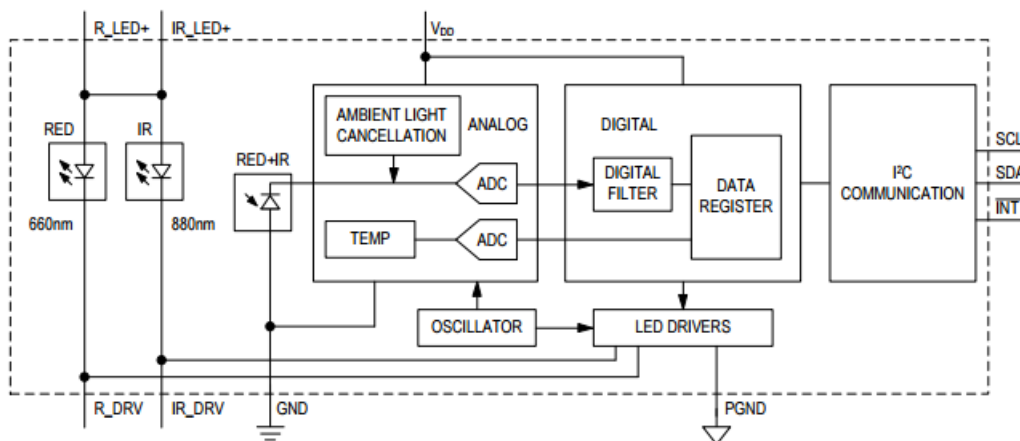


Figure 3.3: MAX30100 block diagram from the datasheet

The MAX30100 uses a 3.3V supply and programmable current sources to drive the LEDs, whilst digital operations are done at 1.8V. It draws between 6 and 12 mA while recording red and infrared PPGs. It has a digital 50Hz/60Hz notch filter to reject powerline interference. LEDs can be varied individually from 0 to 50 mA and the alternating LED pulse widths can be varied from 0.2 to 1.6 ms. A sample rate can be selected between 5 and 1000 samples per second. An important feature of the MAX30100 is its 64-byte deep FIFO register which is used to store the output values. Each output set consists of a 16-bit red and 16-bit infrared value, which means that there are 4 bytes per output and therefore 16 sets of output values can be held in the FIFO at any time. The MCU reads 4 bytes at a time from the FIFO to obtain the latest red and infrared values.

### 3.2.2.4 Heart rate sensor choice

The MAX30100 is selected for use in the Ear-Monitor. It has optimized optics to guide outgoing and incoming light. It has integrated ambient light cancellation. Its entire AFE is integrated which means that no additional electronics are needed, apart from the I2C lines and power regulators. This gives it a big

advantage over the more complex separate LEDs and photodetector method. Its small size and reflective mode of operation allows it to be placed inside the ear canal. Data recorded by the MAX30100 is used to calculate heart rate and SpO<sub>2</sub>.

### 3.3 Respiratory Rate

The Ear-Monitor measures respiratory rate from inside the ear canal. The main criteria are sensor size and susceptibility to noise corruption.

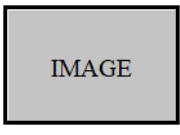
#### 3.3.1 Respiratory rate measuring method

The following three respiratory rate measuring methods from literature are considered.

##### 3.3.1.1 Accelerometer

A small MEMS accelerometer is placed inside the ear canal and measures the movement of the head caused by breathing. Table 3.7 summarises the evaluation.

Table 3.7: Ear Accelerometer

 <b>IMAGE</b>	<p><b>Advantages</b></p> <ul style="list-style-type: none"> <li>• The accelerometer can serve the dual purpose of measuring breathing and heart rate, thus saving space.</li> </ul>
Sensor size: $3 \times 3 \times 1$ mm (ST Electronics, 2016a) Noise: Very high	<p><b>Disadvantages</b></p> <ul style="list-style-type: none"> <li>• This method is extremely vulnerable to noise from other movements.</li> </ul>

##### 3.3.1.2 Microphone

A microphone is placed inside the ear canal and records the sound of air moving through the respiratory tracts, allowing the respiratory rate to be determined. Table 3.8 summarises the evaluation.

Table 3.8: Ear Microphone

<b>IMAGE</b>	<b>Advantages</b> <ul style="list-style-type: none"> <li>• The microphone can serve the dual purpose of measuring breathing and heart rate, thus saving space.</li> </ul>
Sensor size: $4 \times 3 \times 1$ mm (ST Electronics, 2016b) Noise: Very high	<b>Disadvantages</b> <ul style="list-style-type: none"> <li>• This method is extremely vulnerable to noise from other sounds, like talking or ambient noise.</li> </ul>

### 3.3.1.3 Respiratory related heart rate characteristics

The variations in heart rate are used to determine the respiratory rate. These include amplitude modulation, respiratory-induced intensity variation and frequency modulation of the heart rate in synchronization with the respiration rate. Table 3.9 summarises the evaluation.

Table 3.9: Respiratory related heart rate characteristics

<b>IMAGE</b>	<b>Advantages</b> <ul style="list-style-type: none"> <li>• No dedicated sensor is needed.</li> <li>• Less susceptible to noise than the accelerometer or microphone method.</li> </ul>
Sensor size: No sensor needed Noise susceptibility: Low	<b>Disadvantages</b> <ul style="list-style-type: none"> <li>• Only steady and relatively slow respiratory rates can be detected.</li> </ul>

### 3.3.1.4 Respiratory Rate Sensor Choice

Respiration measurement through analysing respiratory related heart rate characteristics, of which heart rate frequency modulation through respiratory sinus arrhythmia (RSA) is found to be the most detectable, is selected for use in the Ear-Monitor. This method saves space by not requiring a dedicated sensor. It is also the least susceptible to noise from other sources. No sensor selection is needed for this vital sign, as all the work is done by the micro controller.

## 3.4 Blood oxygen saturation

Pulse oximetry is the only practical way for the Ear-Monitor to measure blood oxygen saturation. The MAX30100 selected for measuring heart rate is equipped for this task. A red and infrared LED as well as a photo-detector are available for the joint function for measuring heart rate and  $\text{SpO}_2$ .

## 3.5 Final concept

The final concept is obtained by combining the methods and sensors selected in this chapter which are summarised as follows:

- Core body temperature is measured by the TMP006 infrared sensor, located at the tip of the Ear-Monitor's ear probe and pointed at the tympanic membrane.
- Heart rate is measured by the MAX30100 reflective pulse oximeter placed on the side of the ear probe and facing the canal wall. The PPG signal is used to calculate heart rate.
- Respiratory rate is calculated by analysing respiratory sinus arrhythmia (RSA), which is the frequency modulating respiratory related heart rate characteristic.
- $\text{SpO}_2$  is also measured by the MAX30100. The red and infrared PPGs obtained from the ear canal wall are used for this calculation.

Additionally, a microcontroller unit (MCU), battery and wireless transceiver are selected for the Ear-Monitor. The Arduino Pro Mini MCU has the necessary I/O pins for serial communication with the sensors and wireless module. It is also easy to program, making it ideal for the proof of concept version of the Ear-Monitor. Lithium polymer (LiPo) batteries are currently the best choice when regarding capacity, compactness, rechargeability and price. It is therefore selected to supply the power to the Ear-Monitor. Bluetooth is the typically used standard for transmitting data over short distances and is supported by most modern smart devices. The HC-05 Bluetooth modem is selected and allows the Ear-Monitor to send data to a supporting device through a wireless connection. Figure 3.4 shows a diagram of the Ear-Monitor concept with a more detailed drawing of the ear probe with the selected sensors.

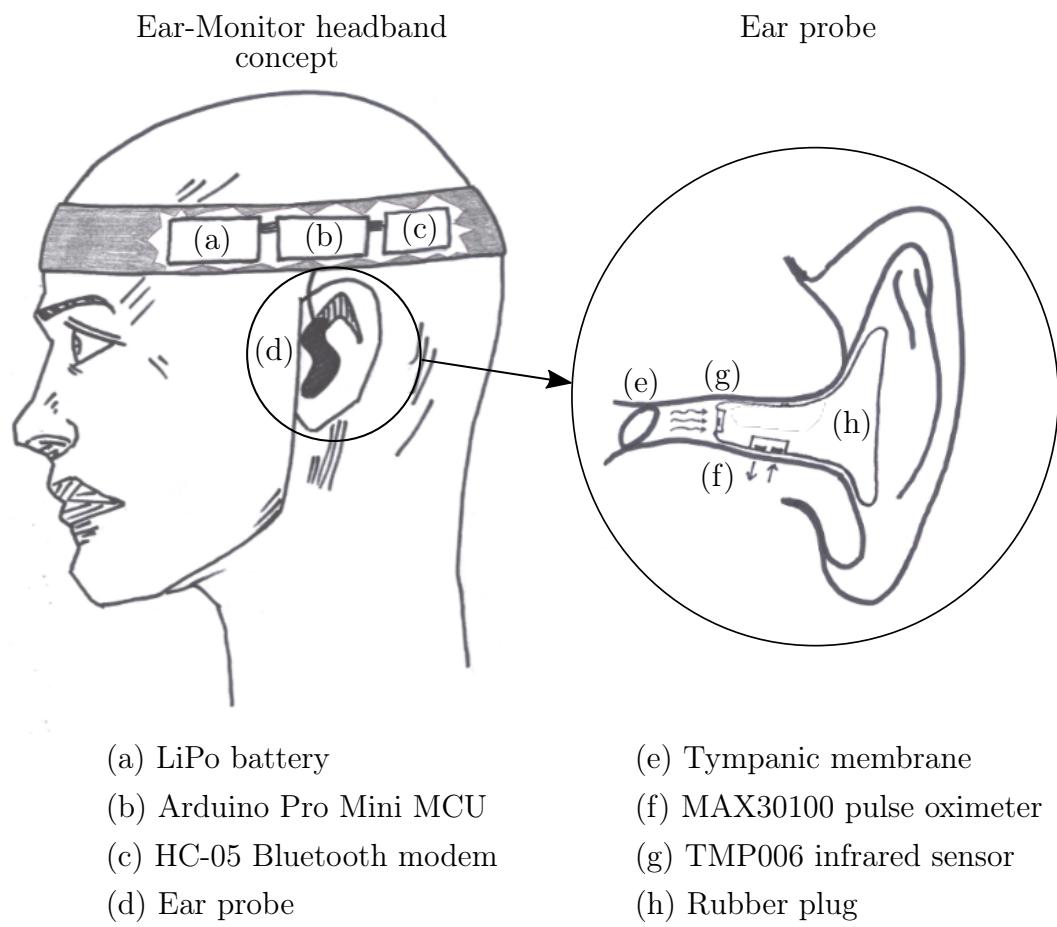


Figure 3.4: Ear-Monitor concept with components labelled

# Chapter 4

## Detailed Design

This chapter documents the detailed design of the subsystems of the Ear-Monitor. The hardware and software facets are discussed separately.

### 4.1 Hardware

A typical telemedicine configuration is used for the Ear-Monitor and its supporting system. It is similar to the configuration used by Wang *et al.* (2010) and Prawiro *et al.* (2016) for their respective wearable health monitors. The ear probe is the signal acquisition module of the Ear-Monitor and contains the sensors. A microcontroller unit (MCU) is used to control the flow of data within the Ear-Monitor. Data is sent by means of a wireless transceiver to a device running supporting software, where data is stored for later access. Figure 4.1 illustrates the flow of information through the hardware set-up.

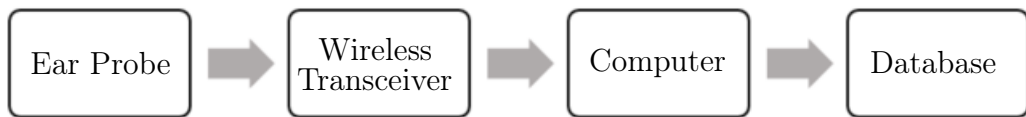


Figure 4.1: Flow of information in a typical telemedicine set-up

The detailed design of each of the key parts of hardware of the Ear-Monitor is documented in the following section.

#### 4.1.1 Temperature sensor

The non-contact infrared TMP006 is selected to measure tympanic membrane temperature in the Ear-Monitor. Four wires are connected for power and serial communication lines. The package has eight solder balls for surface mounting

on a printed circuit board (PCB). A big challenge was to mount this micro-component. Various methods were tested:

- A PCB was designed and manufactured, but mounting the miniature TMP006 on this PCB proved to be problematic.
- The device footprint and wire connection pads were etched into copper clad flexible circuit board sheets. Solder paste and a heat gun was used to mount the TMP006. Etching the flexible circuit board worked well, but mounting the TMP006 proved to be unreliable, for connections were sometimes not made properly or the component got damaged.
- Pre-mounted boards were acquired and the excess material was cut away to allow wires to be soldered to the exposed tracks.

This last method proved to be the best solution for the proof of concept version of the Ear-Monitor. It was necessitated by the lack of advanced facilities to mount micro surface-mount technology (SMT) components. The flexible circuit board method will be preferable when a SMT component placement system is available. Figure 4.2 shows the procured, pre-mounted boards and the cut-out component with the four connections. 3.3V and ground (GND) are connected to a power regulator and the two serial communication wires are connected to the serial communication input/output (I/O) pins of the MCU.

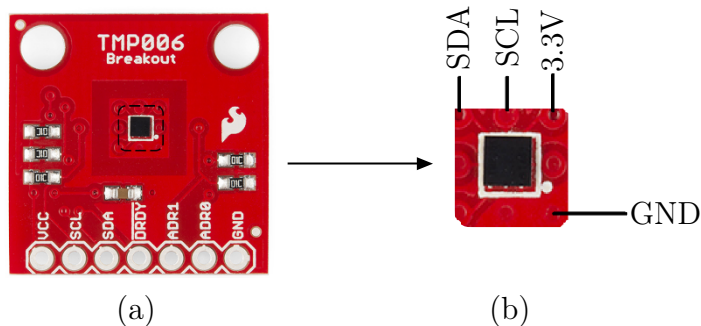


Figure 4.2: (a) TMP006 pre-mounted board and (b) the cut-out sensor segment with four connections labelled

According to the user guide of the TMP006, the sensor captures radiation from almost its entire 180° field of view (FOV), but the most of the received signal comes from sources that are parallel to, and precisely in front of the sensor. The final target object temperature is an integration of all the radiation signals captured across the FOV of the sensor.

The user guide also states that the smaller the object is, the closer it should be placed to the sensor to prevent other objects from entering the field of vision. The TMP006 is placed at the tip of the ear probe within 5 mm of

the tympanic membrane. This position removes the risk of contact with the membrane, while still ensuring thermal radiation from the canal is detected. Energy from the ear canal itself is inevitably detected by the sensor, but the majority of the radiation comes from the membrane and it is assumed that the wall near the membrane is in thermal equilibrium with the membrane within an acceptable margin.

Energy radiated or conducted between the PCB and the sensor can cause temperature calculation errors. To prevent this, the sensor and PCB should be kept at the same temperature. The ear probe set-up of the Ear-Monitor is favourable for this task, as the PCB is very small and contains no other heat generating components. Also, the target object (tympanic membrane), stays at a constant temperature, so the sensor experiences no heat fluctuations. It is, however, necessary to allow time for the sensor and PCB to reach thermal equilibrium once placed inside the ear canal, before accurate measurements can be taken. This is not a problem, for the device is designed to be worn continuously for long periods of time.

#### 4.1.2 Pulse Oximeter

The MAX30100 pulse oximeter is selected to record red and infrared photoplethysmographs from inside the ear canal. These are used for determining heart rate and SpO<sub>2</sub>. The MAX30100 is controlled through 5 connection wires, connected to 7 of the 14 pins of the package. Figure 4.3 shows a diagram of the MAX30100 package and the required connections for operation. 3.3 V, 1.8 V and GND are connected to a power regulator and the two serial communication lines are connected to the serial communication I/O pins of the MCU.

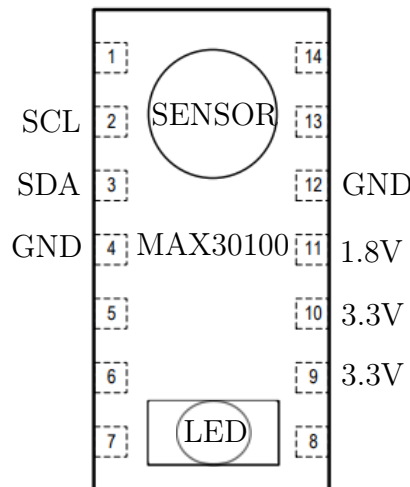


Figure 4.3: MAX30100 package diagram with required connections for operation.

As with the TMP006, the mounting of the extremely small MAX30100 was a great challenge. The first attempt was to design and manufacture a PCB on the typically used, 1.6 mm thick, FR4 PCB material. This PCB proved to be too thick and its inflexibility caused additional problems in ensuring firm contact with the ear canal wall. The solution was to etch the footprint, tracks and pads into flexible circuit board material. The etching process involves the following:

- Design the layout on EAGLE PCB open source software.
- Print the mirrored layout on toner transfer paper.
- Prepare the copper clad material by cleaning it with rubbing alcohol.
- Transfer the ink from the toner transfer paper to the copper clad material by applying heat and pressure.
- Submerge the copper clad material with ink layout in ferric chloride ( $\text{FeCl}_3$ ).
- Remove the remaining ink with acetone to reveal the copper tracks.

The ferric chloride dissolves all the copper that is exposed, leaving copper tracks that were covered by the ink during etching. The flexible copper clad material is 60  $\mu\text{m}$  thick, which is ideal for the size limitations inside the ear canal. Figure 4.4 shows the layout designed and resulting etched flexible circuit

board. The flexible nature of the circuit board allows it to be folded in half to form a two-sided circuit board, saving space and placing all the connection pads on the same end. It also allows for uniform and firm contact between the MAX30100 and the ear canal wall. Wires for power and communication are soldered to the five connection pads.

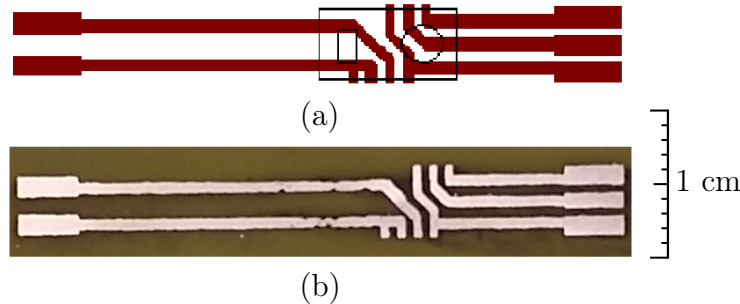


Figure 4.4: (a) is the layout as designed on EAGLE PCB with the outline of the MAX30100 shown in black and (b) is the finished flexible PCB with copper tracks

#### 4.1.3 Control and Communication Hardware

The remaining electronic components consisted of the Arduino MCU, HC-05 Bluetooth modem and battery. A PCB is designed to integrate all the different hardware subsystems. Additional electronics include the power regulators, I<sup>2</sup>C pull-up resistors and a charging circuit for the LiPo battery. An on-off switch and power-on indicator LED are also added.

10 kΩ pull-up resistors on the SDA and SCL lines are recommended for standard I<sup>2</sup>C communication and are therefore included in the design. A 7.4 V, 1000 mA h rechargeable LiPo battery is selected to supply power to the Ear-Monitor. The Ear-Monitor can be operated for XXX minutes on a single charge (Calculations in Appendix A). The Arduino has its own power regulation circuitry on board and can be connected directly to the battery. Two low drop-out voltage regulators are selected to supply 1.8 V and 3.3 V to the sensors and Bluetooth modem. A charging circuit is added to allow the battery to be charged without physically disconnecting it from the device. Decoupling capacitors are added to all power supply lines. Figure 4.5 depicts a block diagram of the hardware of the Ear-Monitor. The diagram is split between the PCB components worn on the head and the components in the ear probe.

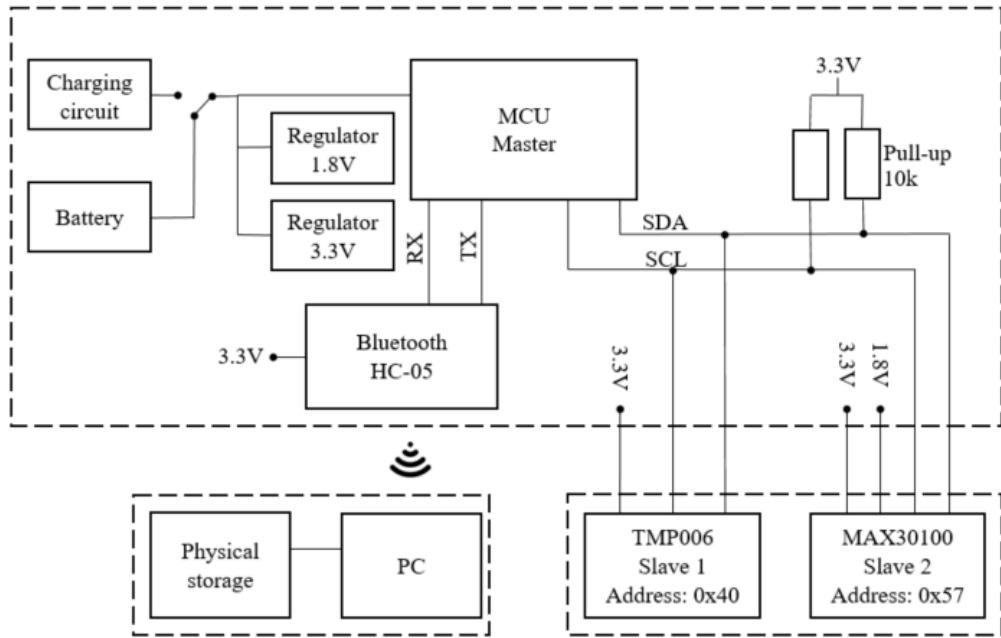


Figure 4.5: Block diagram of the Ear-Monitor’s hardware components

A schematic diagram and PCB layout are included in Appendix ???. Calculations to select passive components is included in Appendix ???. The MCU, battery, Bluetooth modem and PCB are worn in a headband around the head in this proof of concept version of the Ear-Monitor. Only the TMP006 and MAX30100 are located at their correct positions in the ear canal, and held in place by the ear probe. The ear probe is connected by a wire to the electronics in the headband. Data is sent from the headband to the PC through the wireless connection. It is well within the abilities of the current state of technology to reduce the size of all the electronics to a hearing aid, or even ear probe size device. Such miniaturisation is, however, not within the scope of this project.

An ear probe is designed to hold the MAX30100 and TMP006 in the correct positions in the ear canal and restrict their movement to minimize artefacts. Sugru® is the brand name for a mouldable silicone elastomer which is ideal for this application. According to the product documentation it is non-toxic and does not cause skin irritation. The mouldable putty is pressed into the ear and assumes its shape, but does not conform completely. Therefore, it allows the probe to fit in different ear shapes. When cured, it has a sturdy, but flexible structure. Slots and holes are cut into the moulded probe to hold the sensors and wires. Figure 4.6 is a photo of the completed ear probe and Figure 4.7 depicts the entire hardware set-up of the Ear-Monitor.



Figure 4.6: Ear probe with TMP006 visible

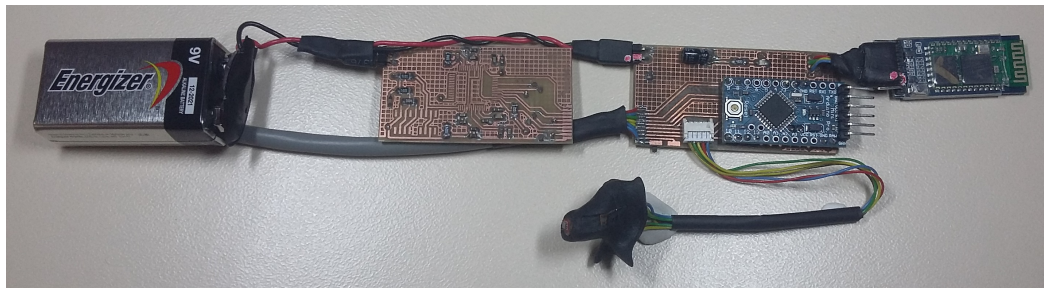


Figure 4.7: Hardware of the Ear-Monitor

## 4.2 Software

Software is written for the MCU and for the PC receiving and storing the data. MCU software is C++ based and developed using the Arduino IDE. MCU software handles sensor communication, timing, selected processing functions and the transmission of collected data via the Bluetooth modem. The PC software is Java based and developed using the Processing IDE. The PC software listens on the Bluetooth serial port, processes received data, displays the data via a user interface and stores the received data on the local hard drive.

Figure 4.8 describes the flow of data through the various software functions. The final calculated vital signs are shown in blue. The diagram is split between the MCU functions and PC functions. MCU and PC software are connected through the Bluetooth connection. The main functions are discussed in this section.

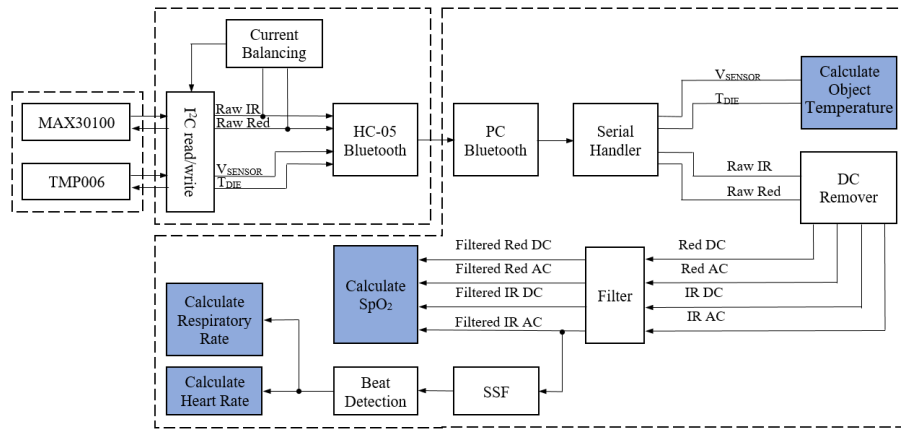


Figure 4.8: Block diagram of the flow of information through the various software functions. Final calculated vital signs are shown in blue

#### 4.2.1 Sensor Communication Software

Software is written for the MCU to communicate with the sensors and Bluetooth module. The MAX30100 and TMP006 have different default addresses and can share one I<sup>2</sup>C bus for communication with the MCU. I<sup>2</sup>C communication happens one byte at a time with no parity and MSB first. The eighth bit of the address indicates a read or write request. Figure 4.9 explains how the software reads 16-bit values from the TMP006 registers. Values form the MAX30100 are read in a similar way.

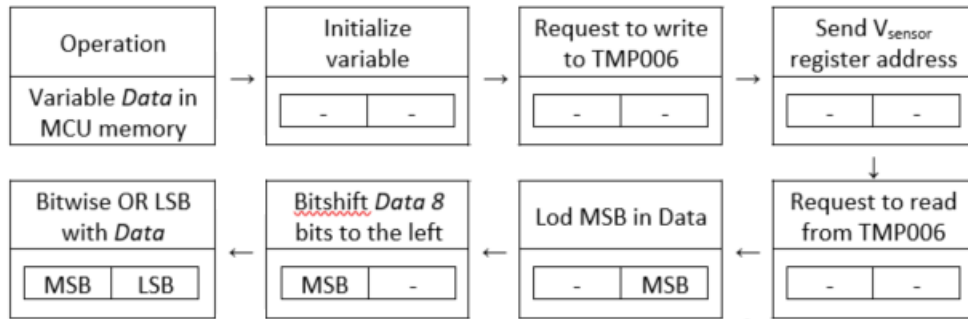


Figure 4.9: How the software reads 16-bit values from the TMP006 registers

Communication with sensors consists of two steps, configuration and reading data.

#### 4.2.1.1 Sensor Configuration

Upon power-on, both sensors start with their default configurations. The MCU is programmed to reconfigure both sensors on start-up. This is done by writing values to the various configuration registers. The MAX30100 is set to SpO<sub>2</sub> mode with 1600 µs LED pulse width, 50 Hz sampling rate and 50 mA current supply to both LEDs. The TMP006 is set to use the average of 16 conversions per output, meaning it will sample at 0.25 Hz. This is done, because the application does not demand a high sampling rate and increasing the number of samples per output will reduce noise ( $\pm 0.125^\circ\text{C}$ ). These configurations are done every time the Ear-Monitor is powered on.

#### 4.2.1.2 Reading data from sensors

After configuration is done, the MCU enters a continuous loop of sensor data reading. The MAX30100 uses one FIFO register to store the latest 16 infrared and red photo-detector voltages and the TMP006 has two separate registers for die temperature and sensor voltage. These registers are read through Arduino's Wiring library. The MAX30100 outputs at 50 Hz and the TMP006 at 0.025 Hz. A timing loop is created to ensure that the values are read from the sensors in time.

### 4.2.2 Temperature related software

After start-up configuration, two values, V<sub>SENSOR</sub> and T<sub>DIE</sub>, are read from the TMP006 through the I<sub>2</sub>C connection every 4 seconds.

T<sub>DIE</sub> is measured by an on-chip precision thermistor and digitalized to a 14-bit value in binary two's compliment, signed integer format with one LSB equal to 0.03125 °C. After two bytes have been read from the TMP006's T<sub>DIE</sub> register (as shown in Figure 4.9), it is bitshifted twice to the right to get the 14-bit value and then divided by 32 to get the temperature in °C. Table 4.1 shows an example calculation to obtain T<sub>DIE</sub>. This conversion is done on the MCU and the value in °C is transmitted over the Bluetooth connection.

Table 4.1: T<sub>DIE</sub> example calculation

Digital output	Right shifted twice	Decimal	$\div 32$
0000 1100 1000 0000	0000 0011 0010 0000	800	25 °C

V<sub>SENSOR</sub> is the output of the thermopile and ranges from -5.12 to 5.12 mV. The 16-bit ADC converts this analogue value to a digital value with a LSB equal to  $\frac{5.12 - (-5.12)}{2^{16}} = 156.25 \text{ nV}$ . Conversion to voltage is done prior to sending the voltage value over the Bluetooth connection.

$T_{DIE}$  and  $V_{SENSOR}$  are received by the PC software, where they are used to calculate  $T_{OBJ}$ . One sensor voltage and die temperature conversion cycle takes 250 ms, and the device gives the designer an option to choose the number of conversions ( $N$ ) per output sample. The average of the  $N$  samples is loaded into the output register every  $N \times 250$  ms. In this design  $N$  is chosen to be 16 and the time per register output equals 4 seconds.

### 4.2.3 Calculating $T_{OBJ}$

$T_{DIE}$  and  $V_{SENSOR}$  are used to calculate  $T_{OBJ}$ . The TMP006's datasheet suggests using the relationship:

$$T_{OBJ} = \sqrt[4]{T_{DIE}^4 - \frac{f(V_{SENSOR})}{S}} \quad (4.1)$$

Where  $f(V_{SENSOR})$  is a function that compensates for heat flow in the form of convection and conduction. The function is described in two stages by:

$$V_{OS} = B0 + B1(T_{DIE} - T_{REF}) + B2(T_{DIE} - T_{REF})^2 \quad (4.2)$$

and

$$f(V_{SENSOR}) = (V_{SENSOR} - V_{OS}) + C(V_{SENSOR} - V_{OS})^2 \quad (4.3)$$

Where  $V_{OS}$  is a compensating offset voltage,  $T_{REF}$  is a reference temperature equal to 25 °C and  $B0$ ,  $B1$ ,  $B2$  and  $C$  are calibration parameters.

$S$  takes into account the object emissivity ( $\varepsilon$ ), Stefan-Boltzman constant ( $\sigma$ ) and the non-ideal absorption of the sensor itself. It is described by:

$$S = S0(1 + A1(T_{DIE} - T_{REF}) + A2(T_{DIE} - T_{REF})^2) \quad (4.4)$$

Where  $S0 = \varepsilon\sigma$ ,  $T_{REF} = 25$  °C and  $A1$  and  $A2$  are parameters experimentally derived through calibration.

The TMP007 is the same sensor as the TMP006, but with a built-in math engine. The recommended calibration parameters from the TMP007's data sheet is shown in Table 4.2. These parameters can also be seen as the default calibration parameters for the TMP006 and is a good starting point for the calibration process.

Table 4.2:  $T_{DIE}$  example calculation

S0	C	A1	A2	B0	B1	B2
4.43e-14	0	9.99e-4	-6.02e-6	-3.09e-5	-8.72e-8	1.30e-8

The TMP006 in the Ear-Monitor will operate in a relatively narrow temperature range. Plotting the  $T_{OBJ}$  equation over the range  $T_{OBJ} = 35$  to  $40^\circ\text{C}$ ,  $T_{DIE} = 35$  to  $39^\circ\text{C}$  and  $V_{SENSOR} = -46.88$  to  $23.44 \mu\text{V}$  with recommended calibration parameters (Table 4.2) relieves a surface resembling a flat plane. This plot can be seen in Figure 4.10.

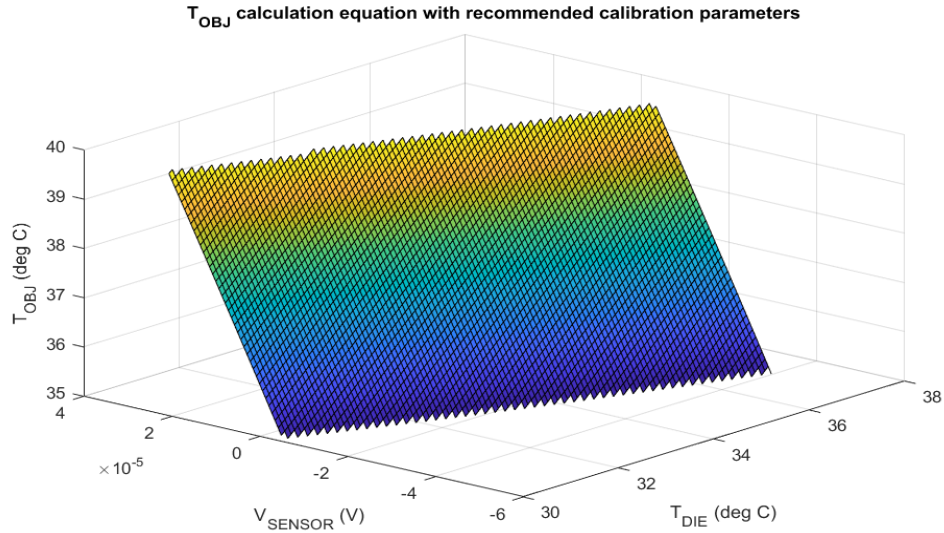


Figure 4.10: Plot of the  $T_{OBJ}$  equation with recommended calibration parameters over the operating temperature range of the Ear-Monitor

This linear characteristic of the TMP006 in the operating temperature range of the Ear-Monitor can be used to simplify the  $T_{OBJ}$  calculation method as described in Equations 4.1 to 4.4. These bulky recommended equations can be replaced by a first-degree polynomial formula for a flat plane as described by:

$$T_{OBJ} = P_0 + P_1 \cdot T_{DIE} + P_2 \cdot V_{SENSOR} \quad (4.5)$$

Where  $P_0$ ,  $P_1$  and  $P_2$  are parameters to be determined by a calibration process that follows the trial stage.

#### 4.2.4 PPG signal processing

The PPG signal is crucial to the calculation of heart rate, respiratory rate and SpO<sub>2</sub>. This signal is captured by the MAX30100 pulse oximeter. Some noise is present in the measured signal. The MAX30100 has on chip digital filters for 50Hz/60Hz interference and low-frequency ambient noise. Despite on-chip filtering, signal drift and high frequency noise still contaminate the signal. This causes the detection of false heartbeat peaks and noisy SpO<sub>2</sub> calculations. An AC and DC extraction algorithm and low-pass filter is designed to prime the signal for further processing. Figure 4.11 shows how the signal samples for the

MAX30100 are processed.  $x_n$  is the PPG signal measured by the MAX30100 in the ear canal and  $y_n$  is the processed signal.

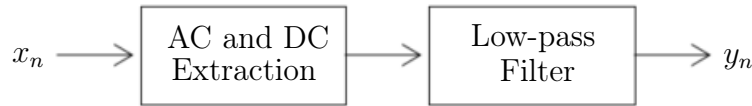


Figure 4.11: The raw PPG signal,  $x_n$ , is sent through AC and DC extraction and filtering functions

#### 4.2.4.1 AC and DC separation

An algorithm is implemented to digitally separate the AC and DC components of the red and infrared signals. Signal separation need to be done in real time and with the minimal computational overhead, because it is executed on the MCU. The following infinite impulse response (IIR) filter is used for AC extraction (Koblenksi, 2015):

$$w_n = x_n + \alpha \cdot w_{(n-1)} \quad (4.6)$$

$$y_n = w_n - w_{(n-1)} \quad (4.7)$$

Where  $x_n$  is the raw ADC value from the MAX30100,  $w_n$  is an intermediate value and  $y_n$  is the filter output. This filter has a narrow stop band at the DC frequency when the scale factor,  $\alpha$ , is close to 1. Scale factor  $\alpha = 0.7$  is chosen as it gives the best DC rejection while maintaining an acceptable response time. Figure 4.12 shows the PPG signal before and afted the C extraction function.

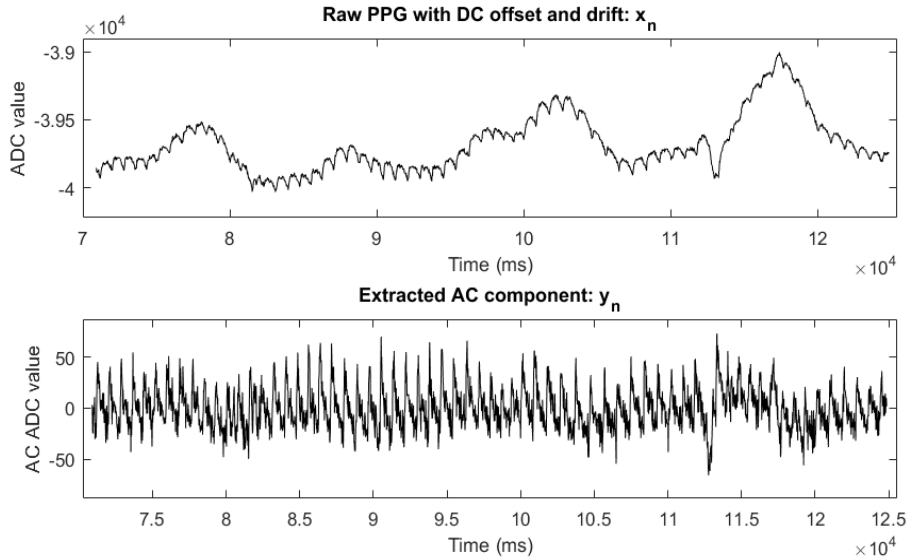


Figure 4.12: (a) the raw infrared signal contaminated by DC offset and drift and (b), the extracted AC component of the signal

The DC component of the signal is used during LED bias adjustment and SpO<sub>2</sub> calculations. To get the DC value, the AC value is subtracted from the raw signal. Alternative AC extraction methods tested were high-pass FIR filtering and moving average subtraction. These methods were rejected, because a high-pass FIR filter is computationally intensive and moving average subtraction will attenuate frequencies close to DC as well.

#### 4.2.4.2 Low-pass filter

The separated AC and DC component of the red and infrared signals are passed through a third order IIR Butterworth filter. The coefficients were calculated with MATLAB for a cut-off frequency of 3 Hz. Equation 4.8 is the transfer function H(z) of the filter.

$$H(z) = \frac{0.0048 + 0.0143z^{-1} + 0.0143z^{-2} + 0.0048z^{-3}}{1.0000 - 2.2501z^{-1} + 1.7564z^{-2} - 0.4683z^{-3}} \quad (4.8)$$

Figure 4.13 shows the effect of the low-pass filter on the AC signal as extracted in the AC and DC separation function.

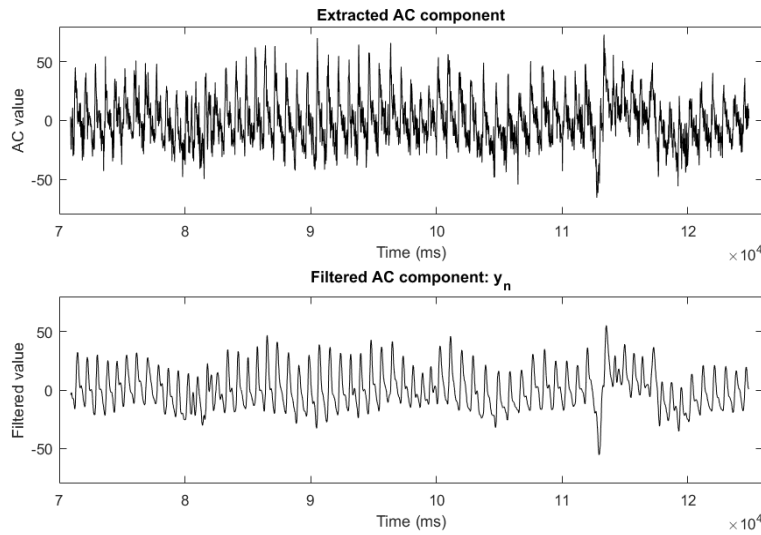


Figure 4.13: (a) the AC component of the infrared signal before filtering and (b), after filtering

#### 4.2.5 Beat Detection

Heartbeats appear as peaks on the inverted PPG signal. The infrared PPG is chosen for beat detection, for infrared light absorption by oxyhaemoglobin is higher than that of red light. Therefore, infrared pulse peaks are more prominent, thus better suited for the detection of heartbeats. A software algorithm is developed to detect these peaks in order to calculate average heart rate, breathing rate and SpO<sub>2</sub>. The algorithm takes as input the filtered infrared PPG signal  $y_n$ , and outputs a timeseries of the heartbeats. Figure 4.14 shows a plot of a PPG signal with characteristic features labelled.

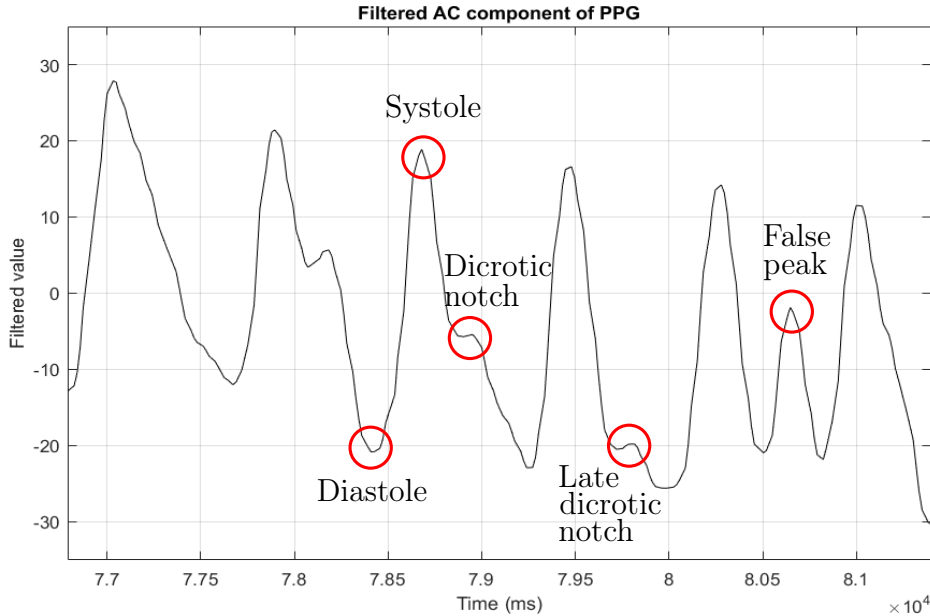


Figure 4.14: Filtered AC component of PPG with important features labelled

This signal extract shows the challenges of the peak detection algorithm. The amplitude of the peaks varies significantly and local maxima which can trigger false positives are present. The intermediate peak in the descending part of the peak is the dicrotic notch, due to the aortic valve closing. Only true systolic peaks should be registered as a heart beat. The beat detection algorithm needs to be robust, computationally inexpensive and should not require any user-specific modifications.

These obstacles are overcome by a two-stage peak detection algorithm developed specifically for the Ear-Monitor's PPG. The algorithm builds on the work done by Park *et al.* (2015), Zong *et al.* (2003) and Elgendi *et al.* (2013) as well as adding new elements like the ...

Stage 1 is a morphological conversion in the form of a slope summing function (SSF). This method is also used by Zong *et al.* (2003), Park *et al.* (2015) and Elgendi *et al.* (2013). The SSF is defined piecewise according to its derivative,  $\Delta y_n$ , as shown by Equation 4.9. The aim of the SSF is to enhance the rising section of the pulse peak while suppressing the falling section.

$$z_n = \sum_{k=n-w}^n \Delta y_k, \quad \text{where} \quad \Delta y_k = \begin{cases} \Delta y_k, & \text{if } \Delta y_k < 0 \\ 0, & \text{if } \Delta y_k \geq 0. \end{cases} \quad (4.9)$$

The  $n^{\text{th}}$  SSF output value,  $z_n$ , equals the sum of the previous  $w$  filtered PPG slopes as defined by the conditions in Equation 4.9. Zong *et al.* (2003) suggest choosing  $w$  as the typical duration of the pulse up-slope, so a moving

sum window of  $w = 10$  was selected. Figure 4.15 shows (a) the extracted and filtered AC component and (b) the output of the SSF.

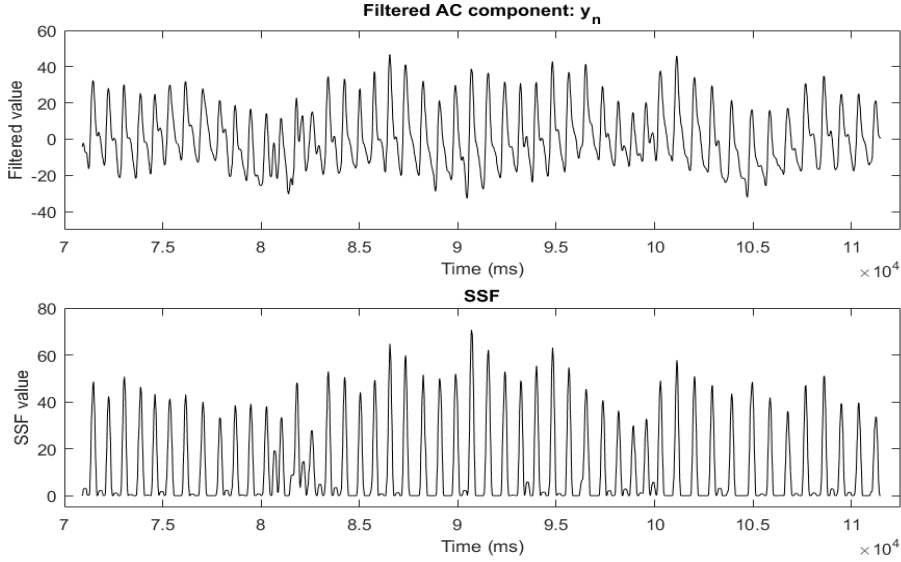


Figure 4.15: (a) the AC component of the infrared signal before filtering and (b), after filtering

Stage 2 of the beat detection function is a set of decision rules determine if a peak is present. Some of the rules were adapted form Park *et al.* (2015). Their algorithm is applied to in-ear pulse waves, which is closer to a ballistocardiogram than a PPG. Therefore, the decision rules in this function are chosen specifically for the Ear-Monitor and determined through experimentation.

Rule 1: Adaptive threshold. The adaptive threshold applied to this algorithm is related to the mean of the previous 3 detected SSF peak heights by Equation 4.10.

$$t = c \frac{\sum_{k=0}^2 z_{n-k}}{3} \quad (4.10)$$

Where  $c$  is an experimentally determined scaling factor equal to 0.5. If the SSF signal amplitude rises above the threshold, a potential peak is awaited. Zong *et al.* (2003) uses a threshold equal to 60% of the previous SSF peak amplitude, but this method proved to miss heartbeats if subsequent SSF maxima varies more than the threshold percentage. This problem is mitigated by basing the threshold on the previous three-peak average.s

Rule 2: Local maximum point. Following the crossing of the threshold, the algorithm monitors the SSF for a local maximum. This occurs at  $SSF_{n-1}$  when:  $SSF_{n-2} < SSF_{n-1} \geq SSF_n$ .

Rule 3: Waiting period If a local maximum is detected, the time elapsed since the previous successfully detected beat is tested. If the time is less than

a dynamic waiting period, the local maximum is rejected. The waiting period is set to be 70% of the mean of the previous 10 beat periods.

Only if all three rules apply to a SSF value, will it be registered as a peak. The time difference between the newly detected peak and the previous one is the heartbeat period. Another element to the beat detection algorithm is the threshold reset. If no local maximal is detected above the threshold for longer than 2 times the mean of the previous 10 beat periods, the threshold is reset to 1. This is in case the amplitude of the SSF peaks drops below the threshold and no beats is registered to update the threshold to a lower value. Figure 4.16 shows the example signal's SSF with detected beats. This example illustrates how the algorithm can successfully detect peaks of varying amplitude and using the threshold method and how the time delay prevent the triggering of a false peak.

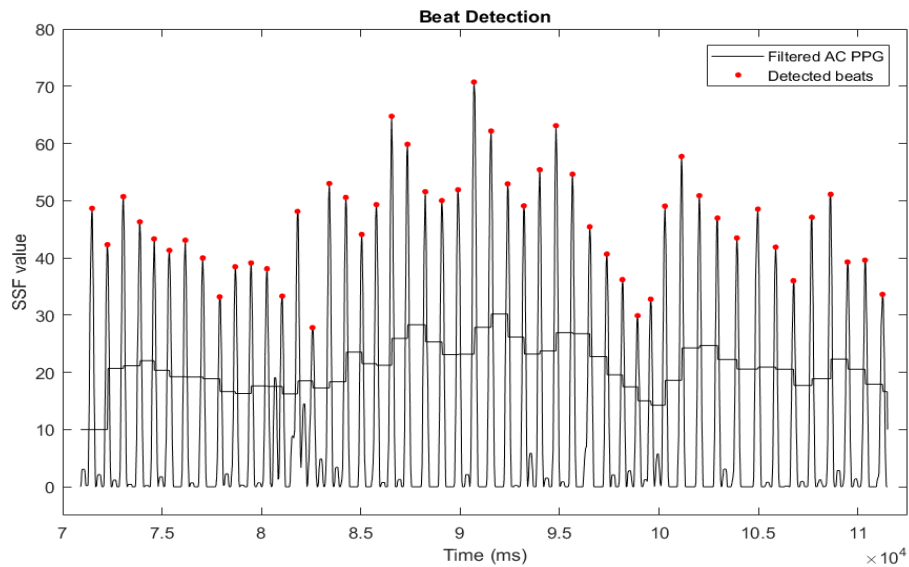


Figure 4.16: SSF with detected beats and threshold plotted.

Figure 4.17 illustrates how the SSF and beat detection algorithm can extract beats, even in a noisy signals. It depicts an especially irregular AC component of the Ear-Monitor PPG signal (blue), the corresponding SSF (orange) and the adaptive threshold (gray). Detected peaks are marked in red. It can be seen how the SFF emphasises the rising slopes of the PPG signal, even when the amplitudes and baseline of the PPG varies significantly. The adaptive threshold prevents the detection of false peaks at (a) and (b), while the time delay prevent false peaks at (c) and (d).

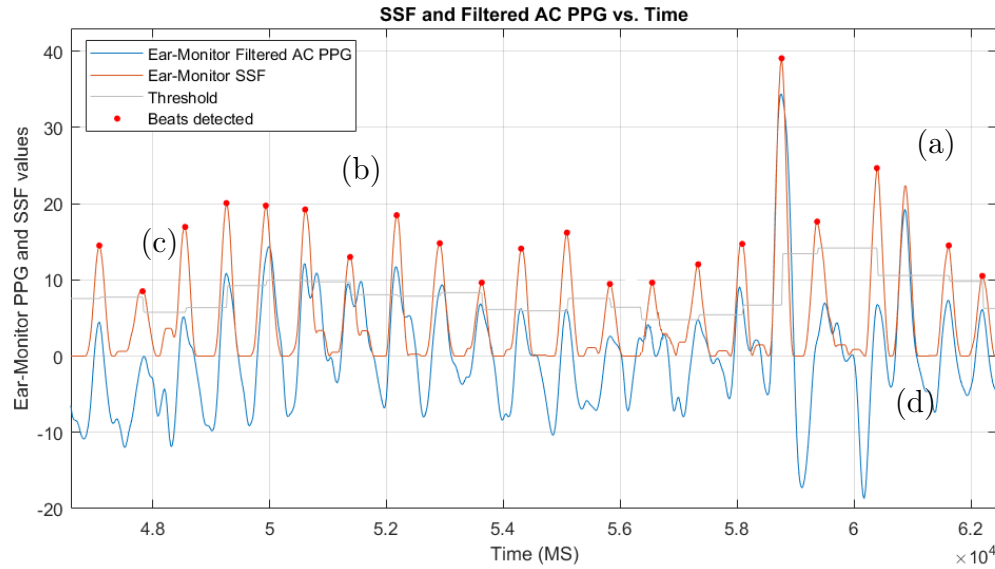


Figure 4.17: Peak detection example

#### 4.2.5.1 Heart- and Respiratory Rate Calculation

The Ear-Monitor uses a moving average of the previous 10 heartbeat periods to calculate heart rate in beats per minute. This calculation is executed every time a heartbeat is detected and is done by the PC software.

Respiration rate is determined by monitoring respiratory sinus arrhythmia (RSA), the frequency modulating respiratory related heart rate characteristic. During inhalation, the heart rate increases and during exhalation it decreases. RSA is not easily observed in a PPG plot, but becomes visible when plotting the heartbeat periods. Figure 4.18 shows plots of the heartbeat period and of the chest expansion due to the respiratory cycle. The synchronisation to the heart period variation and the respiratory rate is clearly visible, with each chest expansion maximum corresponding with a heartbeat period minimum.

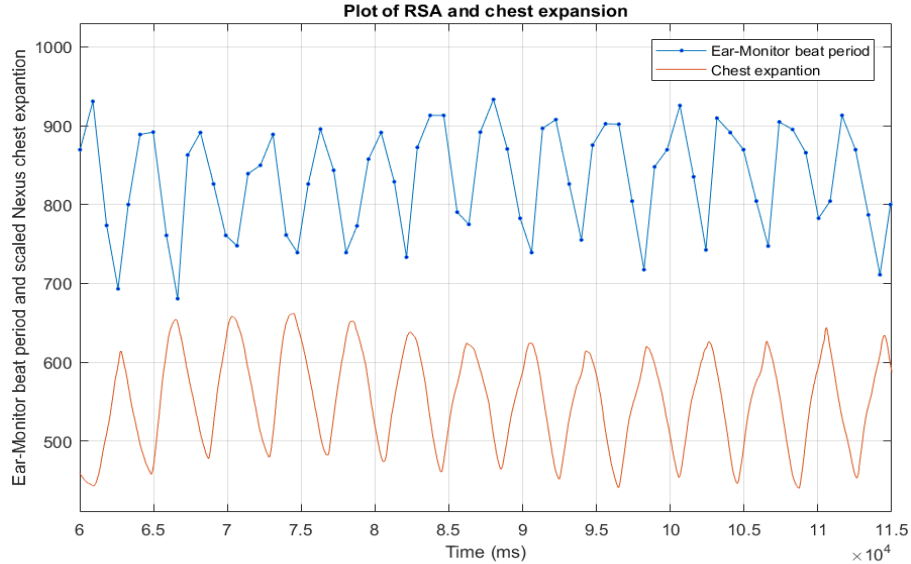


Figure 4.18: Plots of heartbeat periods and chest expansion.

To remove noise and reduce false positives, a two-period moving average is taken of the beat period signal. A inhalation is registered each time a local maximum is detected on this filtered signal. The number of inhalations detected in a minute is used to calculate the respiratory rate in breaths per minute.

The heartbeat periods can be seen as samples, and therefore the heart rate as the sample rate. This means that, according to the Nyquist theorem, the highest theoretical respiration rate that can be measured by the Ear-Monitor will equal half the heart rate.

#### 4.2.6 SpO<sub>2</sub> Calculation

The MAX30100 outputs digital values representing the intensity of red and infrared light reflected by the tissue. Due to the different absorption spectra of oxygenated and deoxygenated blood, these values can be used to determine the fraction of peripheral blood oxygen saturation. PC software is written to calculate the SpO<sub>2</sub> and MCU software is written to control the sensor.

#### 4.2.7 Current Balancing

The ratio of ratios method, discussed in the literature review and shown in Equation 4.11, is used to calculate SpO<sub>2</sub>.

$$R = \frac{\left(\frac{AC}{DC}\right)_{\text{red}}}{\left(\frac{AC}{DC}\right)_{\text{IR}}} \quad (4.11)$$

The motivation behind using this method is that it compensates for differences in DC reflection from person to person. For this to work, the difference between the red and infrared DC values used in the equation needs to be as small as possible. The current to the red and infrared LED of the MAX30100 are set to 50 mA upon start-up configuration. To compensate for the fact that infrared light is reflected differently by the tissue than red light, a dynamic current balancing function is written.

The MAX30100 has a programmable register that allows for the individual current adjustment of red and infrared LED drivers. A negative feedback control system is implemented on the MCU to adjust the individual LED currents in order to lower the difference in reflection. A lower current equal a lower light intensity and subsequently, less reflection. The function checks the difference in infrared and red DC levels every second and adjusts the current to the LEDs until the difference are within an acceptable margin. Figure 4.19 shows a plot of this process. The difference in reflection starts out at 15000, with both LED currents equal to 50 mA, and after five adjustments the difference is lowered to 1000, with the red LED current unchanged and the infrared LED equal to 33.9 mA. As can be seen from Figure 4.19, the current adjustments happen in a stepwise fashion, with each step about 2700. Therefore, to avoid oscillations, the margin is set to 2000.

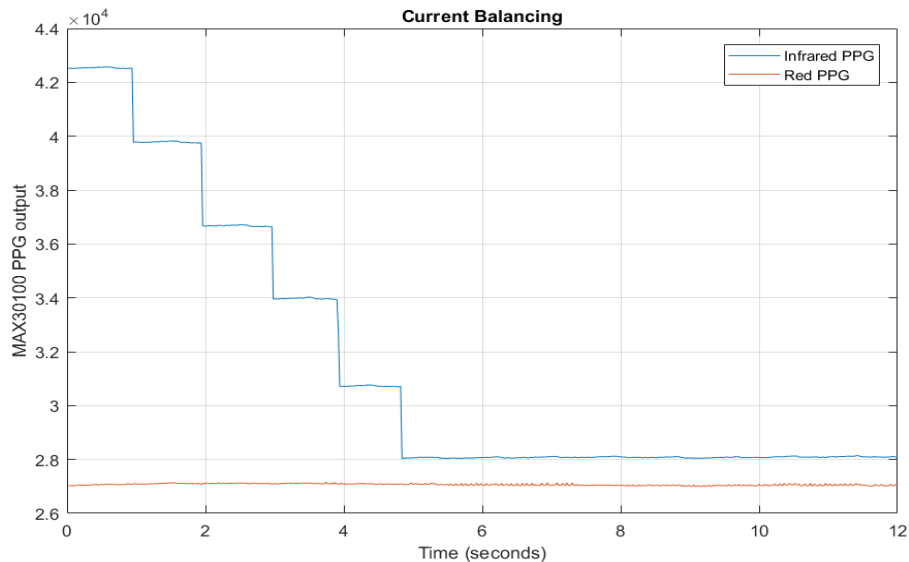


Figure 4.19: Plot showing the effect of the current balancing function implemented on the MAX30100 lowering the difference in detected light between red and infrared LED by adjusting the current to the infrared LED.

### 4.2.8 Moving average SpO<sub>2</sub>

SpO<sub>2</sub> calculation is done by the PC interface software. The filtered AC and DC components of the infrared and red PPG signals, as calculated in the PPG signal processing section, are used in the ratio of ratios method.  $R$  is calculated using the mean of the absolute AC and DC values of the previous 12 heartbeats. These values are updated each time new PPG data is available.

The relationship between  $R$  and SpO<sub>2</sub> is unique for different devices and measurement locations. Calibration is needed to find the relation for the Ear-Monitor. The relationship used in literature (Oak and Aroul, 2015) was adjusted through a calibration process to achieve a desirable level of accuracy. Equation 4.12 shows the relationship used by the Ear-Monitor to calculate SpO<sub>2</sub>.

$$111.2 - (25 \cdot R) \quad (4.12)$$

$R$  and SpO<sub>2</sub> are calculated on every heartbeat using the moving data window of the previous 12 heartbeats.

### 4.2.9 PC Interface

A graphical user interface is written in Processing to display the measurements on the computer screen and allow the user to set alarms and save the data. The interface receives variables from the various functions discussed. It displays these variables along with a series of real-time graphs and has the option to save the measured Ear-Monitor data in a .csv file for later reference or analysis. Figure 4.20 shows a screen-shot of the user interface with (a) the SSF with detected beats, (b) the AC components of the red and infrared PPGs, (c) respiration illustrated in plotting the heartbeat period, (d) temperature, (e) data written to .csv files and (f) alarm conditions.

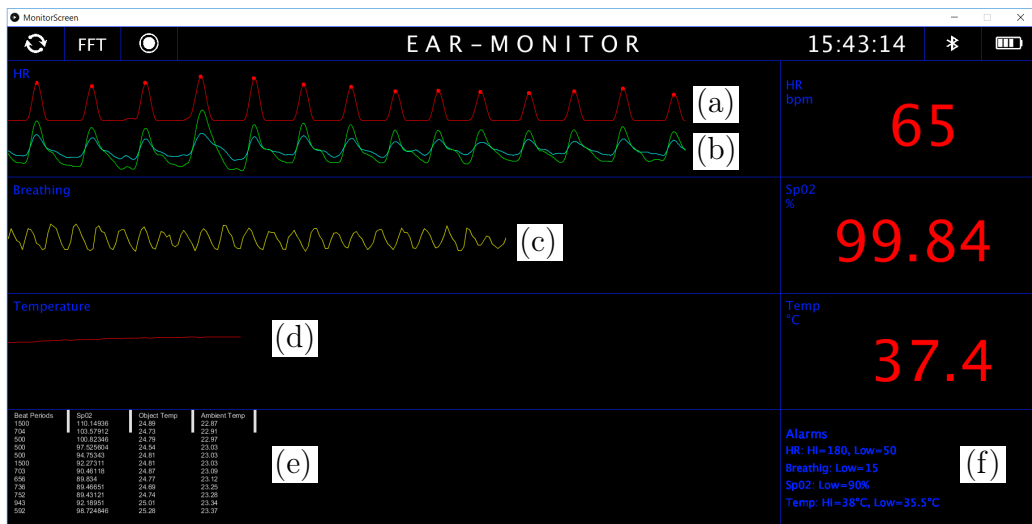


Figure 4.20: Ear-Monitor user interface

# Chapter 5

## Trial Period

A trial is conducted during which the Ear-Monitor is tested on a sample of 16 healthy, adult volunteers. The trial's goal is twofold: firstly, to calibrate the temperature and SpO<sub>2</sub> algorithms and secondly to evaluate the accuracy of the Ear-Monitor's measurements. This chapter describes the trial environment and the method used to collect data for calibration and evaluation. Ethical approval is obtained for this trial from the Health Research Ethics Committee of Stellenbosch University, under the reference number M16/09/038 (proof of approval included in Appendix ??).

### 5.1 Participant Selection

Participants for the study are invited via a recruitment email sent to students and staff at the faculty building. Inclusion criteria are physical health, ages from 18 to 60 years and volunteers of any gender or race. Exclusion criteria are small ear canal size, ear abnormalities or injuries and general health issues. If the individual's ear canal is smaller than 5 mm diameter the Ear-Monitor's probe will not fit. This also applies to ear abnormalities or injuries that will prevent the use of an ear probe, for example an abnormal sharp bend in the ear canal or an inflamed or infected ear canal due to i.e. otitis externa (swimmers ear). Individuals with self-diagnosed illness that will cause them risk if they participate, are also excluded. Potential participants are screened through a pre-test physical examination to determine if they meet all the criteria. Table 5.1 gives a demographic summary of the participants that are selected for the trial.

Table 5.1: Demographic summary of participants

	n	Average age
Male	13	24.5 ± 0.7
Female	3	23.3 ± 0.3
Total	16	24.3 ± 0.6

## 5.2 Benchmark Validation

Evaluation is done for all four vital signs measure by the Ear-Monitor, namely core temperature, heart rate, respiratory rate and SpO<sub>2</sub>. Evaluation entails comparing the vital sign measurements made by the Ear-Monitor to measurements made, in the same conditions, by industry standard medical devices, referred to as benchmark devices. The measurements made by benchmark device is referred to as benchmark measurements. In this trial, a device that conforms to the EC requirements qualifies as a benchmark device. The CE mark is sign that the benchmark device complies with the ISO 13485 standard for medical devices, which requires industry standard accurate measurements.

Three benchmark devices, shown in Figure 5.1, are selected to provide the various benchmark measurements. A concise technical overview is given of each.

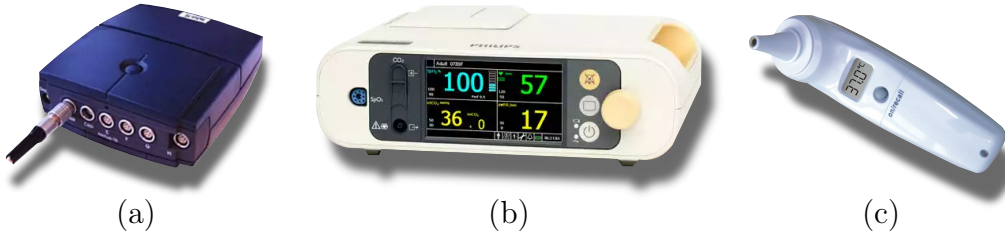


Figure 5.1: Benchmark devices: (a) Nexus-10, (b) SureSigns VM1 and (c) EM 100-A

The Nexus-10 physiological monitoring platform is selected to provide benchmark heart rate and respiratory rate measurements. The Nexus-10 is a data acquisition device with a 24-bit analogue to digital converter and an accuracy of ±2% according to the manufacturer. It has a blood volume sensor, which measures a PPG signal from the fingertip at a sampling rate of 128 Hz. This PPG signal is used to provide the benchmark heart rate measurement. It also has an elastic chest strap to measure respiratory rate. The movement of the chest during the respiratory cycle is converted to a voltage signal and digitalized at a sampling rate of 32 Hz. This signal is used to provide the benchmark respiratory rate measurement. It uses a Bluetooth connection to send data to

a computer. The BioTrace+ software package is used to display the recorded data in real time as well as store the data for later processing.

The SureSigns VM1 patient monitor from Philips is selected to provide benchmark SpO<sub>2</sub> measurements. The SureSigns VM1 uses a pulse oximeter attached to the fingertip to measure SpO<sub>2</sub>. Data is logged on the device's screen and updated at 1 Hz and stored on a computer for later processing. The device is recommended for use by healthcare professionals, emphasizing its accuracy and reliability.

The ET-100A infrared ear thermometer is selected to provide the benchmark tympanic ear temperature measurements. The ET-100A complies with the EN12470-5:2003 standard for clinical thermometers, therefore satisfies an accuracy of  $\pm 0.2^{\circ}\text{C}$  over the range of  $35.5^{\circ}\text{C}$  to  $42^{\circ}\text{C}$ . Its measurements are displayed on the device's screen and data is entered and stored on a computer for later processing.

### 5.3 Method

Data is recorded from one participant at a time. A recording session involves collecting four benchmark- and four Ear-Monitor vital sign measurements simultaneously from one participant. Each recording session lasts for 2 minutes and is conducted twice per participant to ensure repeatability. Figure 5.2 shows a diagram of how all the devices are connected to the participant and which measurements are made by each.

The recording session can be summed up as follows:

- The trial environment is set up before the participant arrives. Equipment is disinfected and connected to the computer, ready for data capture.
- The participant arrives and is briefed about the procedure and signs an informed consent form. The participant is also asked to clean his/her ear with surgical spirits.
- The participant is seated stationary in front of a table containing all the equipment. Sensors are placed on the participant as shown in Figure 5.2. Three tympanic temperature benchmark measurements are taken from the participant with the ET 100-A.
- The recording session starts. The participant sits still the entire time and breaths normally for the first 60 seconds, after which the participant is asked to breath at 15 breaths per minute by following breathing metronome for another 60 seconds.

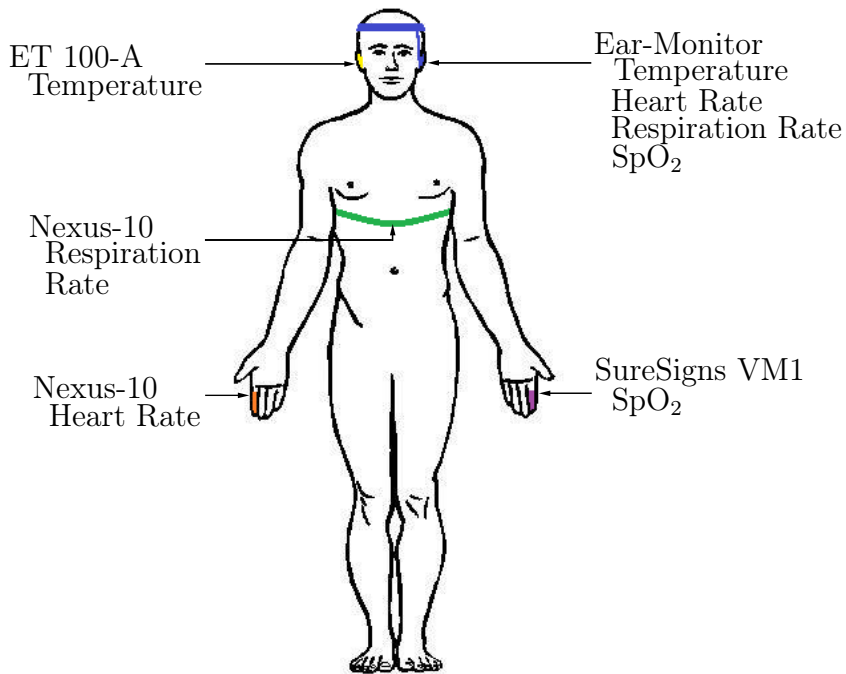


Figure 5.2: Diagram showing how devices are connected to the participant during the recording session

- After 60 of controlled breathing (120 seconds recording time in total) the recording session is concluded. Three more temperature benchmark measurements are taken with the ET 100-A.
- Data from the Ear-Monitor and benchmark devices is stored on a computer in .csv format for later processing and analysis.

The breathing exercise is included due to the uncertainty that the RSA will be detectable during normal breathing. During prototyping, it was more visible in beeper forced breathing. Therefore, if it is not detectable in normal breathing, the controlled breathing data can still be analysed to produce some results.

Figure 5.3 shows an image of one of the participants during a data recording session. The labelled equipment is (a) the computer with the Ear-Monitor user interface, (b) the Ear-Monitor on the participant with the red light of the MAX30100 visible through the tragus. (c) is the SureSigns VM1 and (d) its SpO<sub>2</sub> finger clip. (e) is the Nexus-10 and (f) its blood volume sensor finger clip and (g) its chest strap for measuring respiration. The ET 100-A tympanic thermometer is labelled (h).

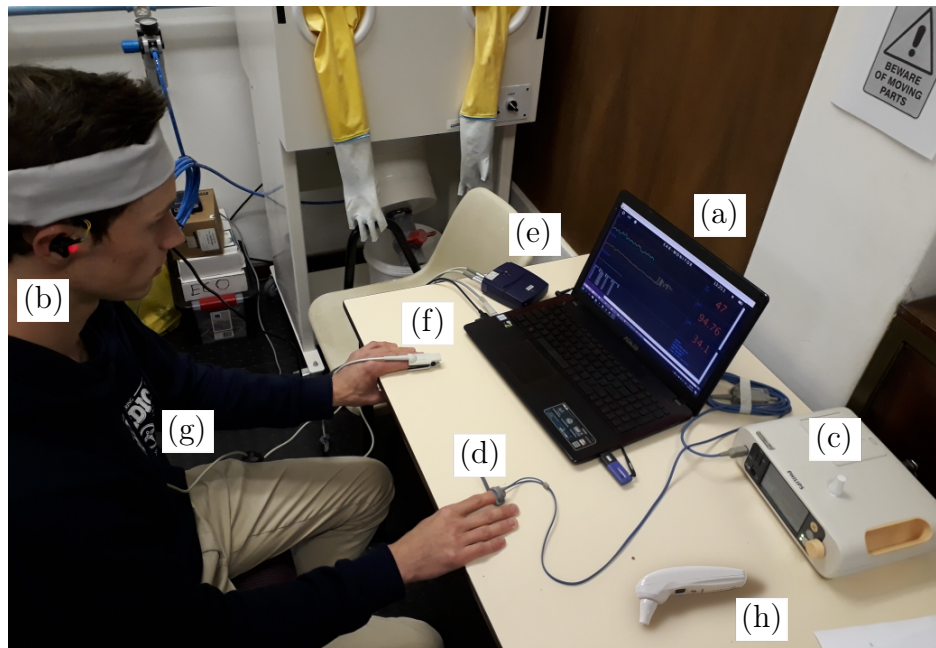


Figure 5.3: Recording session set-up with participant

# Chapter 6

## Calibration

Data collected during the trial is used to calibrate the equations used to calculate tympanic temperature and SpO<sub>2</sub>. The calibration process for the two different vital signs are discussed separately in this chapter.

### 6.1 Temperature Calibration

As discussed in Section 4.2.2, the TMP006 measures die temperature, T<sub>DIE</sub>, and thermopile sensor voltage, V<sub>SENSOR</sub>. These two measurements are used to calculate the temperature of the object, T<sub>OBJ</sub>, which in the case of the Ear-Monitor is the tympanic membrane.

Each data recording session in the trial produced 15 Ear-Monitor measurements and 3 ET 100-A benchmark measurements. Measurements from both devices are averaged separately to get one average Ear-Monitor and one average ET 100-A measurement per session. Two different calibration approaches are discussed: the group calibration approach and the intra-participant calibration approach.

#### 6.1.1 Group Calibration Approach

In this approach, 5 recording sessions are used to calibrate the temperature calculation equation, Equation 4.5. MATLAB's curve fitting tool is used to fit a first order polynomial plane to the data points. The equation with calibration coefficients is shown by Equation 6.1.

$$T_{OBJ} = 22.85 + 0.04803T_{DIE} - 13440V_{SENSOR} \quad (6.1)$$

This equation is applied to all Ear-Monitor temperature measurements. The advantage of the group calibration approach is that calibration is done only once and no patient specific calibration is needed.

A box and whisker plot can be seen in Figure 6.1 and shows the error between the ET 100-A benchmark temperature and the Ear-Monitor temperature before and after calibration. Improvements in accuracy and precision are clearly visible in this graphical representation of the data.

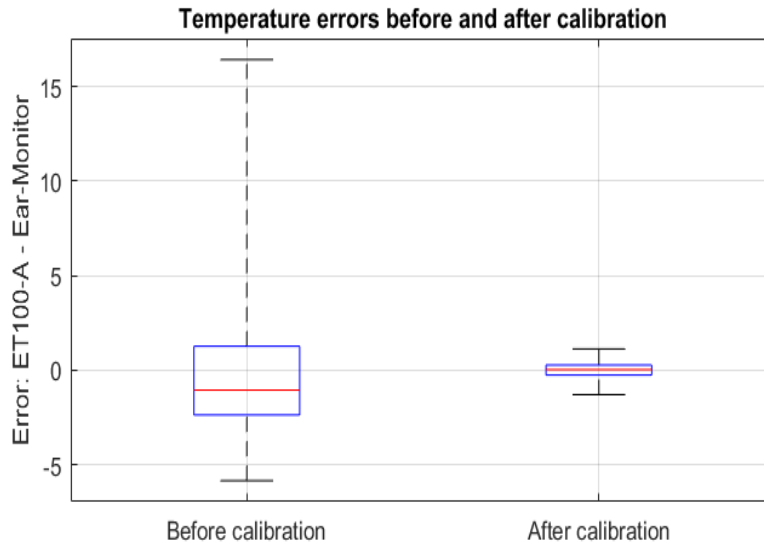


Figure 6.1: Temperature errors before and after calibration

### 6.1.2 Intra-participant calibration approach

In this approach, the first recording session is used to calibrate the calibration coefficients for each participant individually. The first recording session data is entered into Equation 6.1 and the error between the Ear-Monitor and ET 100-A data is used to adjust Equation 6.1.

The advantage of this approach is that the Ear-Monitor can adjust to patient specific parameters, i.e. tympanic membrane size, the sensor's distance from the membrane and the fraction of the FOV that is occupied by the canal wall. The trade-off is that the Ear-Monitor needs to be calibrated for each participant individually. This is not a complicated process, calibration can be done in one minute and is only needed once per individual.

## 6.2 SpO<sub>2</sub> Calibration

According to Oak and Aroul (2015) the modulated ratio, R (Equation 4.11), is linearly related to SpO<sub>2</sub>. The relationship they propose is given by Equation 6.2.

$$SpO_2 = x - m \cdot R \quad (6.2)$$

With  $x$  equal to 110 and  $m$  equal to 25. The relationship will vary for different pulse oximeters, and the calibration parameters for the MAX30100 in the Ear-Monitor are calculated empirically through experimentation. Equation 6.2 is used as a starting point and the gradient,  $m$ , is constrained to be larger or equal to 15 in order to ensure  $R$ 's weight in the calculated  $\text{SpO}_2$  value. The remaining calibration parameter,  $x$ , is systematically incremented until the desired fit is achieved. Equation 6.3 describes the relationship between  $R$  and  $\text{SpO}_2$  selected for the Ear-Monitor.

$$\text{SpO}_2 = 106.32 - 15 \cdot R \quad (6.3)$$

# Chapter 7

## Results and Discussion

This chapter documents the results from the trial conducted on the Ear-Monitor. The aim is to quantify the level of comparability between the measurements of the Ear-Monitor and the benchmark devices. Through this, an understanding of the accuracy of the Ear-Monitor will be obtained. Each participant is acting as his/her own control in this type of comparative analysis. Results are discussed one vital sign at a time.

Correlation between each vital sign and its benchmark is visualised through an interclass correlation (ICC) plot. On each ICC plot, the  $x = y$  line is plotted in black and a blue line is fitted to the data using the least squares method. Some of the terms used to evaluate correlation are defined as follows:

- Correlation coefficient ( $r$ ): This quantifies the strength of the linear dependence between the values in the two datasets.  $r$  varies from -1 to 1. A correlation coefficient close to 1 indicates a high level of positive correlation between the Ear-Monitor and benchmark datasets and is a favourable result.
- p-Value ( $p$ ): The p-value is the probability of the data leading to an incorrect rejection of the null hypothesis, which is that there is no correlation between the Ear-Monitor and benchmark datasets. p-Values smaller than 0.05 indicate strong evidence against the null hypothesis, while p-values larger than 0.05 indicate weak evidence against the null hypothesis.  $p = 0$  indicates a p-value smaller than 0.00005, meaning that the correlation can be accepted with confidence.
- ICC agreement ( $ICC_a$ ): This value ranges from 0 to 1 and the following, often quoted interpretation is suggested by Cicchetti (1994):
  - 0 to 0.40: Poor
  - 0.40 to 0.59: Fair
  - 0.60 to 0.74: Good

- 0.75 to 1.00: Excellent
- ICC consistency ( $ICC_c$ ): This quantifies the consistency of conclusions made by different observers. It ranges from 0 to 1, where values closer to 1 indicates higher consistency.
- 95% confidence intervals: These intervals are given for the  $ICC_a$  and  $ICC_c$  values. If the interval should contain zero, then the ICC is not significant.

## 7.1 Temperature Results

The Ear-Monitor uses the TMP006 infrared sensor to measure the temperature of the tympanic membrane. The ET 100-A tympanic thermometer is used as the benchmark device. During each recording session, 15 Ear-Monitor and 3 ET 100-A data points are collected. It is assumed that the core temperature of the participant stays constant during the duration of the recording session. Therefore, the averages for the ET 100-A and Ear-Monitor measurements are compared. This is a valid assumption, for the standard deviations within recording sessions are found to be between 0.0018 and 0.0814 °C. Datasets recorded from participants 1 and 5 are removed due to faulty recording sessions.

Results from the two calibration approaches are documented separately and then compared in the discussion. The results for the two different calibration methods are summarised in Appendix B. All participants are healthy and benchmark temperatures range from 36.33 to 38.55 °C.

### 7.1.1 Group Calibration Results

Equation 6.1 is used by the Ear-Monitor to calculate the tympanic temperature of participants. Figure 7.1 depicts an ICC plot of the Ear-Monitor versus ET 100-A data points for the 28 recording sessions. The mean error is 0.0180 ± 0.5125 °C.

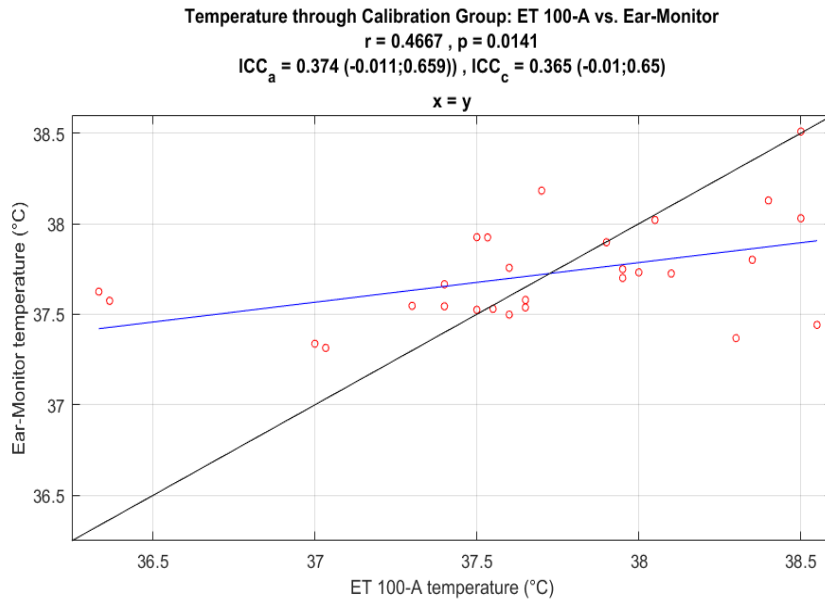


Figure 7.1: Temperature through the Group calibration method: ET 100-A vs. Ear-Monitor

### 7.1.2 Intra-participant Calibration Results

This method uses data from the first recording session to calibrate the Ear-Monitor, and the data from the second session to evaluate the calibration. Figure 7.2 depicts an ICC plot of the Ear-Monitor versus ET 100-A data points for the 14 recording sessions used for evaluation. The recording sessions used for calibration are not plotted, for they all lay on the  $x = y$  line. The mean error is  $-0.0156 \pm 0.29 ^{\circ}\text{C}$ .

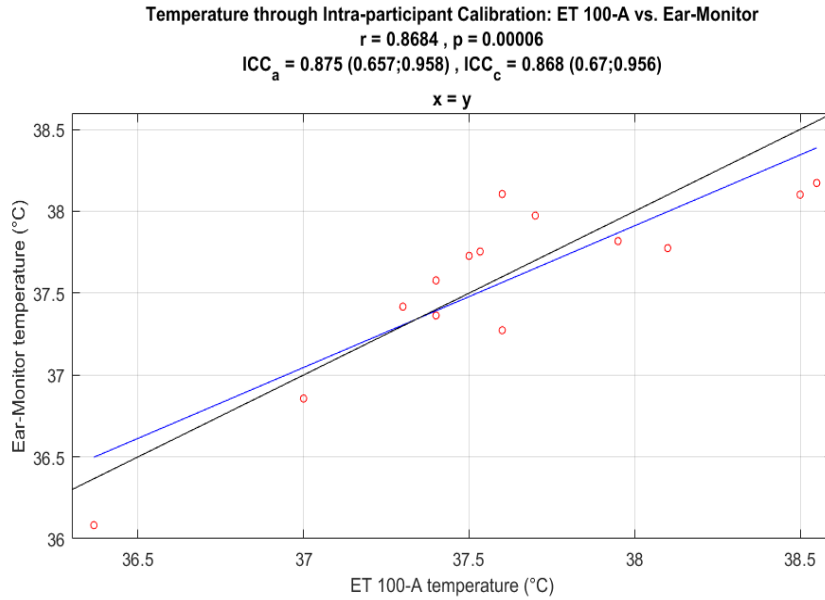


Figure 7.2: Temperature through the Intra-participant calibration method:  
ET 100-A vs. Ear-Monitor

### 7.1.3 Temperature Results Discussion

The measurements inside a recording session are close to one another, with a maximum standard deviation of  $0.0814^{\circ}\text{C}$ . This demonstrates the high precision of the TMP006, making it the right choice for an infrared sensor. This level of precision is owed to the thermal consistency inside the ear canal. Air flow is negligible and the position of objects in the sensor's field of vision stays constant.

The two different calibration methods can be compared through a box and whisker plot of their respective errors, as depicted in Figure 7.3. The superiority of the intra-participant calibration method can be observed in the smaller first and fourth quartiles. This indicates a significant reduction in large errors.

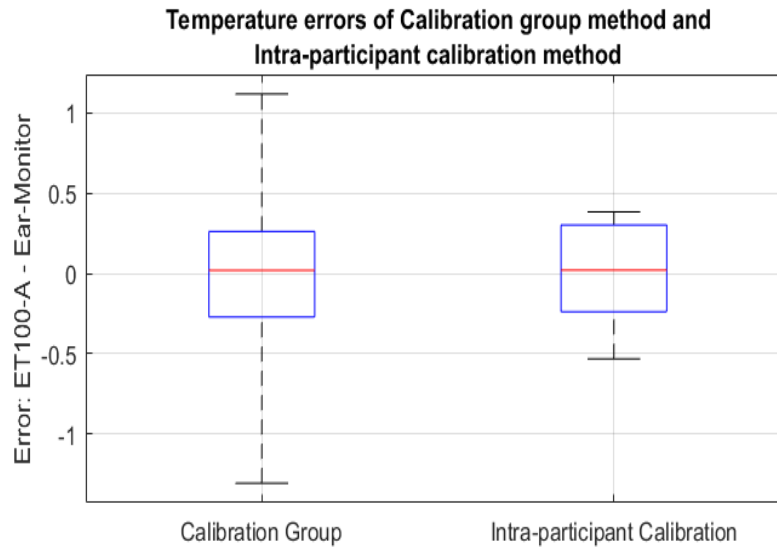


Figure 7.3: Temperature errors of the Group calibration and Intra-participant calibration methods

The 95% confidence intervals for  $ICC_a$  and  $ICC_c$  for the group calibration method includes zero, which means that the correlation is not significant. Whereas, the ICC intervals for the intra-participant calibration method is above zero, indicating good correlation. Furthermore, the p-value is far below 0.05, indicating a negligible probability of zero correlation. The data unanimously indicate that the intra-participant calibration method is superior to the group calibration method with regards to accuracy and correlation.

Although the intra-participant calibration method produces the best results, it should be kept in mind that this method requires a calibration sequences when it is used for the first time on an individual. The merit in the group calibration method lies in the fact that calibration is done only once, during manufacturing. With better probe design, the TMP006 can be located more consistently between different individuals and the group calibration method can become more accurate. But as it is now, the intra-participant calibration method is the preferred.

As mentioned in the literature review, there are not many published results of wearable ear temperature monitors to compare the Ear-Monitor to. There are, however, commercial devices available for comparison. The Novatemper<sup>®</sup> and Starboard<sup>®</sup> both claims a standard accuracy of  $\pm 0.2^\circ\text{C}$  (Novatemper, 2011; Starboard, 2016) and the Cosinuss Degree<sup>®</sup>, a standard accuracy of  $\pm 0.1^\circ\text{C}$  (Cosinuss, 2017b). The Ear-Monitor with intra-participant calibration comes close to this, with a standard accuracy of  $\pm 0.29^\circ\text{C}$ .

## 7.2 Heart Rate Results

The Ear-Monitor uses an infrared PPG obtained by the MAX30100 in the ear canal to detect heartbeats via a beat detection algorithm. The average period between 10 successive detected beats is used to calculate the heart rate. The beat detection algorithm is at the core of the heart rate functionality of the Ear-Monitor, and therefore it is evaluated independently. This is followed by comparative analysis between the individual beat periods and 10-beat moving average heart rates of the Ear-Monitor and Nexus-10 physiological monitor.

### 7.2.1 Beat Detection Algorithm Evaluation Results

The beat detection algorithm used by the Ear-Monitor is first tested on open source data from PhysioNet.org, and then on the data collected during the trial. The results of these two tests are discussed separately.

#### 7.2.1.1 PhysioNet Data Test

The beat detection algorithm is tested on PPG data from the open-source MIMIC Database on PhysioNet.org (Goldberger *et al.*, 2000). This data was recorded from patients in intensive care units and is made available for developing and testing intelligent monitoring systems. PPG data is recorded with clinical finger pulse oximeters. Ten-minute segments from 14 different patients are used to test the algorithm. Each set of data also includes an ECG signal, which is used to identify the benchmark beats. The results for this test can be seen in Appendix B.

Of the 12001 beats in all the PhysioNet test datasets, 13 (0.108%) false positives and 91 (0.758%) false negatives are detected. Even though the beat detection algorithm is designed and tuned using PPGs collected from the ear canal wall, it can accurately detect beats from finger pulse oximeters. This result demonstrates the robustness of the algorithm. Most false detections occurred where signals were corrupted by noise. This result also demonstrates how the SSF can extract beats, even from a noisy signal.

#### 7.2.1.2 Trial Data Test

Subsequently, the algorithm is tested using the data collected during the trial. The number of beats detected for each participant by the Ear-Monitor is compared to the number of benchmark beats. The supporting software for the Nexus-10, BioTrace+, has a peak detection algorithm, but it is found that it misses some peaks. To ensure accurate benchmark peak detection, the PPG from the Nexus-10 is inspected manually and peaks are marked by a human annotator. Figure 7.4 depicts plots of (a) the Ear-Monitor SSF with detected

beats and (b) the Nexus-10 PPG signal with annotated beats. In this example, 100% of the peaks are detected by Ear-Monitor.

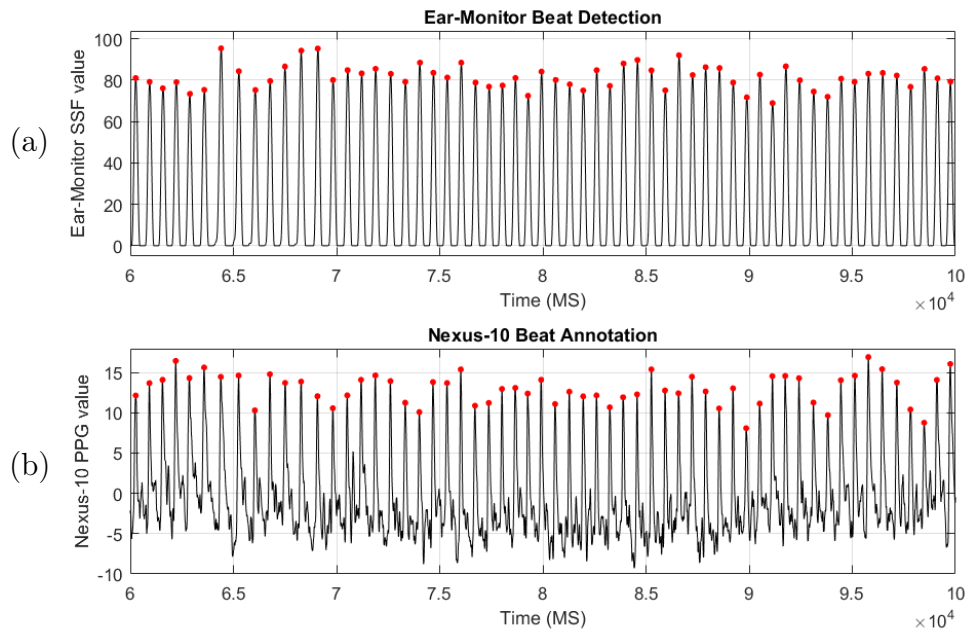


Figure 7.4: Plots of (a) the Ear-Monitor SSF with detected beats and (b) the Nexus-10 PPG signal with annotated beats

Appendix B tabulates the results of the beat detection evaluation. Of the 4713 beats in the participant trial data, 10 (0.21%) false positives and 58 (1.23%) false negatives are detected. The mean error of the sample group is  $-1.5313 \pm 2.8847$  beats. It should also be noted 51 of the false negatives (87.9%) are from the data collected from three of the participants: 5, 9 and 13.

Figure 7.5 depicts an ICC plot of the number of annotated Nexus-10 beats versus the number of detected Ear-Monitor beats. Data recording sessions from all 16 trial participants are used, which means 32 sets of data points are compared.

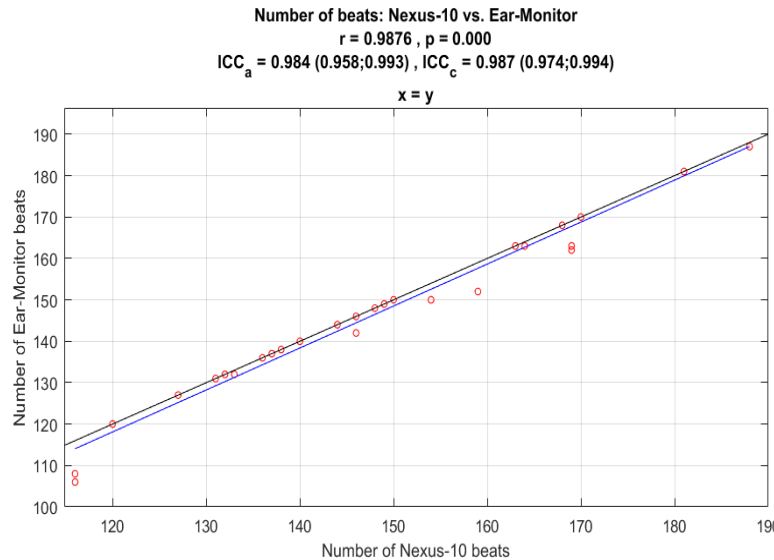


Figure 7.5: Number of beats: Nexus-10 vs. Ear-Monitor

This test demonstrates that the Ear-Monitor performs well in its task of detection beats. The number of false negatives detected for the trial data is higher than for the PhysioNet data. This can be ascribed to the fact that the PPG from three of the participants was of a notably lower quality. Although the adaptive threshold method detected the majority of the peaks, the amplitude of the SSF peaks varied prominently and very low amplitudes were missed by the algorithm. This can be caused by low blood profusion in the ear canal or bad contact between the MAX30100 and the canal wall.

### 7.2.2 Beat Period and Average Heart Rate Results

The accuracy of the heartbeat period is tested to determine if beats are detected at the right position in time. Periods between subsequent beats detected by the Ear-Monitor are compared to periods between beats annotated on the Nexus-10 PPG. Figure 7.6 depicts an ICC plot of Nexus-10 versus Ear-Monitor periods. A total of 4569 periods from the 16 participants is compared. Benchmark periods ranged from 575.65 to 1198 ms. The mean error of the sample group is  $0.0821 \pm 50.71$  ms.

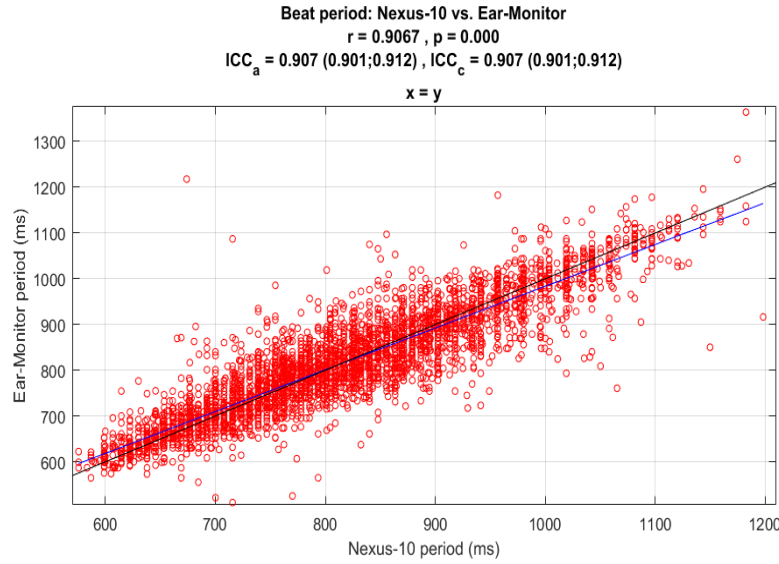


Figure 7.6: Beat period: Nexus-10 vs. Ear-Monitor

The 10-beat average heart rate is calculated from the Ear-Monitor and Nexus-10 data and compared in the same way as with the beat periods. Figure 7.7 depicts an ICC plot of Nexus-10 versus Ear-Monitor heart rates. A total of 4258 periods are compared from 16 participants with benchmark heart rates varying from 54.2 to 100.0 bpm. The mean error of the sample group is  $0.0306 \pm 0.7174$  bpm.

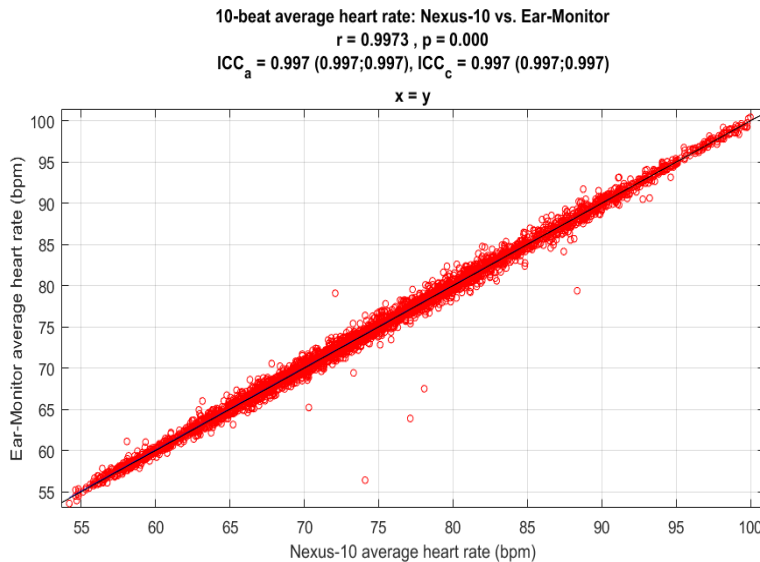


Figure 7.7: 10-beat average heart rate: Nexus-10 vs. Ear-Monitor

### 7.2.3 Heart Rate Results Discussion

The beat detection algorithm is evaluated based on PhysioNet data and data collected from participants during the trial. The algorithm performed better on the PhysioNet data than on the trial data. This can be ascribed to the fact that three of the participants contributed to 87.9% of the false negatives detected in the trial data. These are all participants with smaller external ears, which is emphasized by the fact that two of them are female. This highlights the effect the fit of the ear probe in the ear has on the accuracy of the beat detection algorithm. A bad fit causes non-ideal contact between the MAX30100 and the canal wall, as well as reducing subcutaneous blood perfusion. This is a patient specific inaccuracy and can be overcome by a more customised ear probe.

Even with these three individuals, the beat detection algorithm performs exceptionally good. On average  $1.5313 \pm 2.8847$  beats are missed per 2-minute recording session. The correlation of the number of beats detected between the Ear-Monitor and the benchmark device is high, with a correlation coefficient of 0.9876 and a p-value of zero. The  $ICC_a$  and  $ICC_c$  are both excellent within a 95% confidence interval.

The beat period ICC plot in Figure 7.6 depicts a clear correlation. The large number of data points reveals the normal distribution of the data. The correlation coefficient, p-value,  $ICC_a$  and  $ICC_c$  all indicate an excellent correlation. The Ear-Monitor can measure the period between heartbeats with a mean error of  $0.0821 \pm 50.71$  ms. This notably high accuracy is improved even further by calculating the 10-beat average heart rate. The ICC plot of the average heart rate in Figure 7.7 illustrates an exceptional correlation between the Ear-Monitor and benchmark measurements. The Ear-Monitor can measure the heart rate of participants with a mean error of  $0.0306 \pm 0.7174$  bpm relating to a 1.04% error at 72 bpm. This compares favourably to the commercial wrist worn heart rate monitors reviewed by Shcherbina *et al.* (2017).

## 7.3 Respiratory Rate Results

The Ear-Monitor uses respiratory sinus arrhythmia (RSA), the frequency modulating respiratory related heart rate characteristic, to extract a respiratory rate. The chest strap connected to the Nexus-10 physiological monitoring platform is used to measure the benchmark respiration rate. Benchmark breaths from the Nexus-10 are manually annotated. The recording session consisted of one minute of normal breathing followed by one minute of regulated breathing at 15 breaths per minute. Appendix B tabulates the results of the breaths detected for the 16 participants. Benchmark respiratory rates of the participants varied from 7 to 28 breaths per minute. The mean error is  $0.0156 \pm 3.9081$  breaths per minute.

It should be noted, however, that the majority of the inaccuracies can be traced to the recording sessions of participants 5, 9 and 13. Upon closer inspection, the following explanation can be given. Participant 5 and 13 both have a large number of false positives, the highest and third highest average heart rates and very low heartbeat period variation due to RSA. Participant 9 has an unusually high resting respiratory rate (more than double that of the average of the rest of the participants), bordering on the maximum measurable rate according to the Nyquist theorem, which is equal to half the heart rate. This caused 51% of breaths to be missed during normal breathing. As expected, when the respiratory rate was lowered during the controlled breathing exercise, the breath detection accuracy returned to the group average. These three participants are regarded as outliers and are isolated from the rest in order to reveal the trends present in the bulk of the recording sessions.

The mean errors in respiratory rate between the benchmark Nexus-10 and the Ear-Monitor can be seen in Table 7.1. Standard deviations are included and all values are in breaths per minute. When removing the outliers, the mean error of the normal and controlled breathing groups are closer to one another and the standard deviation of the errors are reduced by more than half.

Table 7.1: Mean errors of the respiratory rate measurements

Group	Outliers removed	Outliers included
Normal breathing	$-0.6154 \pm 1.6752$	$0.4375 \pm 4.9183$
Breathing exercise	$-0.5000 \pm 1.1045$	$-0.40625 \pm 2.4476$
All	$-0.5577 \pm 1.4061$	$0.0156 \pm 3.9081$

Figure 7.8 depicts an ICC plot of the Nexus-10 benchmark breaths versus the Ear-Monitor detected breaths. Triangles mark the number of breaths after 1 minute of normal breathing and circles mark the total number of breaths in the recording session, which includes the breathing exercise.

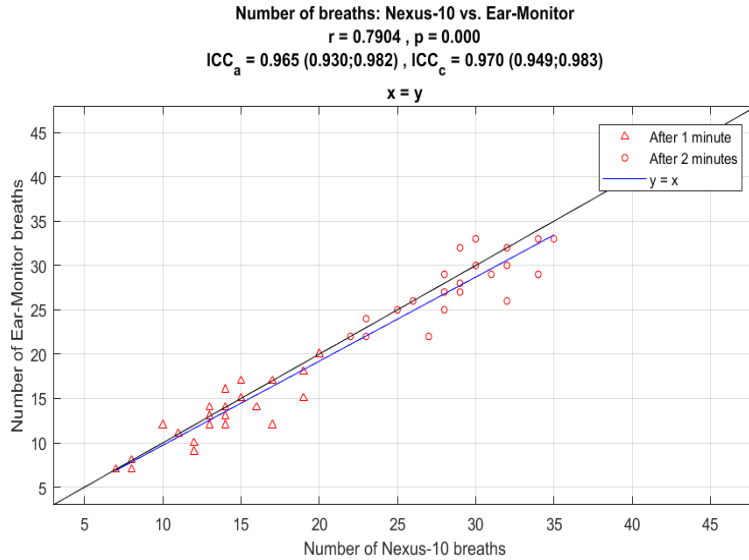


Figure 7.8: Number of breaths detected: Nexus-10 vs. Ear-Monitor  
(Excluding outliers)

### 7.3.1 Respiratory Rate Discussion

The breathing exercise was included in the trial, due to the uncertainty that the RSA will be visible during normal breathing. In general, participants started breathing deeper during the breathing exercise. This resulted in a more accurate detection of breaths.

During normal breathing, the standard deviation for the data from the breathing exercise is lower, however, the Ear-Monitor still measured normal respiratory rate better than expected. According to the trial data (excluding the outliers), the Ear-Monitors correlates with the benchmark device with a coefficient of 0.7604 and a p-value of zero.  $ICC_a$  and  $ICC_c$  indicate exceptional correlation agreement and consistency with in the 95% confidence interval. The Ear-Monitor is able to calculate the respiratory rate of a participant breathing normally to within a mean accuracy of -0.6154 breaths per minute with a standard deviation of 1.6752 breaths per minute (11.45% standard deviation at 15 breaths per minute). This is slightly worse, but comparable, to the 1 breath per minute accuracy from Clifton *et al.* (2007) and the 7.6% accuracy from Leonard *et al.* (2006). This can be ascribed to the fact that they used the more advanced approach of neural networks for detecting breaths from the RSA.

It can be seen that, on average, the Ear-Monitor detects a respiratory rate that is slightly lower ( $-0.5577 \pm 1.4060$  breaths per minute) than the actual rate. This means that the algorithm misses some breaths. This can be ascribed to intermittent shallower and shorter breaths that do not cause a big enough variation in heartbeat period.

The outliers are removed to emphasize the normal results, but they are not random and provide a valuable insight into the limitations of using RSA to measure respiratory rate. It can be stated that elevated heart rates (higher than 80 bpm in this trial) reduces the magnitude of RSA and causes the detection of false breaths. Also, if the breathing rate approaches half the heart rate (Nyquist theorem), the sampling frequency is too low and many breaths are missed by the detection algorithm. These results can be summarised by saying that respiratory rate measurement through RSA is most accurate at a combination of low heart and respiratory rates.

## 7.4 SpO<sub>2</sub> Results

The Ear-Monitor uses the MAX30100 pulse oximeter to measure the blood oxygen saturation of the tissue in the wall of the ear canal. One SpO<sub>2</sub> calculation is done every time the Ear-Monitor detects a heartbeat. The SureSigns VM1 from Philips is used to provide the benchmark SpO<sub>2</sub> measurement. The SureSigns VM1 samples at 1 Hz, resulting in 120 samples per recording session. As with temperature, the SpO<sub>2</sub> of a participant is assumed to stay constant over the duration of the 2-minute recording session. Therefore, the average of the SureSigns VM1 measurements and Ear-Monitor measurements are compared for each recording session.

All trial participants are in good health and benchmark SpO<sub>2</sub> levels ranged between 96.38 and 100 %. The measurements from the Ear-Monitor varied between 96.27 and 100%. The mean error between the SureSigns VM1 and Ear-Monitor measurements is  $-0.22 \pm 1.50\%$ . When plotting the Ear-Monitor and SureSigns VM1 measurements, no significant correlation is observed. This plot can be seen in Figure 7.9.

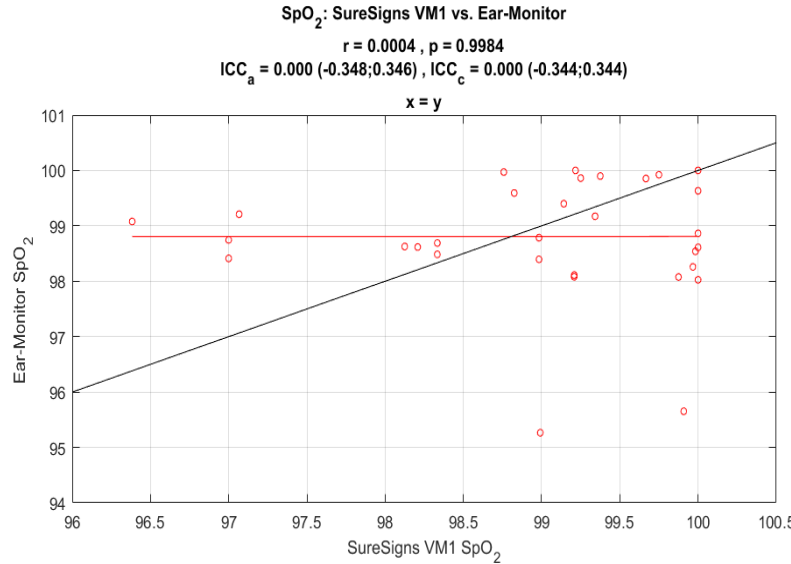


Figure 7.9: SpO<sub>2</sub>: SureSigns VM1 vs. Ear-Monitor

#### 7.4.1 SpO<sub>2</sub> Results Discussion

Analysing the trial data, it is calculated that the Ear-Monitor can measure SpO<sub>2</sub> in healthy individuals, with a mean error of  $-0.22 \pm 1.50\%$ .

However, because of the insignificant correlation, it can not be proven that this accuracy will continue if individuals with lower SpO<sub>2</sub> levels are monitored. An attempt was made to induce hypoxia during pilot testing by holding the breath. However, this did not cause a detectable change in SpO<sub>2</sub> measurements by the Ear-Monitor or SureSigns VM1. Clarity about the SpO<sub>2</sub> performance of the Ear-Monitor can be obtained by testing it on hypoxic patients, but testing on unhealthy individuals is not within the scope of this project.

The SpO<sub>2</sub> calculation method relies on the difference in the detected red and infrared light. According to the relationship found in literature, the magnitude of the infrared PPG should be higher than that of the red PPG (Oak and Aroul, 2015; Stroganovs, 2017). This can be observed in all the data recorded by the Ear-Monitor. If the wearer's SpO<sub>2</sub> decreases, the difference between the infrared and red PPGs should decrease, resulting in a higher SpO<sub>2</sub> modulation ratio (R) and, according to Equation 2.6, a lower calculated SpO<sub>2</sub> value. This can not be observed in the trial data. The most probable reason is that the relationship is obscured by the inherent margin of error in pulse oximeters. The SpO<sub>2</sub> benchmark of the group is constant, meaning there is not a big enough variation in SpO<sub>2</sub> among individuals to be detected by the Ear-Monitor.

The lack of correlation within the testing range of values does not prove that the Ear-Monitor fails to measure SpO<sub>2</sub> accurately. Within the trial group,

$\text{SpO}_2$  measurements all indicated participants are above the 95% mark required for healthy adults. This is the same result as found by Aziz *et al.* (2006). Future testing can include hypoxic subjects and comparison with a blood gas test.

## 7.5 Results Summary

The statistical analysis values for the trial data is summarised in Table 7.2.

Table 7.2: Summary of Statistical Results

Vital Sign	Mean Error	Correlation coefficient	p-value	ICC <sub>a</sub>	ICC <sub>c</sub>
Temperature Group Calibration	0.018 ±0.513	0.467	0.014	0.374 (-0.01;0.66)	0.365 (-0.01;0.65)
Temperature Intra-participant Calibration	-0.016 ±0.290	0.868	0	0.875 (0.66;0.96)	0.868 (0.67;0.96)
Heart Rate	0.031 ±0.717	0.997	0	0.997 (0.99;0.99)	0.997 (0.99;0.99)
Respiratory Rate	-0.558 ±1.406	0.790	0	0.965 (0.93;0.98)	0.97 (0.95;0.98)
SpO	-0.22 ±1.50	0	0.998	0 (-0.35;0.35)	0 (-0.34;0.34)

# Chapter 8

## Conclusion

This document reports on the development and evaluation of the Ear-Monitor, a wireless device that monitors multiple vital signs through the external ear. Vital signs include core temperature, heart rate, respiratory rate and blood oxygen saturation ( $\text{SpO}_2$ ). The motivation for this project is the need for a wearable device that can continuously and inconspicuous monitor the health of the wearer while not constraining movement. Three objectives are set to guide the project towards reaching the aim:

- Develop a device to measure core temperature, heart rate, respiratory rate and blood oxygen saturation through the external ear of the wearer.
- Conduct a trial experiment to test the device on a sample of human participants.
- Use the data collected from the trial to evaluate the accuracy of the measurements made by the device.

This section aims to clarify to what extent these objectives are achieved. Attention is also given to the findings regarding the measurement of each vital sign and suggestions for future work.

### 8.1 Device development

The Ear-monitor uses the TMP006 infrared sensor to measure tympanic temperature. The MAX10300 pulse oximeter is used, along with a beat detection algorithm, to measure heart rate and  $\text{SpO}_2$ . Respiratory rate is measured through analysing respiratory sinus arrhythmia, the frequency modulation respiratory related heart rate characteristic. The MCU, battery and Bluetooth modem are located in a headband around the wearers head. A PCB is designed and manufactured to integrate all the electronic components in the headband. Sensors are located on a silicone ear probe that is connected the headband

and placed in the external ear of the wearer. Collected data is sent through the wireless Bluetooth connection to a computer. Software is developed for the computer to analyse the data, calculated the vital sign values, display the information through a graphical user interface and stores the data for later use.

## 8.2 Experimental Trial

A trial is designed and conducted to test the Ear-Monitor on a sample of human participants. Each vital sign measured by the Ear-Monitor is compared to measurements made by selected benchmark devices. 16 participants are recruited for the trial. Data is collected from each participant in two 2-minute recording sessions.

## 8.3 Data Analysis and Results

The data captured by the Ear-Monitor and various benchmark devices are compared one vital sign at a time. The Ear-Monitor is evaluated in terms of accuracy and correlation with the benchmark measurements.

### 8.3.1 Core Temperature

The TMP006 proves to be a precise sensor, making 15 consecutive measurements within a recording session with a mean standard deviation of  $0.0814^{\circ}\text{C}$ . Two calibration approaches are tested. Group calibration produced a statistically weak correlation with the benchmark ET 100-A ( $r = 0.467$ ,  $\text{ICC}_a = 0.374$ ,  $\text{ICC}_c = 0.365$ ). Changing the calibration approach to intra-participant calibration, improved the correlation considerably ( $p = 0$ ,  $r = 0.868$ ,  $\text{ICC}_a = 0.875$ ,  $\text{ICC}_c = 0.868$ ). These results indicate that the Ear-Monitor is capable of measuring consistent and accurate temperature, assuming that it is calibrated to the ear of the individual. This is due to the variation in ear canal shape and size between individuals. This leads to the conclusion that, in order to improve core temperature measurements further, an ear probe is needed that can place the TMP006 in the same position relative to the tympanic membrane between individuals, regardless of differences in external ear shape and size.

### 8.3.2 Heart Rate

The Ear-Monitor can detect heartbeats in the data captured by the MAX10300 by means of a beat detection algorithm. Beats are detected from trial data with a mean error of  $-1.5313 \pm 2.8847$  per 2-minute recording sessions. When comparing beat period length between the Ear-Monitor and the Nexus-10, a statistical significant correlation is found ( $p = 0$ ,  $r = 0.9067$ ,  $\text{ICC}_a = 0.907$ ,

$ICC_c = 0.907$ ). The 10-beat average heart rate is calculated from the beat period and the results show that the Ear-Monitor can measure heart rate with a mean error of  $0.031 \pm 0.717$  bpm. Excellent correlation is found between the average heart rate of the Ear-Monitor and the Nexus-10 ( $p = 0, r = 0.997$ ,  $ICC_a = 0.997$ ,  $ICC_c = 0.997$ ). This leads to the conclusion that the Ear-Monitor succeeds aptly in the task of measuring the heart rate of the wearer.

### 8.3.3 Respiratory Rate

Respiratory sinus arrhythmia (RSA) is used by the Ear-Monitor to calculate the respiratory rate of the wearer. The results from the trial data lead to a mean accuracy of  $0.0156 \pm 3.9081$  breaths per minute. It is observed that most of the inaccuracy is from the recording sessions of three of the participants. Upon closer inspection, it is noted that these participants had either a high heart rate or high respiratory rate. Two deductions are made from this finding. Firstly, the effects of RSA is attenuated by a high heart rate. And secondly, a respiratory rate approaching half the heart rate causes many false negatives due to the Nyquist sampling limit. This leads to the conclusion that respiratory rate measurement through RSA is most effective at low heart and respiratory rates. Removing the 3 outlier participants gives the Ear-Monitor an accuracy of -0.5577 breaths per minute with a greatly reduced standard deviation of 1.4061 breaths per minute.

### 8.3.4 SpO<sub>2</sub>

The MAX30100 is used to collect the data used to calculate SpO<sub>2</sub>. A modulation ratio between red and infrared AC and DC components of the PPG signals collected from the ear canal wall is used. The mean error between the Ear-Monitor and SureSigns VM1 benchmark device is  $-0.22 \pm 1.50\%$ . This is a good accuracy within the testing range. The Ear-Monitor also indicates that all participants are healthy, with a SpO<sub>2</sub> of above 95%, which is correct. However, the ICC analysis reveals no statistically significant correlation. Therefore, no predictions can be made about the accuracy of measurements made by the Ear-Monitor when the wearer has a SpO<sub>2</sub> of lower than 96%. The lack of correlation can be ascribed to the inherent variability in pulse oximeter measurements.

## 8.4 Suggestions for Future Work

As a whole, the Ear-Monitor achieved all of its objectives. However, there is an opportunity for improvements and additions in future versions.

Firstly, research can be done regarding an ear probe that better conforms to different ear shapes. It should place the infrared sensor in the same po-

sition relative to the tympanic membrane, regardless of the ear canal shape of the wearer. Analysis of the trial data suggests that will greatly improve the accuracy of the core temperature measurements. Furthermore, the probe should ensure uniform contact between the MAX30100 and the canal wall, even for smaller ear canal shapes. Considerations for the probe should include material, shape and different sizes.

Secondly, a more extensive trial can be done to test the Ear-Monitor. More participants can be tested, including hypoxic patients, to more test the SpO<sub>2</sub> capabilities of the Ear-Monitor more thoroughly. The benchmark measurements from the SureSigns VM1 should be replaced or supplemented by a blood gas test for more accurate benchmarking.

Finally, the vital signs measurement capabilities can be extended to include the monitoring of electrical brain activity and can research can be done into monitoring blood pressure through the ear canal. Diagnostic algorithms can be added to the supporting system on the computer and alarms can be triggered when health warning signs are detected.

## 8.5 Conclusion

Overall, the Ear-Monitor project is a success. The functional device and supporting software prove that it is possible for a wearable device to collect vital signs from the external ear and transmit data over a wireless connection to a nearby computer. Core temperature, heart rate, and respiratory rate are measured with sufficient accuracy, while SpO<sub>2</sub> was measured, but no significant correlation was found with the benchmark measurements, and further testing is needed. This Ear-Monitor project adds valuable academic information to the body of knowledge concerning wearable vital sign monitoring through the external ear and lays the groundwork towards a commercial medical device.

# Appendices

# Appendix A

## Calculations

### A.1 Ear-Monitor power supply

# Appendix B

## Proof of Ethical Approval

# Appendix C

## Data Tables

### C.1 Temperature Results

The calibration group method is labelled and A and the intra-participant calibration method as B. The temperature values are recording session averages with standard errors indicated in brackets. All values are in °C.

Table C.1: Summary of the temperature results

Participant No.	ET 100-A Temp	Ear-Monitor Temp A	Error A	Ear-Monitor Temp B	Error B	Ear-Monitor standard error
2a	36.33	37.63	-1.29	-	-	±0.0043
2b	36.37	37.57	-1.21	36.08	0.28	±0.0017
3a	37.65	37.54	0.11	-	-	±0.0031
3b	37.40	37.67	-0.27	37.58	-0.18	±0.0172
4a	38.30	37.37	0.93	-	-	±0.0012
4b	38.55	37.44	1.11	38.17	0.38	±0.0014
6a	38.35	37.80	0.55	-	-	±0.0032
6b	37.60	37.76	-0.16	38.11	-0.51	±0.0015
7a	37.03	37.31	-0.28	-	-	±0.0008
7b	37.00	37.34	-0.34	36.86	0.14	±0.0016
8a	38.40	38.13	0.27	-	-	±0.0072
8b	38.50	38.03	0.47	38.10	0.40	±0.0009
9a	37.55	37.53	0.02	-	-	±0.0005
9b	37.40	37.54	-0.14	37.36	0.04	±0.0007
10a	37.95	37.70	0.25	-	-	±0.0031
10b	38.10	37.73	0.37	37.77	0.33	±0.0007
11a	37.50	37.52	-0.02	-	-	±0.0006
11b	37.60	37.50	0.10	37.27	0.33	±0.0051
12a	38.50	38.51	-0.01	-	-	±0.021

12b	37.70	38.18	-0.48	37.97	-0.27	$\pm 0.0028$
13a	38.05	38.02	0.03	-	-	$\pm 0.012$
13b	37.53	37.92	-0.39	37.75	-0.22	$\pm 0.0016$
14a	38.00	37.73	0.27	-	-	$\pm 0.001$
14b	37.95	37.75	0.20	37.82	0.13	$\pm 0.0004$
15a	37.65	37.58	0.07	-	-	$\pm 0.0033$
15b	37.30	37.55	-0.25	37.42	-0.12	$\pm 0.0008$
16a	37.90	37.90	0.00	-	-	$\pm 0.0016$
16b	37.50	37.93	-0.43	37.73	-0.23	$\pm 0.0038$

## C.2 PhysioNet Beat Detection Results

Table C.2: Results of the beat detection algorithm on the PhysioNet data

Record No.	Actual No. Beats	False Positives	False negatives
039	1337	0	0
041	1030	1	7
055	1021	0	0
211	891	2	8
212	845	0	15
216	763	0	1
218	697	0	1
219	720	0	0
221	776	0	4
224	863	0	0
230	871	7	36
237	777	2	17
240	816	1	2
252	594	0	0

Table C.3: Results of the beat detection algorithm on the PhysioNet data

Participant No.	No. Nexus-10 Beats	No. Ear-Monitor Beats	False Positives	False Negatives	%
1a	150	150	0	0	100
1b	148	148	0	0	100
2a	116	108	2	10	93.1
2b	116	106	1	11	91.4
3a	136	136	0	0	100
3b	138	138	0	0	100
4a	132	132	0	0	100
4b	133	132	0	1	99.2
5a	181	181	0	0	100
5b	188	187	0	1	99.5
6a	120	120	0	0	100
6b	127	127	0	0	100
7b	144	144	0	0	100
7c	140	140	0	0	100
8a	163	163	0	0	100
8b	164	163	0	1	99.4
9a	149	149	0	0	100
9b	146	142	0	4	97.3
10a	146	146	0	0	100
10c	146	146	0	0	100
11a	131	131	0	0	100
11b	131	131	0	0	100
12a	144	144	0	0	100
12b	137	137	0	0	100
13a	169	163	0	6	96.45
13b	169	162	0	7	95.86
14a	168	168	0	0	100
14b	170	170	0	0	100
15a	149	149	0	0	100
15c	149	149	0	0	100
16a	154	151	1	4	98.05
16b	159	152	6	13	95.6

### C.2.1 Respiratory Rate Results

Table C.4: Summery of breaths recorded during each recording session

Participant No.	No. Nexus-10 Breaths	No. Ear-Monitor Breaths	Error
1a	30	30	0
1b	23	22	1
2a	27	22	5
2b	27	22	5
3a	28	25	3
3b	25	25	0
4a	28	29	-1
4b	28	27	1
5a	24	33	-9
5b	24	44	-20
6a	34	29	5
6b	32	30	2
7b	28	29	-1
7c	26	26	0
8a	29	27	2
8b	29	32	-3
9a	42	31	11
9b	43	29	14
10a	31	29	2
10b	32	32	0
11a	29	28	1
11b	29	28	1
12a	32	26	6
12b	34	33	1
13a	30	39	-9
13b	28	43	-15
14a	22	22	0
14b	23	24	-1
15a	32	32	0
15c	30	33	-3
16a	29	28	1
16b	35	33	2

### C.2.2 Ball mass and inertia parameters

Consider a volume element  $dV$  with respect to a static base  $S$  of an arbitrary solid body with density  $\rho$ . The mass of the body is obtained by integrating

over the volume of the body,

$$m = \int_{\text{body}} \rho dV \quad (\text{C.1})$$

In figure C.1, a ball with radius  $R_i$  and uniform density  $\rho_i$  is depicted. The mass of the ball is after integration of equation (C.1)

$$m_i = \frac{4}{3}\pi\rho_i R_i^3. \quad (\text{C.2})$$

# Appendix D

## Discrete Element Method Theory

### D.1 Ball elements

#### D.1.1 Ball mass and inertia parameters

Consider a volume element  $dV$  with respect to a static base  $S$  of an arbitrary solid body with density  $\rho$ . The mass of the body is obtained by integrating over the volume of the body,

$$m = \int_{\text{body}} \rho dV \quad (\text{D.1})$$

In figure C.1, a ball with radius  $R_i$  and uniform density  $\rho_i$  is depicted. The mass of the ball is after integration of equation (C.1)

$$m_i = \frac{4}{3}\pi\rho_i R_i^3. \quad (\text{D.2})$$

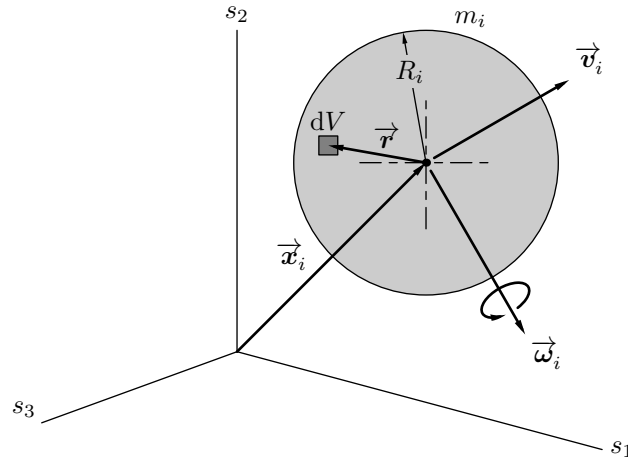


Figure D.1: Ball Element Parameters

# List of References

- Alvord, L.S. and Farmer, B.L. (1997). Anatomy and orientation of the human external ear. *Journal-American academy of audiology*, vol. 8, pp. 383–390.
- Aoyagi, T. (2003). Pulse oximetry: its invention, theory, and future. *Journal of anesthesia*, vol. 17, no. 4, pp. 259–266.
- Aziz, O., Lo, B., King, R., Darzi, A. and Yang, G.-Z. (2006). Pervasive body sensor network: an approach to monitoring the post-operative surgical patient. In: *Wearable and Implantable Body Sensor Networks, 2006. BSN 2006. International Workshop on*, pp. 4–pp. IEEE.
- Bagha, S. and Shaw, L. (2011). A real time analysis of ppg signal for measurement of spo2 and pulse rate. *International journal of computer applications*, vol. 36, no. 11, pp. 45–50.
- Barfield, W., Papile, L., Baley, J. *et al.* (2012). American academy of pediatrics committee on fetus and newborn. *Levels of neonatal care. Pediatrics*, vol. 130, no. 3, pp. 587–597.
- Bheema lingaiah, T., Hanumesh Kumar, D. and Nagaraja, C. (2013). Measurement of pulse rate and spo2 using pulse oximeter developed using labview. *Journal of Electrical and Electronics Engineering*, vol. 8.
- Blahd, W. (2016 09). Mebmd sleep apnea.  
Available at: <http://www.webmd.com/sleep-disorders/sleep-apnea/sleep-apnea>
- Bragi (2017). Meet the dash pro.  
Available at: <https://www.bragi.com/thedashpro/>
- Buske, O., Neils, C. and Regnier, M. (2009). Heartbeat: Design and development of a headphone.
- Chan, E.D., Chan, M.M. and Chan, M.M. (2013). Pulse oximetry: understanding its basic principles facilitates appreciation of its limitations. *Respiratory medicine*, vol. 107, no. 6, pp. 789–799.
- Chan, V. and Underwood, S. (2005 11). *A Single-Chip Pulsoximeter Design Using the MSP430*. Texas Instruments. Rev. Feb 2012.

- Charbek, E. (2015 08). Medscape normal vital signs.  
Available at: <http://emedicine.medscape.com/article/2172054-overview>
- Cicchetti, D.V. (1994). Guidelines, criteria, and rules of thumb for evaluating normed and standardized assessment instruments in psychology. *Psychological assessment*, vol. 6, no. 4, p. 284.
- Clifton, D., Douglas, J.G., Addison, P.S. and Watson, J.N. (2007). Measurement of respiratory rate from the photoplethysmogram in chest clinic patients. *Journal of clinical monitoring and computing*, vol. 21, no. 1, pp. 55–61.
- Cosinuss (2017a). Cosinuss one.  
Available at: <https://www.cosinuss.com/en/products/one>
- Cosinuss (2017b). Degreee.  
Available at: <https://www.degreee-fever-assistant.com/>
- Da He, D., Winokur, E.S., Heldt, T. and Sodini, C.G. (2010). The ear as a location for wearable vital signs monitoring. In: *Engineering in Medicine and Biology Society (EMBC), 2010 Annual International Conference of the IEEE*, pp. 6389–6392. IEEE.
- DeMeulenaere, S. (2007). Pulse oximetry: uses and limitations. *The Journal for Nurse Practitioners*, vol. 3, no. 5, pp. 312–317.
- DerSarkissian, C. (2016). Flu or cold symptoms?  
Available at: <http://www.webmd.com/cold-and-flu/cold-guide/flu-cold-symptoms>
- Duun, S., Haahr, R.G., Birkelund, K., Raahauge, P., Petersen, P., Dam, H., Nørgaard, L. and Thomsen, E.V. (2007). A novel ring shaped photodiode for reflectance pulse oximetry in wireless applications. In: *Sensors, 2007 IEEE*, pp. 596–599. IEEE.
- Elgendi, M., Norton, I., Brearley, M., Abbott, D. and Schuurmans, D. (2013). Systolic peak detection in acceleration photoplethysmograms measured from emergency responders in tropical conditions. *PLoS One*, vol. 8, no. 10, p. e76585.
- Encyclopædia Britannica, T.E. (2015 01). External auditory canal.  
Available at: <https://global.britannica.com/science/external-auditory-canal>
- Encyclopædia Britannica, T.E.O. (2009). Spectrophotometry.  
Available at: <https://www.britannica.com/science/spectrophotometry>
- Erickson, R.S. and Kirklin, S.K. (1993). Comparison of ear-based, bladder, oral, and axillary methods for core temperature measurement. *Critical care medicine*, vol. 21, no. 10, pp. 1528–1534.
- Fahy, B., Lareau, S. and Sockrider, M. (2011). Pulse oximetry. *American Journal of Respiratory and Critical Care Medicine*, vol. 184.

- Gasim, G.I., Musa, I.R., Abdien, M.T. and Adam, I. (2013). Accuracy of tympanic temperature measurement using an infrared tympanic membrane thermometer. *BMC research notes*, vol. 6, no. 1, p. 194.
- Goldberger, A.L., Amaral, L.A.N., Glass, L., Hausdorff, J.M., Ivanov, P.C., Mark, R.G., Mietus, J.E., Moody, G.B., Peng, C.-K. and Stanley, H.E. (2000). PhysioBank, PhysioToolkit, and PhysioNet: Components of a new research resource for complex physiologic signals. *Circulation*, vol. 101, no. 23, pp. e215–e220. Circulation Electronic Pages: <http://circ.ahajournals.org/content/101/23/e215.full> PMID:1085218; doi: 10.1161/01.CIR.101.23.e215.
- Goverdovsky, V., von Rosenberg, W., Nakamura, T., Looney, D., Sharp, D.J., Papavassiliou, C., Morrell, M.J. and Mandic, D.P. (2016). Hearables: Multimodal physiological in-ear sensing. *arXiv preprint arXiv:1609.03330*.
- Holland, K. (2016 09). Thermoregulation.  
Available at: <http://www.healthline.com/health/thermoregulation#overview1>
- Huang, C.-Y., Chan, M.-C., Chen, C.-Y. and Lin, B.-S. (2014). Novel wearable and wireless ring-type pulse oximeter with multi-detectors. *Sensors*, vol. 14, no. 9, pp. 17586–17599.
- Johansson, A. (2003). Neural network for photoplethysmographic respiratory rate monitoring. *Medical and Biological Engineering and Computing*, vol. 41, no. 3, pp. 242–248.
- Jones, D. (2010). *Biomedical Sensors*. Sensor technology series. Momentum Press. ISBN 9781606500569.  
Available at: <https://books.google.co.za/books?id=7cI83Y0IUTkC>
- Karaki, H. and Polyziev, V. (2014). Demystifying thermopile ir temp sensors.  
Available at: <http://www.sensorsmag.com/components/demystifying-thermopile-ir-temp-sensors>
- Karriem-Norwood, V. (2017). Stress symptoms.  
Available at: <http://www.webmd.com/balance/stress-management/stress-symptoms-effects-of-stress-on-the-body>
- Kennedy, S.M. (2015). An introduction to pulse oximeters: Equations and theory. *University of Wisconsin-Madison*, vol. 20.
- Khalifa, O.O., Khan, T. and HM, H. (2014). Development of wearable pulse oximetry for telehealth monitoring system. *Journal of Electrical Engineering*, vol. 14, no. 4, pp. 1–6.
- Koblenksi, S. (2015). Everyday dsp for programmers: Dc and impulsive noise removal.  
Available at: <http://sam-koblenksi.blogspot.co.za/2015/11/everyday-dsp-for-programmers-dc-and.html>

- König, V., Huch, R. and Huch, A. (1998). Reflectance pulse oximetry—principles and obstetric application in the zurich system. *Journal of Clinical Monitoring and Computing*, vol. 14, no. 6, pp. 403–412.
- Laskowski, E.R. (2015). What's a normal resting heart rate? Available at: <http://www.mayoclinic.org/healthy-lifestyle/fitness/expert-answers/heart-rate/faq-20057979>
- Lee, H., Ko, H. and Lee, J. (2016). Reflectance pulse oximetry: Practical issues and limitations. *ICT Express*, vol. 2, no. 4, pp. 195–198.
- Lefrant, J.-Y., Muller, L., de La Coussaye, J.E., Benbabaali, M., Lebris, C., Zeitoun, N., Mari, C., Saissi, G., Ripart, J. and Eledjam, J.-J. (2003). Temperature measurement in intensive care patients: comparison of urinary bladder, oesophageal, rectal, axillary, and inguinal methods versus pulmonary artery core method. *Intensive care medicine*, vol. 29, no. 3, pp. 414–418.
- Leonard, P.A., Douglas, J.G., Grubb, N.R., Clifton, D., Addison, P.S. and Watson, J.N. (2006). A fully automated algorithm for the determination of respiratory rate from the photoplethysmogram. *Journal of clinical monitoring and computing*, vol. 20, no. 1, pp. 33–36.
- Lin, B.-S., Chou, W., Wang, H.-Y., Huang, Y.-J. and Pan, J.-S. (2013). Development of novel non-contact electrodes for mobile electrocardiogram monitoring system. *IEEE journal of translational engineering in health and medicine*, vol. 1, pp. 1–8.
- Louw, A., Cracco, C., Cerf, C., Harf, A., Duvaldestin, P., Lemaire, F. and Brochard, L. (2001). Accuracy of pulse oximetry in the intensive care unit. *Intensive care medicine*, vol. 27, no. 10, pp. 1606–1613.
- Mayo Clinic (2017). Pneumonia. Available at: <http://www.mayoclinic.org/diseases-conditions/pneumonia>
- Moody, G.B., Mark, R.G., Bump, M.A., Weinstein, J.S., Berman, A.D., Mietus, J.E. and Goldberger, A.L. (1986). Clinical validation of the ecg-derived respiration (edr) technique. *Group*, vol. 1, no. 3.
- Nitzan, M., Noach, S., Tobal, E., Adar, Y., Miller, Y., Shalom, E. and Engelberg, S. (2014). Calibration-free pulse oximetry based on two wavelengths in the infrared—a preliminary study. *Sensors*, vol. 14, no. 4, pp. 7420–7434.
- Novatemper (2011). Accuracy is key for tympanic temperature monitoring. Available at: [http://www.novamed-usa.com/tympanic\\_temperature\\_sensors.html](http://www.novamed-usa.com/tympanic_temperature_sensors.html)
- Oak, S. and Aroul, P. (2015 3). *How to Design Peripheral Oxygen Saturation ( $SpO_2$ ) and Optical Heart Rate Monitoring (OHRM) Systems Using the AFE4403*. Texas Instruments.
- Olive, S., Twentyman, O. and Ramsay, C. (2016). Comparison of fingertip and earlobe pulse oximetry with arterial blood gas results.

- Optotherm (2017). Emissivity table.  
Available at: <http://www.optotherm.com/emiss-table.htm>
- Park, J.-H., Jang, D.-G., Park, J.W. and Youm, S.-K. (2015). Wearable sensing of in-ear pressure for heart rate monitoring with a piezoelectric sensor. *Sensors*, vol. 15, no. 9, pp. 23402–23417.
- Pearce, J. (2002). A brief history of the clinical thermometer. *Qjm*, vol. 95, no. 4, pp. 251–252.
- Poh, M.-Z., Swenson, N.C. and Picard, R.W. (2010). Motion-tolerant magnetic earring sensor and wireless earpiece for wearable photoplethysmography. *IEEE Transactions on Information Technology in Biomedicine*, vol. 14, no. 3, pp. 786–794.
- Prawiro, E.A.P.J., Yeh, C.-I., Chou, N.-K., Lee, M.-W. and Lin, Y.-H. (2016). Integrated wearable system for monitoring heart rate and step during physical activity. *Mobile Information Systems*, vol. 2016.
- Pujary, C., Savage, M. and Mendelson, Y. (2003). Photodetector size considerations in the design of a noninvasive reflectance pulse oximeter for telemedicine applications. In: *Bioengineering Conference, 2003 IEEE 29th Annual, Proceedings of*, pp. 148–149. IEEE.
- Shcherbina, A., Mattsson, C.M., Waggott, D., Salisbury, H., Christle, J.W., Hastie, T., Wheeler, M.T. and Ashley, E.A. (2017). Accuracy in wrist-worn, sensor-based measurements of heart rate and energy expenditure in a diverse cohort. *Journal of personalized medicine*, vol. 7, no. 2, p. 3.
- Shin, K., Kim, Y., Bae, S., Park, K. and Kim, S. (2009). A novel headset with a transmissive ppg sensor for heart rate measurement. In: *13th International Conference on Biomedical Engineering*, pp. 519–522. Springer.
- Sinex, J.E. (1999). Pulse oximetry: principles and limitations. *The American journal of emergency medicine*, vol. 17, no. 1, pp. 59–66.
- ST Electronics (2016a). Mems digital output motion sensor ultra low-power high full-scale 3-axes "nano" accelerometer.  
Available at: <https://www.sparkfun.com/datasheets/Sensors/Accelerometer/LIS331HH.pdf>
- ST Electronics (2016b). Mems audio sensor omnidirectional digital microphone.  
Available at: <http://www.st.com/content/ccc/resource/technical/document/datasheet/group3/10/65/67/7c/98/c2/4b/69/DM00333876/files/DM00333876.pdf/jcr:content/translations/en.DM00333876.pdf>
- Starboard (2016). Tympanic temperature sensors.  
Available at: <http://starboardmedical.com/tympanic-temperature-sensors/>

- Stratton, J.R., Levy, W.C., Caldwell, J.H., Jacobson, A., May, J., Matsuoka, D. and Madden, K. (2003). Effects of aging on cardiovascular responses to parasympathetic withdrawal. *Journal of the American College of Cardiology*, vol. 41, no. 11, pp. 2077–2083.
- Strogonovs, R. (2017 03). Implementing pulse oximeter using max30100. Available at: <https://morf.lv/implementing-pulse-oximeter-using-max30100>
- Stumme, L.D., Baldini, T.H., Jonassen, E.A. and Bach, J.M. (2003). Emissivity of bone. In: *Summer Bioengineering Conference*, pp. 25–29.
- Sund-Levander, M., Forsberg, C. and Wahren, L.K. (2002). Normal oral, rectal, tympanic and axillary body temperature in adult men and women: a systematic literature review. *Scandinavian journal of caring sciences*, vol. 16, no. 2, pp. 122–128.
- Tamura, T., Maeda, Y., Sekine, M. and Yoshida, M. (2014). Wearable photoplethysmographic sensors-past and present. *Electronics*, vol. 3, no. 2, pp. 282–302.
- Tavakoli Dastjerdi, M. (2006). *An analog VLSI front end for pulse oximetry*. Ph.D. thesis, Massachusetts Institute of Technology.
- Thach, B. (2008). Tragic and sudden death. *EMBO reports*, vol. 9, no. 2, pp. 114–118.
- ThermoWorks (). Emissivity table. Available at: [http://www.thermoworks.com/learning/emissivity\\_table](http://www.thermoworks.com/learning/emissivity_table)
- Tytler, J. and Seeley, H. (1986). The nellcor n-101 pulse oximeter. *Anaesthesia*, vol. 41, no. 3, pp. 302–305.
- Wang, I.-J., Liao, L.-D., Wang, Y.-T., Chen, C.-Y., Lin, B.-S., Lu, S.-W. and Lin, C.-T. (2010). A wearable mobile electrocardiogram measurement device with novel dry polymer-based electrodes. pp. 379–384.
- Watthanawisuth, N., Lomas, T., Wisitsoraat, A. and Tuantranont, A. (2010). Wireless wearable pulse oximeter for health monitoring using zigbee wireless sensor network. In: *Electrical Engineering/Electronics Computer Telecommunications and Information Technology (ECTI-CON), 2010 International Conference on*, pp. 575–579. IEEE.
- Winokur, E.S., Da He, D. and Sodini, C.G. (2012). A wearable vital signs monitor at the ear for continuous heart rate and pulse transit time measurements. In: *Engineering in Medicine and Biology Society (EMBC), 2012 Annual International Conference of the IEEE*, pp. 2724–2727. IEEE.
- World Health Organization (2011). Using the pulse oximeter. Available at: [http://www.who.int/patientsafety/safesurgery/pulse\\_oximetry/who\\_ps\\_pulse\\_oxymetry\\_tutorial2\\_advanced\\_en.pdf?ua=1](http://www.who.int/patientsafety/safesurgery/pulse_oximetry/who_ps_pulse_oxymetry_tutorial2_advanced_en.pdf?ua=1)

- Yasuma, F. and Hayano, J.-i. (2004). Respiratory sinus arrhythmia: why does the heartbeat synchronize with respiratory rhythm? *Chest Journal*, vol. 125, no. 2, pp. 683–690.
- Zong, W., Heldt, T., Moody, G. and Mark, R. (2003). An open-source algorithm to detect onset of arterial blood pressure pulses. In: *Computers in Cardiology, 2003*, pp. 259–262. IEEE.